Lawrence Berkeley National Laboratory
LBL Dissertations

Title
RESONANCES IN THE REACTION Kn -> 2~rtV FROM 1600 MeV TO 1900 MeV

Permalink
https://escholarship.org/uc/item/7420374m

Author
Bell, Robert Brooks.

Publication Date
1967-08-01

Thesis/dissertation

eScholarship.org Powered by the California Digital Library
University of California

UCRL-17089

eg. 2

University of California

Ernest O. Lawrence Radiation Laboratory

RESONANCES IN THE REACTION $K^- n \rightarrow \Sigma^- \pi^+ \pi^-$
FROM 1660 MeV TO 1900 MeV

Robert Brooks Bell

August 1966

UCRL-17089
Eg. 2

Berkeley, California

DISCLAIMER

This document was prepared as an account of work sponsored by the United States Government. While this document is believed to contain correct information, neither the United States Government nor any agency thereof, nor the Regents of the University of California, nor any of their employees, makes any warranty, express or implied, or assumes any legal responsibility for the accuracy, completeness, or usefulness of any information, apparatus, product, or process disclosed, or represents that its use would not infringe privately owned rights. Reference herein to any specific commercial product, process, or service by its trade name, trademark, manufacturer, or otherwise, does not necessarily constitute or imply its endorsement, recommendation, or favoring by the United States Government or any agency thereof, or the Regents of the University of California. The views and opinions of authors expressed herein do not necessarily state or reflect those of the United States Government or any agency thereof or the Regents of the University of California.

UCRL-17089

UNIVERSITY OF CALIFORNIA

Lawrence Radiation Laboratory
Berkeley, California

AEC Contract No. W-7405-eng-48

RESONANCES IN THE REACTION $K^- n \rightarrow \Sigma^- \pi^+ \pi^-$ FROM 1660 MeV TO 1900 MeV

Robert Brooks Bell

(Ph. D. Thesis)

August 1966

RESONANCES IN THE REACTION $K^- n \to \Sigma^- \pi^+ \pi^-$ FROM 1660 MeV TO 1900 MeV

Contents

Abstract v

I. Introduction 1

II. Experimental Procedure 4

A. Beam Momenta 4

B. Beam Normalization and Contamination 6

C. Data Processing 9

D. Selection Criteria 12

E. Biases 19

III. Data Analysis 26

A. $\Sigma^- \pi^+$ Spectrum 32

1. $Y_0^*(1520)$ Events 35

2. $Y_0^*(1405)$ Events 55

B. $\Sigma^- \pi^-$ Spectrum 60

Acknowledgments 66

Appendix 67

References 80

Figure Captions 83

RESONANCES IN THE REACTION $K^- n \to \Sigma^- \pi^+ \pi^-$ FROM 1660 MeV TO 1900 MeV

Robert Brooks Bell

Lawrence Radiation Laboratory
University of California
Berkeley, California

August 1966

ABSTRACT

We have studied the reaction $K^- n \to \Sigma^- \pi^+ \pi^-$ in the $K^- n$ center of mass energy range from 1660 MeV to 1900 MeV. Three strangeness minus one baryon resonances are definitely observed; two of these isobars, the $Y_0^*(1520)$ and $Y_0^*(1405)$, are produced with the negative pion and then decay into the $\Sigma^- \pi^+$ final state. The third, the $Y_1^*(1760)$, undergoes the decay $Y_1^*(1760) \to Y_0^*(1520) \pi^-$. It is also possible that the high energy tail of the $Y_1^*(1660)$ is present in our data. The $\Sigma^- \pi^-$ final state has isospin two and an extensive search was made for any enhancement which might indicate the presence of a Y_2^*; no evidence for the existence of a doubly charged strange resonance decaying into $\Sigma^- \pi^-$ was found anywhere in the available energy region of this experiment.

It was possible to unambiguously determine the spin and parity of the $Y_1^*(1760)$ by an examination of the production angular distribution of the $Y_0^*(1520)$ produced in the reaction $K^- n \to Y_1^*(1760) \to Y_0^*(1520) \pi^-$ and the decay distribution of the $Y_0^*(1520)$ into $\Sigma^- \pi^+$. No information concerning the quantum numbers of the $Y_1^*(1660)$ could be obtained from our data.

I. INTRODUCTION

This thesis is a study of the reaction $K^- n \to \Sigma^- \pi^+ \pi^-$ in the $K^- n$ c.m. energy range from 1660 MeV to 1900 MeV. The primary motivation for this experiment was to investigate the broad asymmetric peak which is known to exist in the $K^- p$ total cross section in this energy region. Originally it was thought that this enhancement was due to the presence of a single isospin zero resonance--the $Y_0^*(1815)$.[1] However, in 1963, a study of the reaction $K^- n \to K^- p \pi^-$ at a K^- momentum of 1.51 BeV/c suggested that another resonance, of isospin one and energy around 1760 MeV, might also exist.[2] To investigate this possibility a beam designed to yield separated K^- mesons in the approximate momentum range from 850 MeV/c to 1150 MeV/c was set up at the Bevatron in the early part of 1964. The detector was the new LRL 25-inch hydrogen bubble chamber. Film was exposed with both hydrogen and deuterium as the target liquid. Analysis of the $K^- p$ interactions has led to the determination of the quantum numbers of the $Y_0^*(1815)$;[3] the presence of a resonance near 1760 MeV with isospin one has been detected in final states produced from both $K^- p$ and $K^- n$ reactions.[4]

The channel $\Sigma^- \pi^+ \pi^-$ is strongly dominated by the production of the $Y_0^*(1520)$ baryon resonance; in fact, it has been possible to establish the existence of the process

$$K^- n \to Y_1^*(1760) \to Y_0^*(1520)\, \pi^-$$
$$Y_0^*(1520) \to \Sigma^- \pi^+ .$$

The $Y_1^*(1760)$ resonant parameters were determined by fitting a Breit-Wigner resonance curve to the $Y_0^*(1520)\, \pi^-$ production cross section. They are $M = 1760 \pm 5$ MeV and $\Gamma = 70 \pm 20$ MeV. An analysis of the

$Y_0^*(1520)$ production and decay angular distributions has shown the $Y_1^*(1760)$ to have spin 5/2 and negative parity.

Another resonance which decays into the final state $\Sigma^- \pi^+$ is also produced in this experiment--the $Y_0^*(1405)$; it is thought that the $Y_1^*(1660)$ decays into $Y_1^*(1405)\ \pi^-$.[5] If this is true our data can be interpreted as showing the high energy tail of the $Y_1^*(1660)$. However, the background is extremely severe and contains high order partial waves; this fact, coupled with our inability to observe any polarizations, precludes any possibility of a determination of the $Y_1^*(1660)$ quantum numbers from our data. The only statement that can be made is that spin greater than 3/2 is not required for the $Y_1^*(1660)$.

The final state combination $\Sigma^- \pi^-$ is of particular interest since it must have an isospin of two. Possible doubly charged strange resonances have been reported from time to time, most recently in the $\Sigma^- \pi^-$ final state with a mass near 1420 MeV.[6] Because of the importance of the Y_2^* as a candidate for a member of the 27 representation of SU_3, we have made an extensive search for its existence. No evidence for resonant structure in the $\Sigma^- \pi^-$ system anywhere within the available energy range is present in our data.

The reaction $K^- n \rightarrow \Sigma^+ \pi^- \pi^-$ would, at first thought, supply additional information about the $\Sigma\pi\pi$ final state, particularly because it would be possible to observe polarization of the sigma when it undergoes decay by the protonic mode. However, there are several difficulties connected with this channel. From the point of view of event selection, the presence of the protonic decay of the sigma plus causes severe scanning biases to be present; also there is a larger contamination of non-sigma events in the candidates and the constraint is less reliable.

The most important point is that two identical bosons are present in the $\pi^- \pi^-$ final state and symmetrization effects wash out the features of the angular distributions peculiar to the production of a resonance. It is fortunate that it is not necessary to analyze both charge states of the sigma (as is the case with the reactions $K^- p \rightarrow \Sigma^{\pm} \pi^{\mp}$) in order to uniquely determine the quantum numbers of the $Y_1^*(1760)$. Since the reaction $K^- n \rightarrow \Sigma^- \pi^+ \pi^-$ can supply all information about the $Y_1^*(1760)$ derivable from the $\Sigma\pi\pi$ final state, we shall not consider the $\Sigma^+ \pi^- \pi^-$ channel in this thesis.

II. EXPERIMENTAL PROCEDURE

The interaction of the external proton beam of the Bevatron with a copper target produced the K^- mesons used in this experiment. The beam line employed two stages of electro-static separation and was capable of separating K^- mesons in the approximate momentum range from 850 MeV/c to 1150 MeV/c and K^+ mesons from 800 MeV/c to 1600 MeV/c. The beam is shown schematically in Fig. 1; a more complete description of its characteristics exists elsewhere.[7] Both the external beam and the 25-inch bubble chamber can be pulsed twice during each Bevatron acceleration cycle and this was done whenever possible. An attempt was made to have, on the average, ten incident tracks per picture; at a K^- momentum setting of 850 MeV/c $2X10^{11}$ protons in the EPB channel were needed, while at a setting of 1150 MeV/c only 3 or $4X10^{10}$ protons were required. It was not possible to double pulse effectively below a K^- momentum of 1 BeV/c. Approximately 95% of the incident particles proved to be K^- mesons as is discussed in a later section. About 750,000 three view stereo pictures were taken during the course of the run, of which about one-third were exposed while the chamber was filled with deuterium as a source of neutrons. Four thousand frames were rejected as unusable; the remaining 252,000 pictures served as the basis of the following analysis.

A. Beam Momenta

The beam was tuned to the four nominal K^- momentum values of 850 MeV/c, 950 MeV/c, 1050 MeV/c, and 1150 MeV/c during the deuterium exposure. Due to the Fermi momentum of the neutron in the deuteron, these four momenta are sufficient to yield K^- n c.m. energies throughout the range

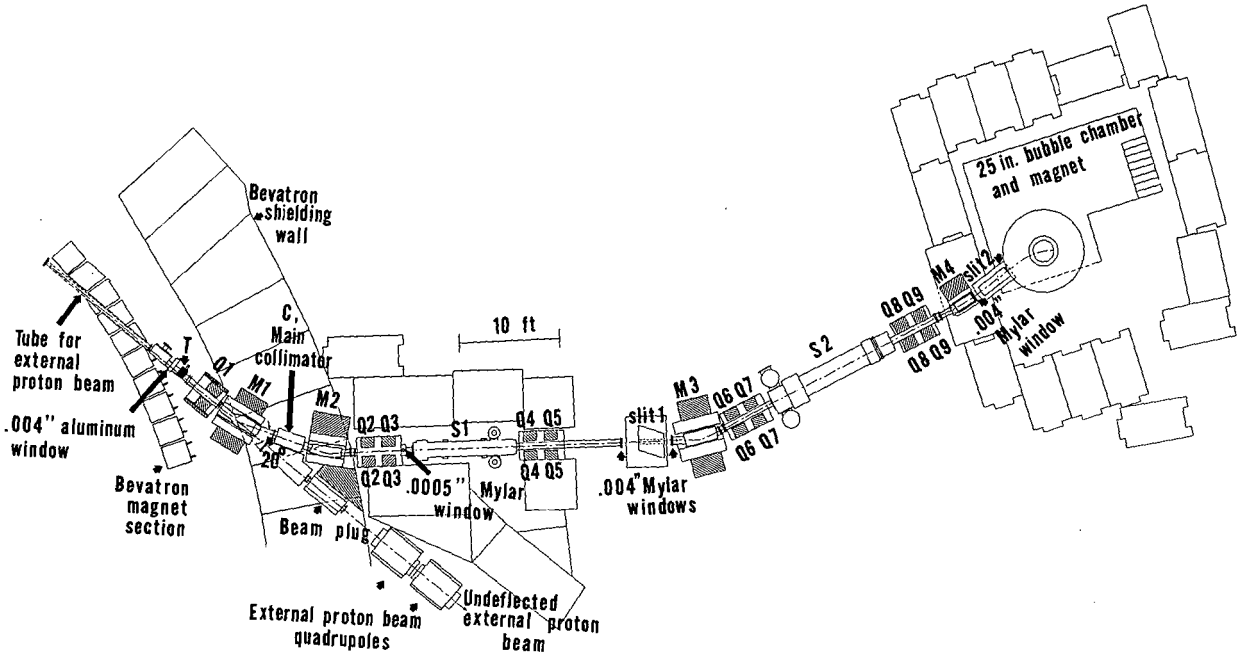

Bevatron shielding wall
C, Main collimator
10 ft
25 in. bubble chamber and magnet
Tube for external proton beam
.004" aluminum window
Bevatron magnet section
T
Q1
M1
M2
20°
Q2 Q3
S1
Q4 Q5
.0005" window
Mylar
Beam plug
External proton beam quadrupoles
Undeflected external proton beam
slit1
M3
Q6 Q7
.004" Mylar windows
S2
Q8 Q9
M4
slit2
.004" Mylar window
MUB-3362

Fig. 1

from 1660 MeV to 1900 MeV. To determine the actual momentum values several hundred beam tracks of length greater than 7 cm were selected from film taken at each magnet and spectrometer settings. Each momentum sample was made up of several of these batches. The tracks were measured by digitized microscope, Franckenstein measuring machine, or the FSD. The mean entrance angles of the beam tracks entering the chamber were determined for each batch and any track whose angles deviated by two degrees or more from these values was rejected. The K^- meson was also required to enter the bubble chamber through the entrance window. Using the remaining tracks, it was possible to determine the actual momentum values from the histograms of Fig. 2; they were 820 MeV/c, 917 MeV/c, 1015 MeV/c, and 1115 MeV/c. An error of ±1.5% was assigned to each of these values which is the momentum bite of the beam. These momenta and errors served as editing values in the constraining process for a given event as outlined in a later section.

B. Beam Normalization and Contamination

In order to calculate cross sections it is necessary to determine the value of the K^- flux at each momentum. With deuterium as the target liquid certain problems arise in making this determination. With hydrogen as the target one can simply count the number of distinctive tau decays of the K^- mesons ($K^- \rightarrow \pi^+ \pi^- \pi^-$) in the film. This number, together with a knowledge of the branching ratio into this mode (5.66%), the beam momentum, and K^- mean life (1.224×10^{-8} sec.) allows an absolute determination of the K^- flux. However, when the chamber contains deuterium, there are a large number of reactions which are topologically identical to a tau decay. Therefore, we proceeded as follows: The number of tracks entering the chamber was counted in

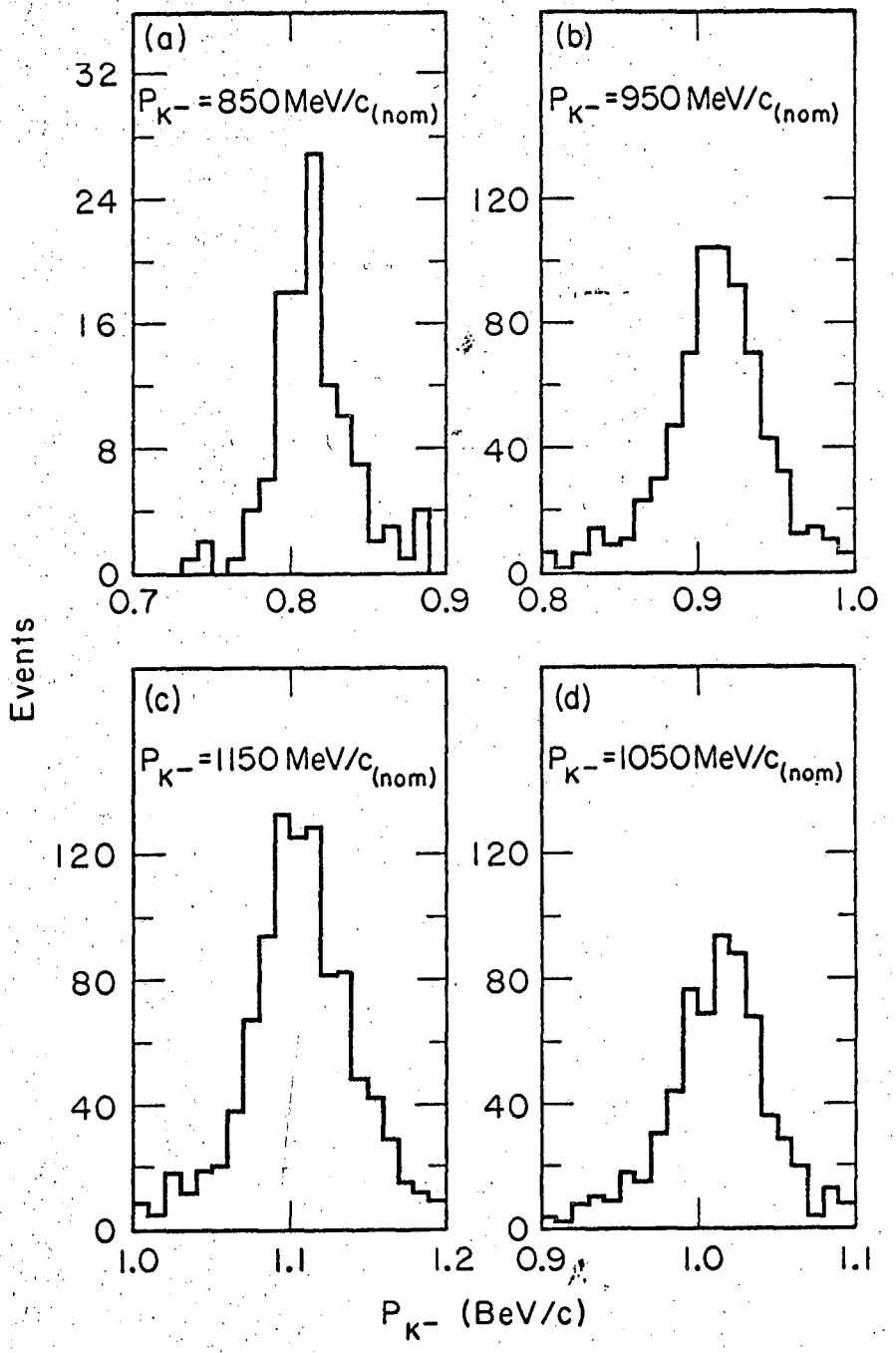

(a)
P_{K^-} = 850 MeV/c(nom)
(b)
P_{K^-} = 950 MeV/c(nom)
(c)
P_{K^-} = 1150 MeV/c(nom)
(d)
P_{K^-} = 1050 MeV/c(nom)
Events
P_{K^-} (BeV/c)
MUB 11597

Fig. 2

every fiftieth frame through the entire film; again the track was required to enter the chamber through the thin window and have entrance angles within the four degree interval about the mean angle used in the momentum determination. All that now remained was to estimate what percentage of these counted tracks were in reality K^- mesons. We again return to the hydrogen situation; by comparing the K^- flux as determined by a tau count to a direct count of beam tracks it was possible to determine the beam contamination. This contamination should be the same for both the hydrogen and deuterium exposures. Because a large amount a time passed between the hydrogen and deuterium runs (during which time the beam was tuned to yield K^+ mesons), it was considered desirable to check the value of the beam contamination by another method, namely by searching the good beam tracks for large delta rays. As is well known, the cross section for delta ray production is a function of the mass of the incident particle for a given momentum. For example, a 1 BeV/c K^- meson cannot yield a delta ray with an energy above 5 MeV. For a given bubble chamber magnetic field this can be translated into the maximum allowed diameter of the delta ray. It was found that the contamination as found from the delta ray count and that determined in the hydrogen film agreed within the errors. The beam contained 95.7%, 95.1%, 95.9%, and 91% K^- mesons for the 850 MeV/c, 950 MeV/c, 1050 MeV/c, and 1150 MeV/c setting, respectively.

During the beam count the total number of decays and interactions was noted. This allowed a determination of the attenuation of the beam as it passed through the chamber. This method was used because the total cross section was not known at the time the analysis was carried out. (This number has been recently determined.[8])

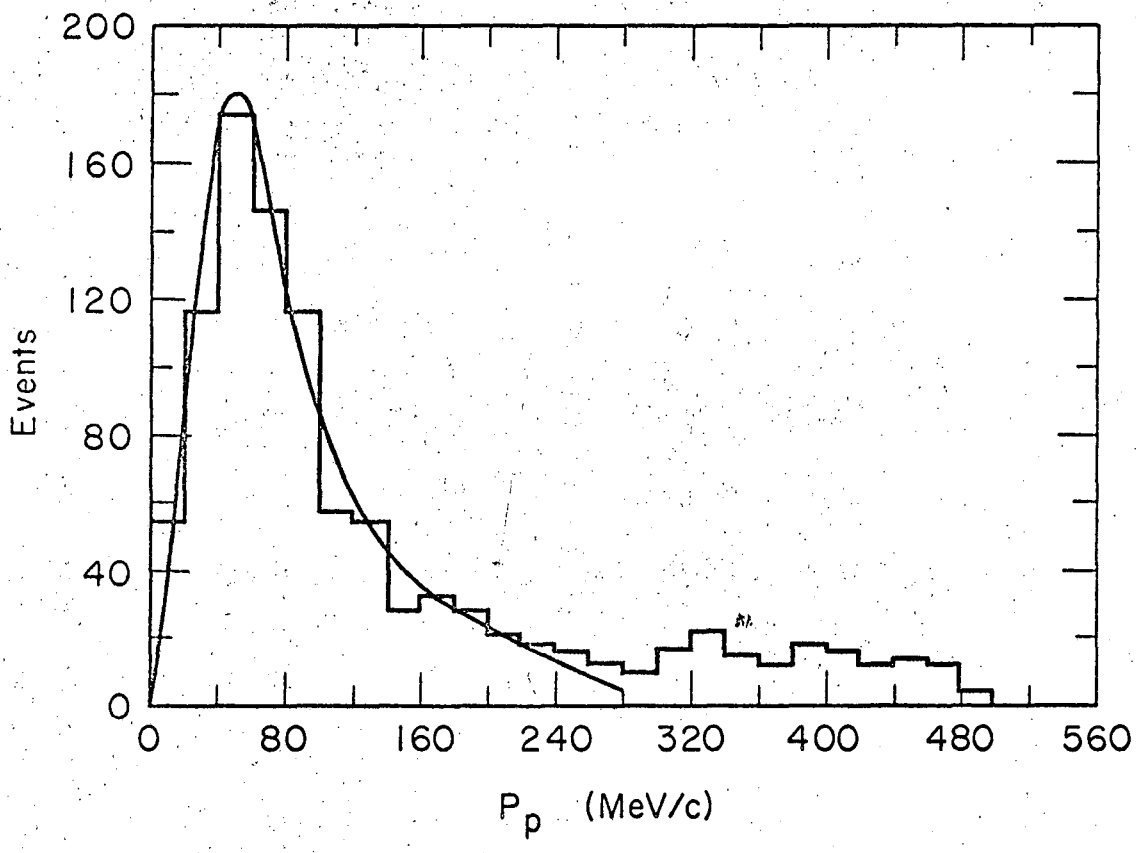
Finally it was necessary to choose a fiducial volume in the chamber. As is discussed later, the exact choice depends to a considerable degree on the event type under consideration. For the reaction $K^- n \rightarrow \Sigma^- \pi^+ \pi^-$, 46 cm in the beam direction was chosen. After correcting the beam count for contamination and attenuation, and using the known values of the number of frames and path length per frame, the total path length for each momentum was determined; they are given in Table I.

C. Data Processing

The final state of interest is $K^- n \rightarrow \Sigma^- \pi^+ \pi^-$ which appears in a bubble chamber as a three-prong event with a kink or change in ionization in one of the negative tracks. Sometimes a fourth track is present; this is possible if the spectator proton in the deuteron has a momentum of 90 MeV/c or greater during the $K^- n$ interaction. This momentum will cause a proton to travel a distance of 2 mm, on the average, in deuterium. Even if the proton stub was visible, it was required to be at least 3 mm in length to be accepted for measurement. The non-appearance of the recoil proton is in itself a form of constraint on the reaction kinematics as will be discussed in the next section. It is also necessary to insure that the recoil proton did not take part in an interaction with the K^- meson and neutron. This was done in the usual manner which consists of rejecting all events whose recoil momentum is greater than a particular value. This value is determined by comparing the distribution of recoil proton momenta with the predictions of the deuteron wave function. The exact cut off value is a matter of choice; in this experiment the limit was taken to be 300 MeV/c. Figure 3 shows the histogram from which this choice was made.

Table I. Path Lengths for the four beam momenta of our experiment.

Nominal Beam Momentum	Actual Beam Momentum	Path Length cm.
850 MeV/c	820 MeV/c	$(6.31 \pm 0.12) \times 10^6$
950 MeV/c	917 MeV/c	$(28.21 \pm 0.25) \times 10^6$
1050 MeV/c	1015 MeV/c	$(25.68 \pm 0.25) \times 10^6$
1150 MeV/c	1115 MeV/c	$(39.56 \pm 0.31) \times 10^6$



MUB 11590

Fig. 3

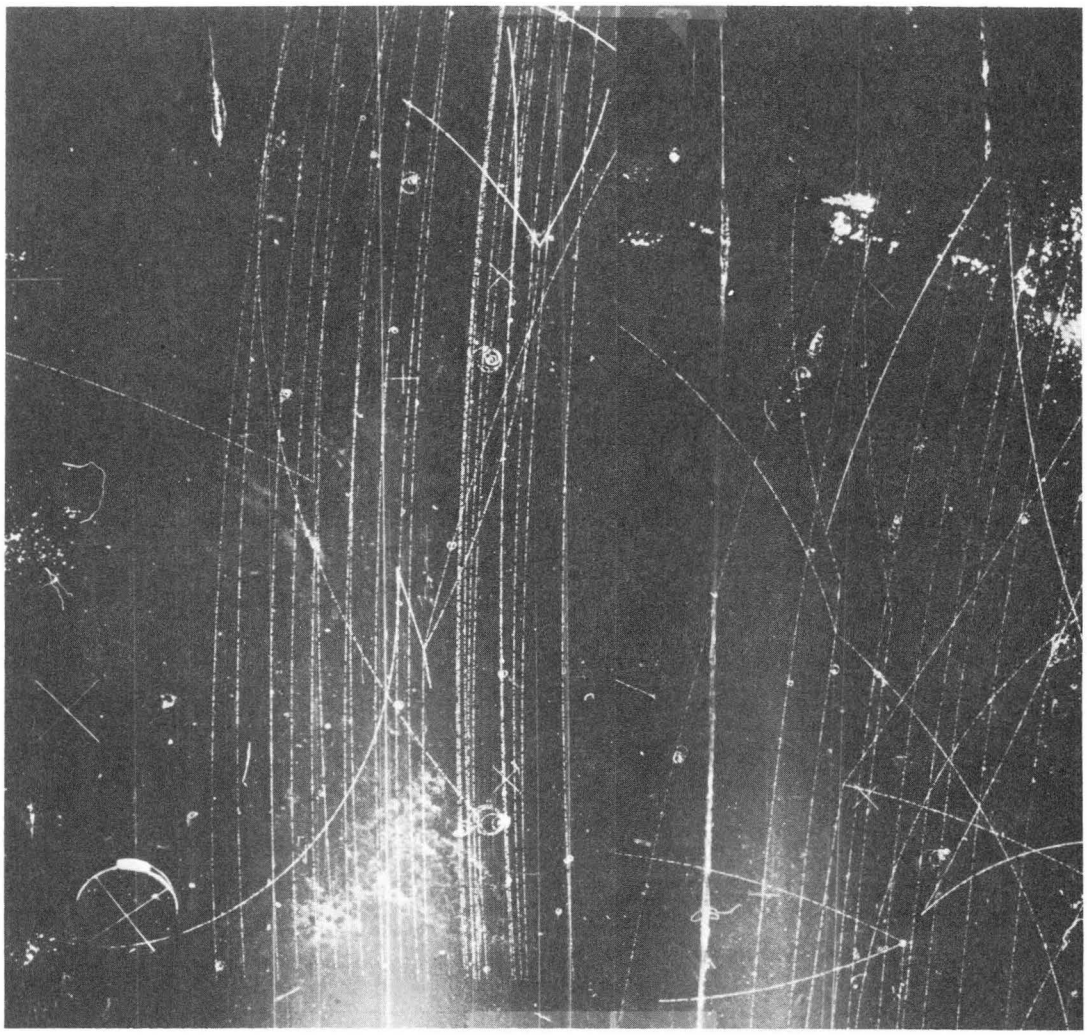
All 252,000 pictures were scanned with the very general criteria that any three- or four-prong event with a kink or change in ionization in a negative track was accepted for measurement provided the assumed sigma was 3 mm or greater in length; the event was also required to fall within the fiducial volume. An example of a three- and four-prong candidate is shown in Fig. 4. Approximately 3100 candidates were found in the scan of which 31% had a visible fourth track; no cut on the proton momentum was made by the scanners. These events were then measured by a digitized microscope and processed through the FOG-CLOUDY-FAIR data reduction programs. These programs are described in full elsewhere.[9] In brief, FOG checks the format of the measured data for errors and then reconstructs the event in space using the necessary chamber constants; in particular, FOG calculates momentum values and their errors for each track. This information is then used by CLOUDY as starting points for kinematic constraining. (As mentioned above, the beam momenta and errors are replaced by edited values.) CLOUDY varies the measured values until the quantity

$$M = (m_n - m_o)^T \underset{\sim}{U} (m_n - m_o) + 2\alpha^T F$$

is minimized. m_n are the current values of the measured values after n iterations; m_o are the original values; U is the error matrix, α the Lagrangian multipliers, and F the constraint equations of energy and momentum conservation. If these conservation equations are satisfied by the values m_n, then M can be interpreted as chi-squared.[10]

D. Selection Criteria

A candidate event was required to satisfy several conditions to be accepted for use in the analysis. They were as follows:

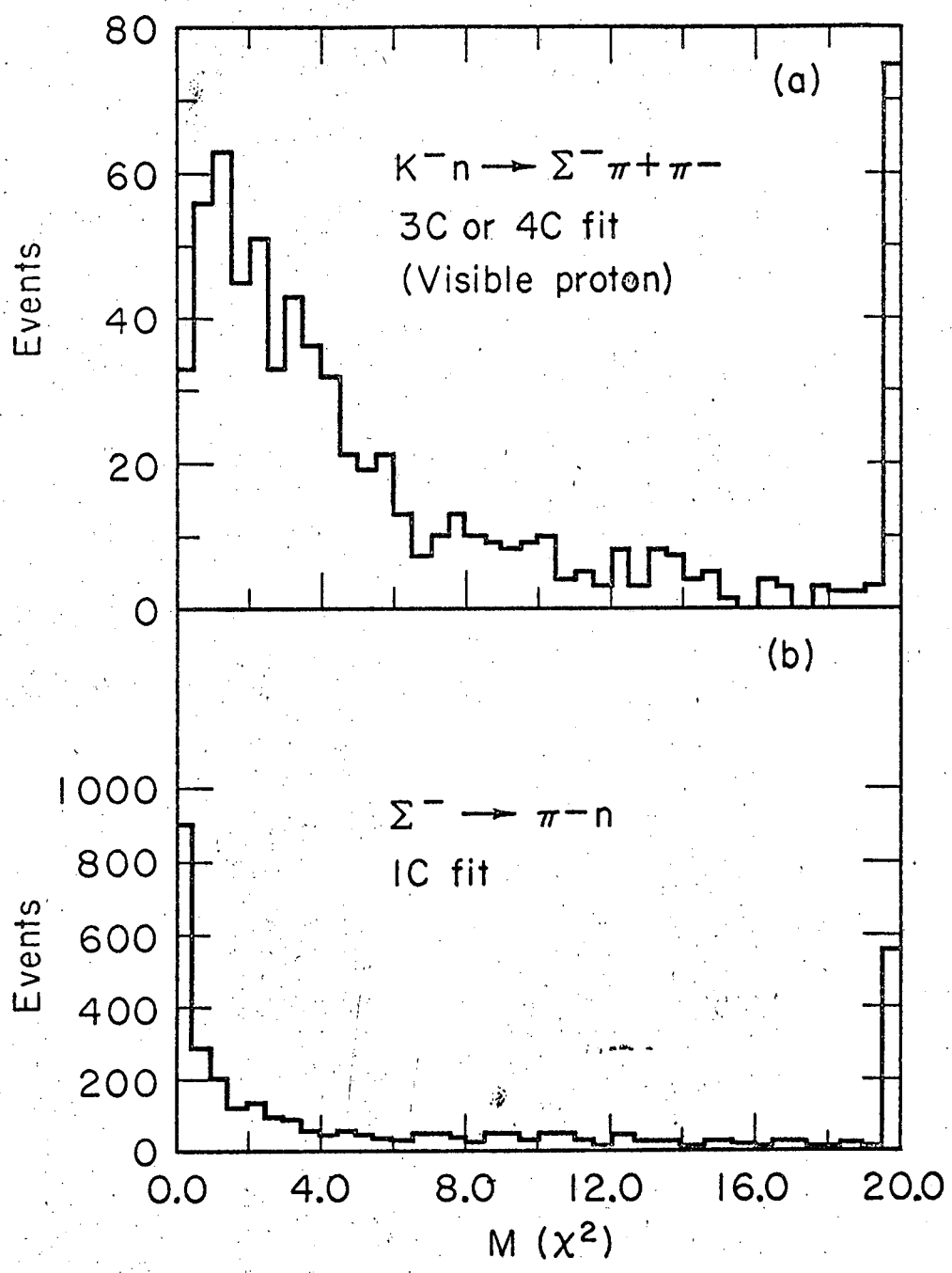


Bub Ch 1838

Fig. 4

(1) The event must have taken place within the fiducial volume mentioned in connection with the beam count; this region was chosen so that at least 3 cm of beam track was visible and so that essentially no sigmas leave the chamber before decaying. Since a sigma will travel, on the average, about 1.5 cm during a sigma mean lifetime, it was possible to use almost the full length of the chamber. To check that no bias was introduced by this choice of fiducial volume we plotted the distribution of events as a function of position in the chamber; it was found that all parts of the fiducial volume were equally populated. The beam track which produced the event was required to enter the chamber through the thin window and have entrance angles in the four degree interval mentioned twice before. The scanners made a preliminary fiducial cut on events that would obviously not be accepted; final cutting was done in FAIR.

(2) The event must have constrained to the reaction $K^- n \rightarrow \Sigma^- \pi^+ \pi^-$. The first condition to be met was that the energy and momentum conservation equations be satisfied at the production origin, that is F=0. If the spectator proton was visible the event is three or four times overdetermined, depending on whether or not the sigma yields a reliable momentum measurement. This momentum is determined from the sigma's curvature; thus short or straight sigma tracks result in the loss of one constraining equation. The M (chi-squared) distribution for events with spectators is shown in Fig. 5a where both 3C and 4C events are plotted together. As can be seen, the distribution peaks somewhat too low and has too many events at large chi-square values. This implies that



MUB 11589

Fig. 5

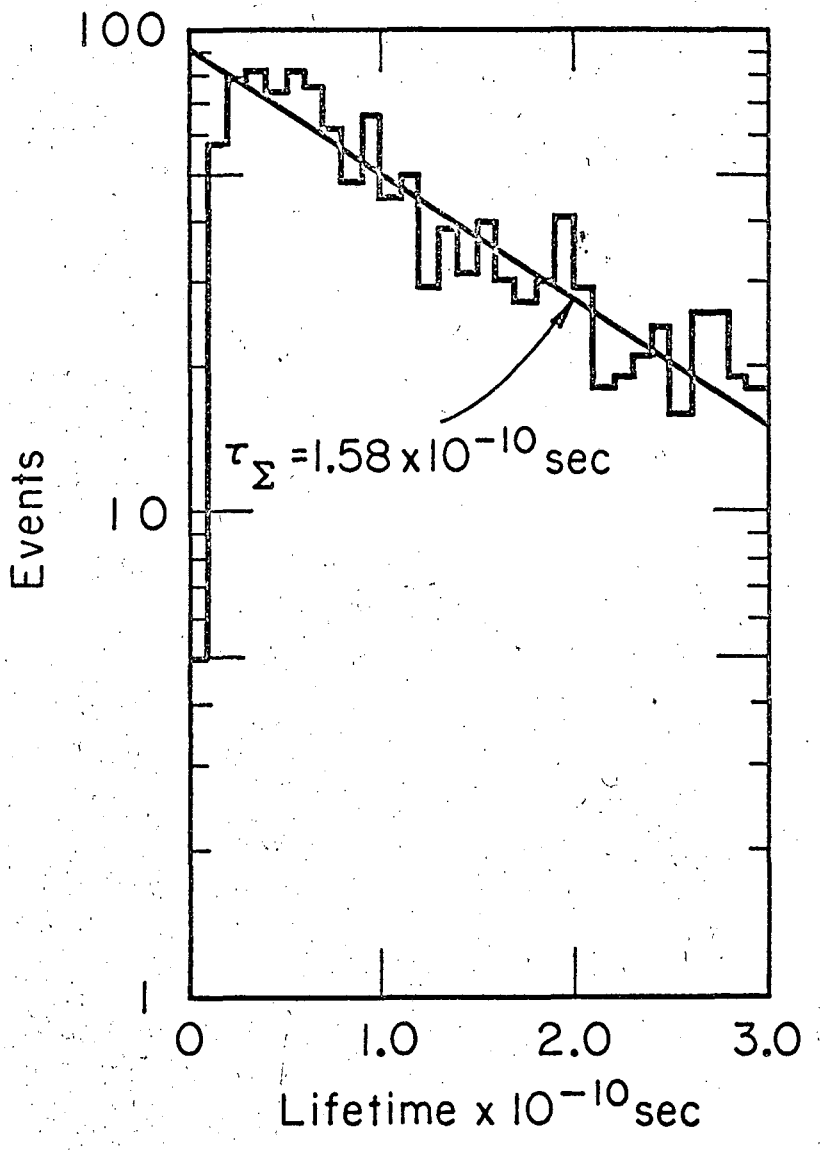
the measurement errors are being overestimated and are non-normally distributed. For the 4C fits we demanded that M be less than 20; for the 3C cases it was required to be less than 15. The sigma momentum determined by this first orgin constraint was then extrapolated to the sigma decay vertex where a 1C constraint was imposed. The chi-squared distribution for this fit is shown in Fig. 5b. We demanded that chi-squared be less than 7 and that the constraint equations F=0 be satisfied.

If no spectator proton is visible, the constraint at the production orgin is much looser, being at best on a 1C and often a zero C. If the constraint was a 1C we required the chisquared to be less than 7 and F=0; again the sigma momentum was used in a 1C fit at the decay vertex as described above. If the situation is a 0C then there is no chisquared at all and in general two solutions for the sigma momentum. In this case we were able to pick the best solution by an examination of the decay vertex fit, imposing kinematical constraints on the allowed range of sigma momentum and by demanding that the invisible proton momentum be less than 100 MeV/c. (This limit on the recoil momentum was imposed on all events with no visible spectator.) A summary of the number of events which constrained in various categories is given in Table II.

(3) The projected length of the sigma was required to be greater than 0.3 cm.. All events were then weighted by the inverse of the probability that the given sigma went that distance. In this connection we made a least mean square fit to the distribution of sigma lifetimes as shown in Fig. 6. This fit

Table II. Disposition of events in this experiment.

Category	3-Prong	4-Prong	All Events
Candidates (after fiducial cut)	2041	1018	3059
Good on first measure	1257	480	1737
Additional good events from remeasure	89	6	95
4-Prong with proton momentum > 300 MeV/c	--	132	132
Non-fitting events after two measures	695	400	1095
$K^- p \rightarrow \Sigma^- \pi^+ \pi^- \pi^+$	--	298	298
Estimate of event $K^- n \rightarrow \Sigma^- \pi^+ \pi^- \pi^o$	210	90	300
Non sigmas or difficult to measure	350	10	360
Unexplained events	135	2	137



MUB-11584

Fig. 6

gave a value of $(1.6 \pm 0.2) \times 10^{-10}$ seconds, which is in good agreement with the current value of 1.58×10^{-10} seconds. It is well known that in the case of a two body final state this type of cut biases the angular distributions since a given sigma momentum corresponds to a definite c.m. angle. In the case of our three body final state we found that the weighting factors were rather independent of the sigma production angle.

E. Biases

There are a number of possible biases to be considered in this experiment. One has already been mentioned in the last section, namely the effect of missing slow short lived sigmas. Other biases considered were:

(1) Sigma events are extremely difficult to measure due to the short length and broadness of the sigma track; with three or even four tracks connected to the production origin, it is often difficult to determine the exact location of that origin. Consequently,

a sample of about 500 events of all types were remeasured and reprocessed through FOG-CLOUDY-FAIR in an attempt to determine how many events failed to meet our selection criteria because of bad measurements. The results are indicated in Table II. This information was used as a correction to the values of the cross sections. The sigma momentum and angular distributions of the events which changed categories (of acceptability or non-acceptability) were examined and found to be the same as events which did not change categories. Thus we expect the angular distributions not to be biased as a result of bad measurements.

(2) As can be seen from Table II, a large number of events did not fit on either measure. In order to determine the nature of these non-constraining events a sample of about 25% of the candidates of all types were examined on the scan table. In general, it might be said that the scanners, in their zeal to be efficient, were reluctant to reject events. For example, 15% of the candidates were found to have a sigma of length greater than 5 cm, where only about 3% of the events should be this long. An examination of the non-constraining four-prongs showed a large number to be of the type $K^- p \rightarrow \Sigma^- \pi^+ \pi^- \pi^+$ and that the scanner had been unwilling to make the choice between calling the fourth track a proton and a pion. Although this event type was easily removed by the momentum cut of 300 MeV/c imposed on the recoil proton track (which was actually a cut on the length of that track), it was a matter of concern that almost 40% of the candidate four-prongs did not constrain. The only source of real background for the event $K^- n \rightarrow \Sigma^- \pi^+ \pi^-$ is the event $K^- n \rightarrow \Sigma^- \pi^+ \pi^- \pi^0$ which is known

to have a cross section too small to explain the large number of non-fitting four-prongs. Another commonly misidentified event was a tau decay followed by a scatter or decay of negative pion. These events were easily identified by the curvature, ionization, and forward motion of the three pions.

Actually, it would have been possible to reject many of the events which did not constrain to the reaction $K^- n \rightarrow \Sigma^- \pi^+ \pi^-$ on the scan table on the basis of reaction kinematics. For example, the laboratory angle between the outgoing sigma and incident K^- cannot be greater than about 60 degrees for either the reaction $K^- n \rightarrow \Sigma^- \pi^+ \pi^-$ or the reaction $K^- n \rightarrow \Sigma^- \pi^+ \pi^- \pi^o$. A cut on events with a lab angle greater than this value was easily made in FAIR which allowed a count of the number of candidates in this category. A small number of events were covered by beam tracks or were difficult to see or measure.

A source of real background, as mentioned before, is the event $K^- n \rightarrow \Sigma^- \pi^+ \pi^- \pi^o$. Several methods exist for determining the number of these reactions in this experiment. Perhaps the easiest is to count the number of $K^- p \rightarrow \Sigma^- \pi^+ \pi^- \pi^+$ events; although this reaction differs from the one in question in that there is another isospin state involved, it is reasonable to assume that the I=0 and I=1 cross sections for the production of the final state $\Sigma 3\pi$ are about equal. The numbers in Table II are the result of this method; it is interesting to note that if the above statement concerning the $\Sigma 3\pi$ cross section is correct, all four-prong candidate events have a reasonable explanation. The other methods for determining the existence of an extra pion involves determining the sigma momentum from the momentum and angles of the decay pion

and then plotting the missing mass at the production origin. The situation is hopeless unless the recoil proton is seen. Even then there are two difficulties; first, the calculation of the sigma momentum is OC and, in general, yields two solutions which are often very different and impossible to chose between; second, a glance at the kinematics of the pionic decay of the sigma shows that in the decay pion momentum range from about 150 MeV/c to 200 MeV/c a small error in measurement in either that momentum or in the decay angle can result in a tremendous error in the sigma momentum. Thus it is expected that the peak in the missing mass spectrum which corresponds to extra pion production will be distorted in a non-predictable manner. Table II contains a complete disposition of the candidate events of this experiment. As can be seen, only about 5% of the candidate events remain unexplained.

(3) There are some categories of track configurations which were expected to be difficult for the scanners to detect; the first of these is the case in which the sigma track is coming toward or going away from the cameras. It is also expected that this possible dip bias would be most serious for short sigma tracks. To investigate this possibility, we plotted the azimuthal angular distribution of the sigma as a function of its production angle. This distribution is shown in Fig. 7a and is seen to be reasonably isotropic; the suggestion of losses in the up and down direction is due to the short or slow sigma events. As pointed out in connection with the length cut we made, the angular distributions are not sensitive functions of the sigma momentum and thus we

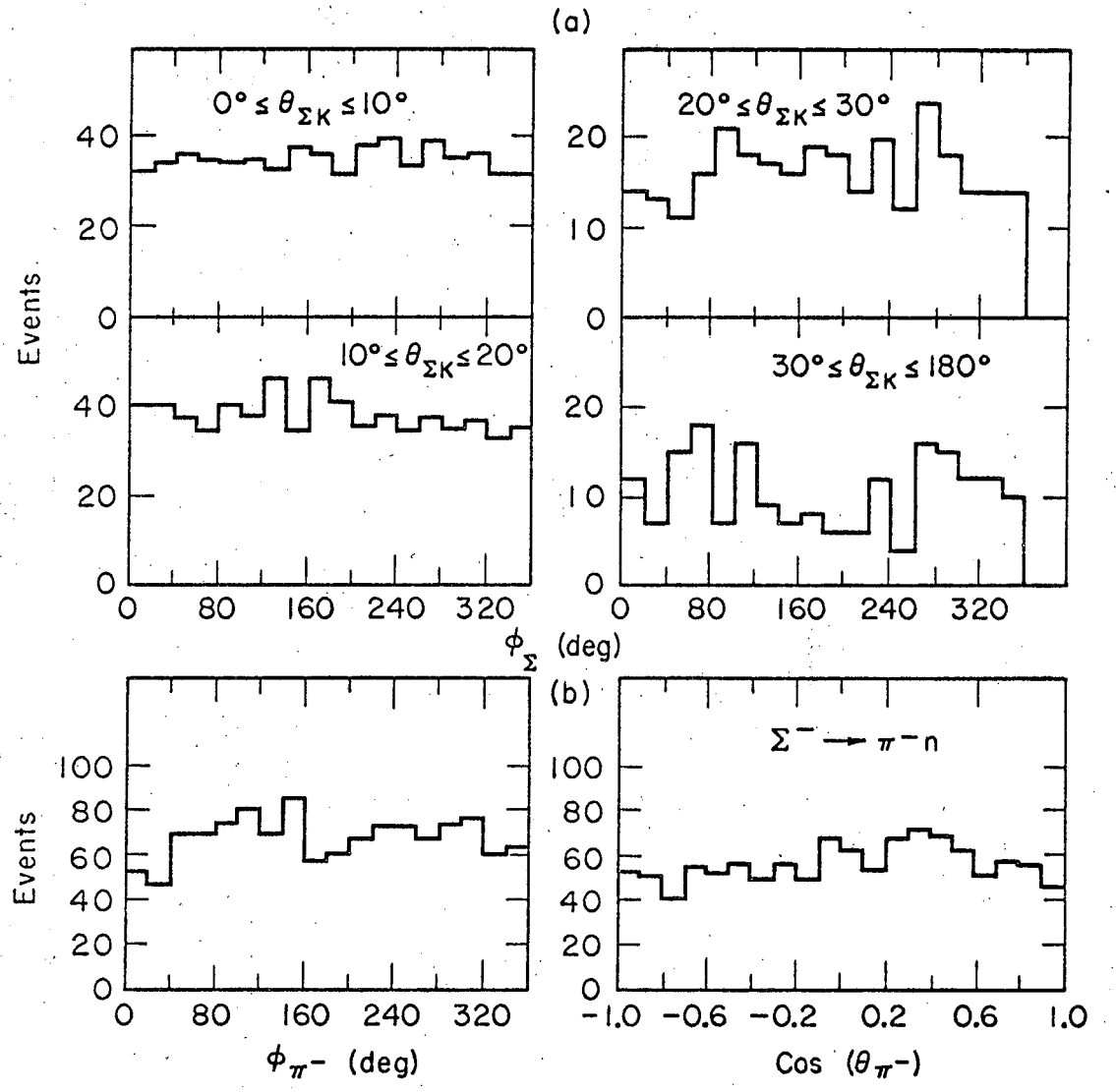

(a)
$0° \le \theta_{\Sigma K} \le 10°$
$10° \le \theta_{\Sigma K} \le 20°$
$20° \le \theta_{\Sigma K} \le 30°$
$30° \le \theta_{\Sigma K} \le 180°$
Events
ϕ_Σ (deg)
(b)
$\Sigma^- \rightarrow \pi^- n$
Events
ϕ_{π^-} (deg)
Cos (θ_{π^-})
MUB 11601

Fig. 7

expect them to be unbiased by dip losses.

The azimuthal distribution of the decay pion was also examined and found to be isotropic; this is to be expected since the pion is usually quite long. Decay pions which decay forward might be expected to be difficult to detect; however it must be remembered that the sigma tracks are usually very dark while the pion tracks are almost always minimum ionizing. Further, the pion can decay into the entire solid angle in the laboratory. Therefore, our criterion of accepting events with a change in ionization would be expected to minimize this loss. The decay angular distribution of the pion in the sigma c.m. is shown in Fig. 7b; since this decay is known to be essentially parity conserving, the distribution is expected to be isotropic. This is the case experimentally.

(4) To determine the scanners' efficiencies, approximately two-thirds of the film was rescanned with no scanner repeating a roll he had done on the first scan. The very general scan criteria resulted in efficiencies ranging from 94% to 98% with a mean efficiency of 97.4%. The small correction necessary in the cross section was easily made.

(5) Finally, it is necessary to consider possible lost events in the data processing. A check of scan records against a listing of processed events showed bookkeeping losses which varied from 5.2% for the 950 MeV/c sample to 9.8% for the 850 MeV/c batch. Most of these events were either lost through computer errors or were contained on input tapes that had inadvertently not been processed at the time of the analysis. It is difficult to imagine any possible bias introduced into the data by these lost events (except

for the exact values of the cross sections where their effect is easily correctable).

III. DATA ANALYSIS

Figure 8 shows a Dalitz plot of the acceptable $K^- n \rightarrow \Sigma^- \pi^+ \pi^-$ events; also shown are the kinematically allowed regions for various $K^- n$ c.m. energies. Events from all four beam momenta are included in this figure and since not all $K^- n$ energies are equally probable, the interpretation of this plot is more difficult than would be the case if only one energy were available. However, there is one very striking feature, namely the large clustering of events in a band around a $M^2(\Sigma^- \pi^+)$ value of 2.31 BeV^2. This enhancement is due to the production of the $Y_0^*(1520)$ which is known to decay strongly into the $\Sigma^- \pi^+$ final state; it has spin 3/2 and negative parity.[11] As can be seen from Fig. 8, this isobar is strongly produced through the available energy region above its threshold value of 1660 MeV. There also appears to be another, less pronounced, band around 2.0 BeV^2 which may be identified with production of the $Y_0^*(1405)$; this resonance is thought to have spin 1/2 and negative parity.[12] Because of the dominance of these two bands in the Dalitz plot, it is difficult to detect any possible enhancement in the $\Sigma^- \pi^-$ channel.

To better study the $\Sigma^- \pi^+$ and $\Sigma^- \pi^-$ mass spectra, we have projected the events onto the $M^2(\Sigma^- \pi^+)$ and $M^2(\Sigma^- \pi^-)$ axes as shown in Fig. 9. The $M^2(\pi^+ \pi^-)$ spectrum is also shown in this figure; no resonances in the pi-pi system are known to exist in the available energy region of this experiment and our data is in agreement with this. Thus, no reflections from pion resonances will be present in the $\Sigma^- \pi^+$ and $\Sigma^- \pi^-$ mass distributions.

Since we are dealing with a distribution of $K^- n$ c.m. energies, the expected three-body phase space is actually the weighted sum of

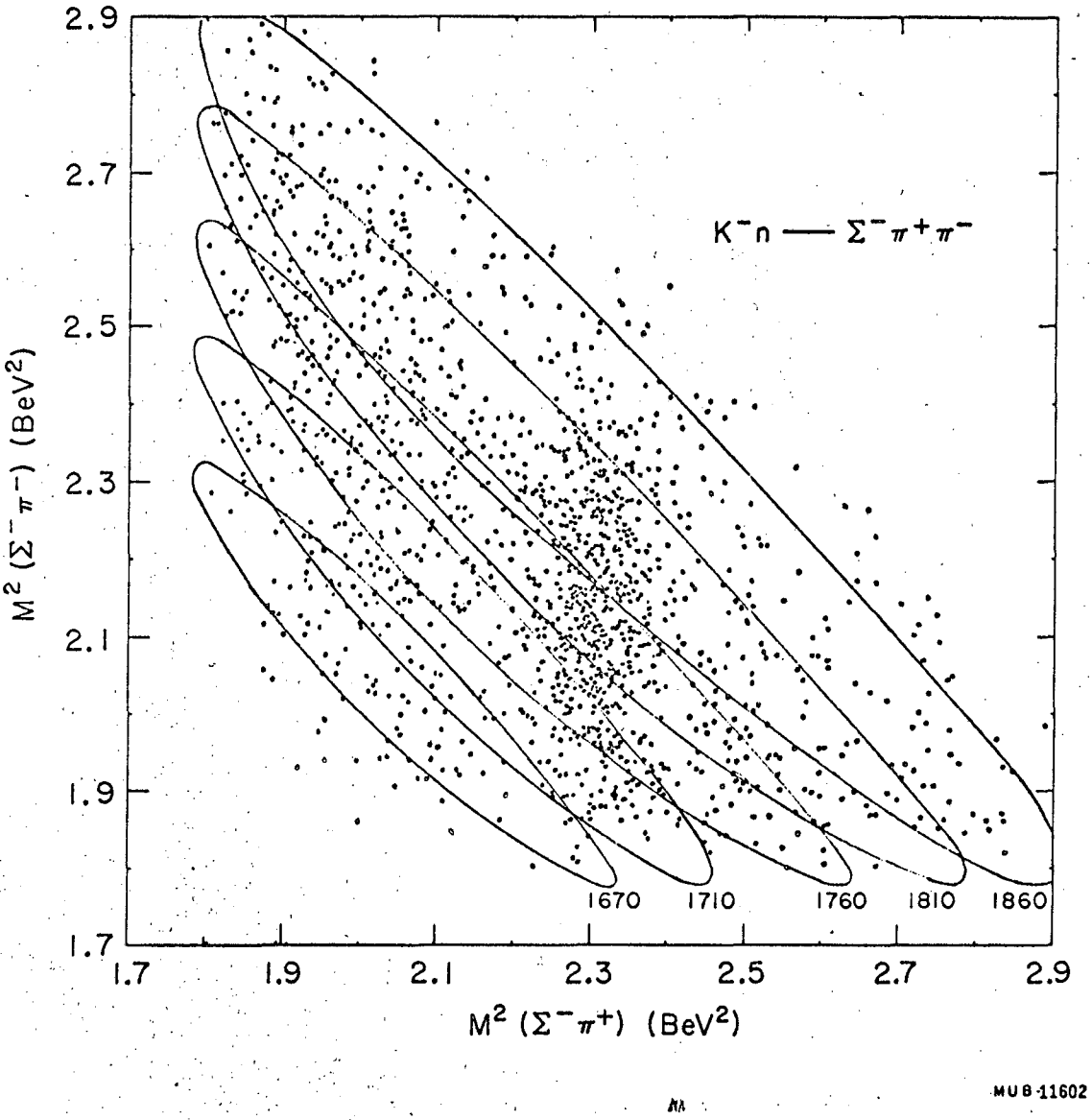
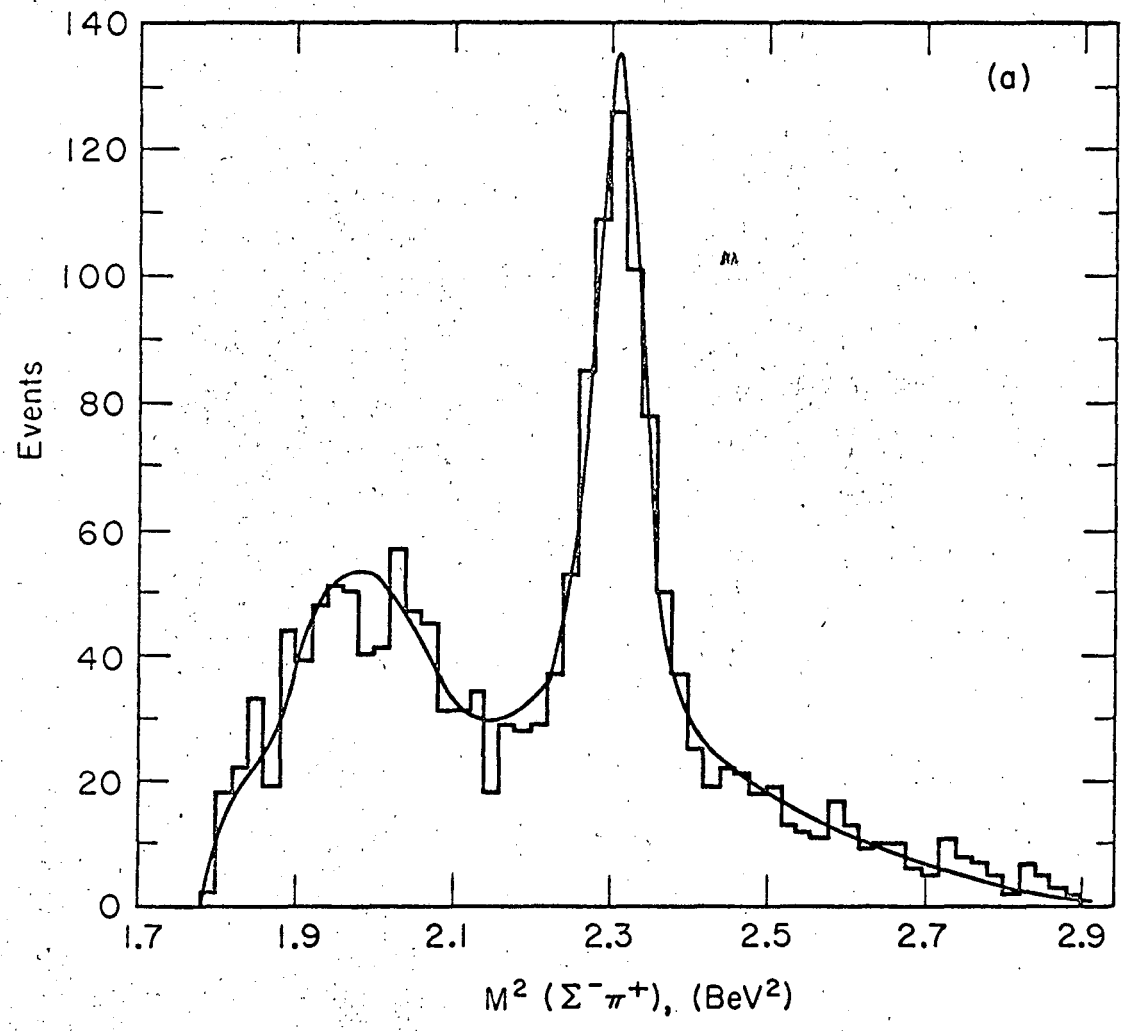
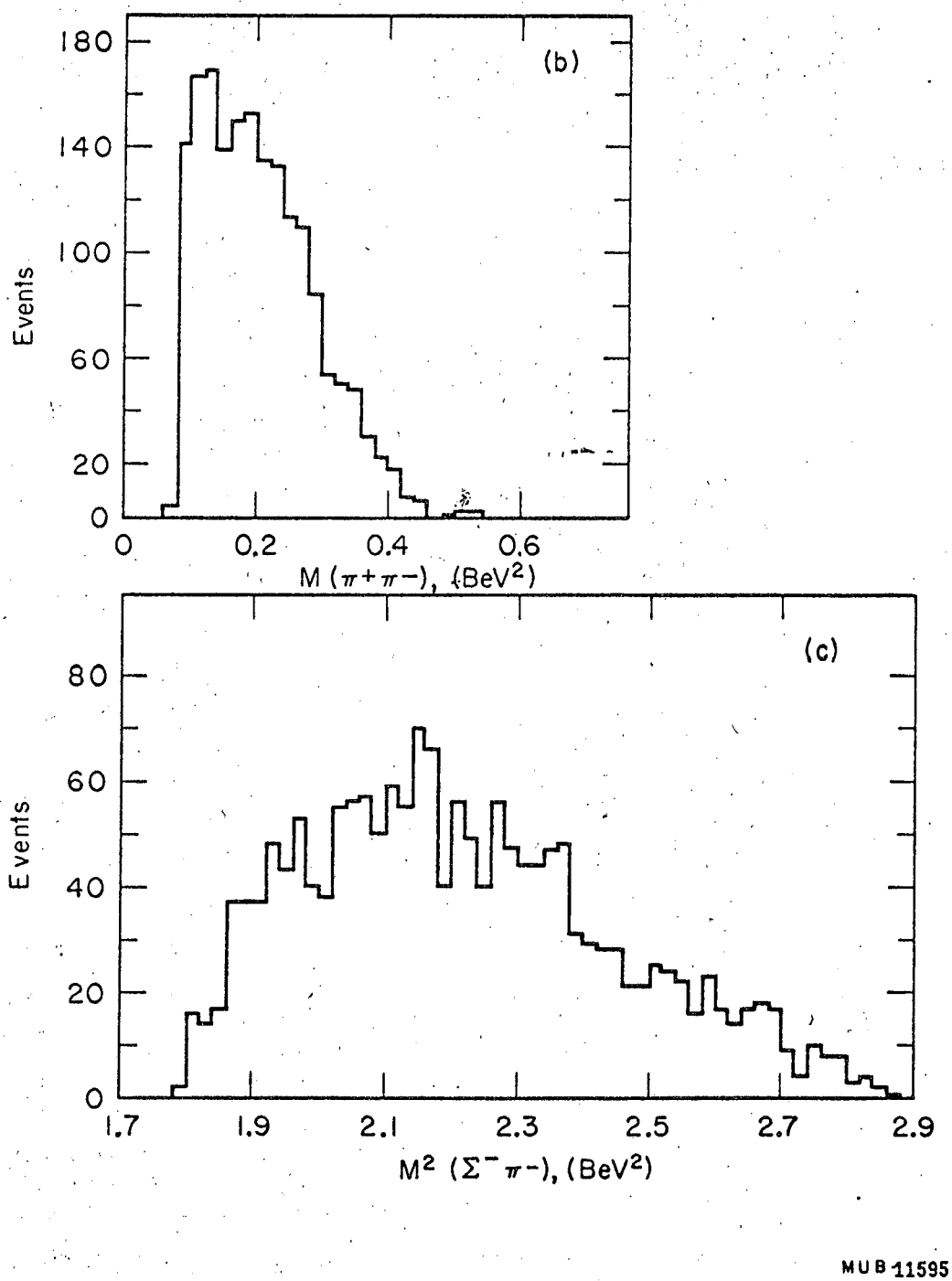

2.9
2.7
2.5
2.3
2.1
1.9
1.7
1.7
1.9
2.1
2.3
2.5
2.7
2.9
$M^2(\Sigma^-\pi^-)$ (BeV^2)
$M^2(\Sigma^-\pi^+)$ (BeV^2)
$K^-n \longrightarrow \Sigma^-\pi^+\pi^-$
1670
1710
1760
1810
1860
MUB-11602

Fig. 8



MUB 11596

Fig. 9a



MUB 11595

Fig. 9b, c

phase spaces from each available energy. The weighting factor is just the probability for finding a given K^- n energy and can be found in the following way: We have shown that the spectator proton momentum, and thus presummably the target neutron momentum, is distributed according to the predictions of the deuteron wave function provided a cut is made to eliminate two nucleon interactions. For a given K^- momentum it is a straightforward calculation to predict the expected distribution of K^- n c.m. energies from this wave function. (The momentum cut was again taken to be 300 MeV/c.) The distributions for the four beam momenta of our experiment are shown in Fig. 10a. Each of these curves was then weighted by the path length for the corresponding beam momentum and all curves added. What resulted is the expected distribution of K^- n c.m. energies as shown in Fig. 10b. A nice pictorial way to interpret this plot is to say that

$$L(E1, E2) = \frac{A(E1, E2)}{A} L_{tot}$$

is the effective path length for the energy interval from E1 to E2; $A(E1, E2)/A$ is the ratio of the area under the curve in the range E1 to E2 to the total area and L_{tot} is the total path length. $L(E1, E2)$ is precisely the needed weighting factor. This method allows the determination of cross sections as a function of K^- n energy rather than with respect to K^- beam momentum. In order to estimate the errors in these effective path lengths, the momenta were varied by the 1.5% error which is assigned in the beam editing process and the distribution of Fig. 10b recalculated. The errors in beam normalization are not significant. As would be expected, only path lengths at the high and low energy ends of the distribution depend sensitively on the exact value of the beam momenta. The errors found in this way were folded

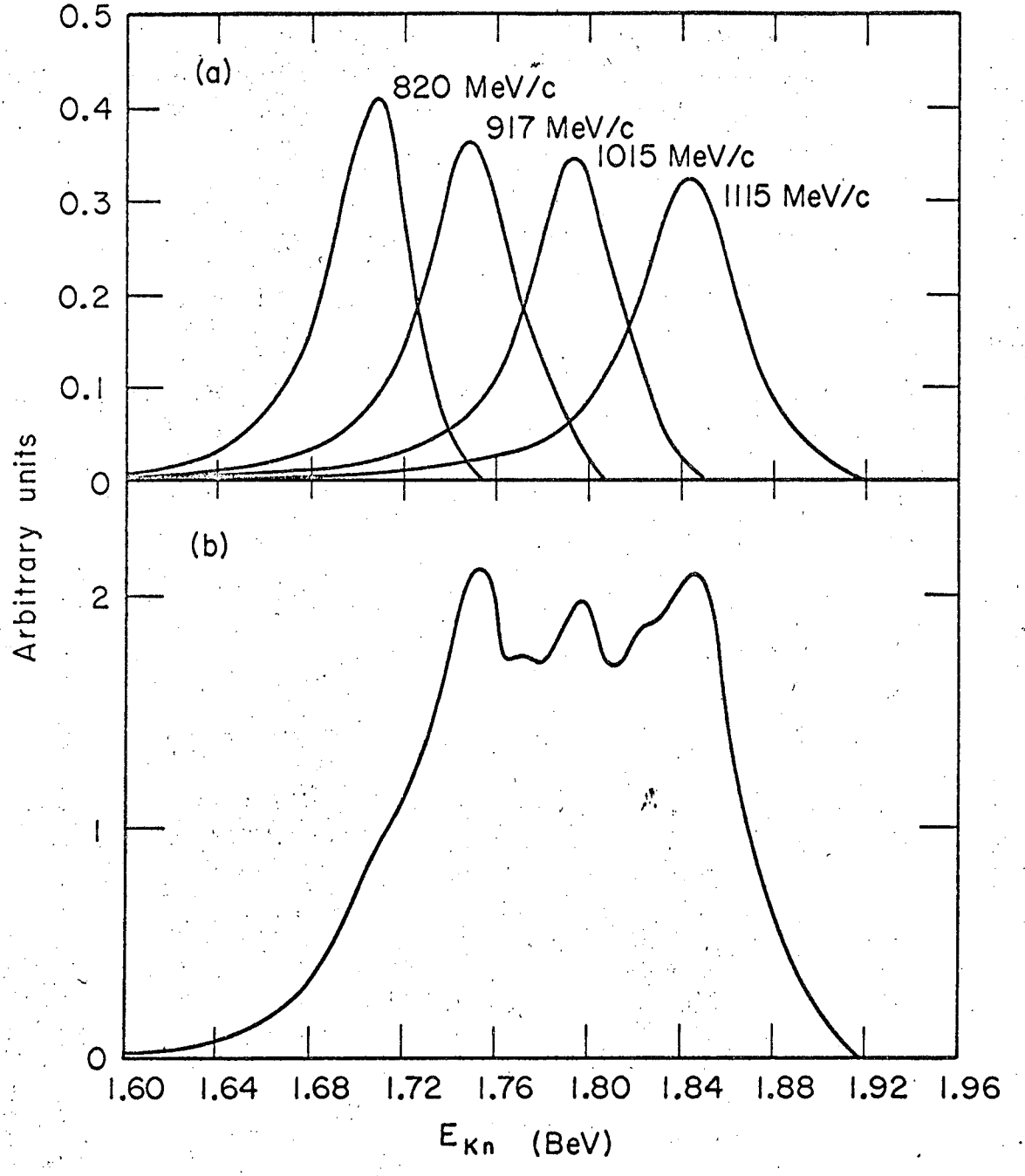

(a)
820 MeV/c
917 MeV/c
1015 MeV/c
1115 MeV/c
(b)
Arbitrary units
0.5
0.4
0.3
0.2
0.1
0
2
1
0
1.60
1.64
1.68
1.72
1.76
1.80
1.84
1.88
1.92
1.96
E_{Kn} (BeV)
MUB 11599

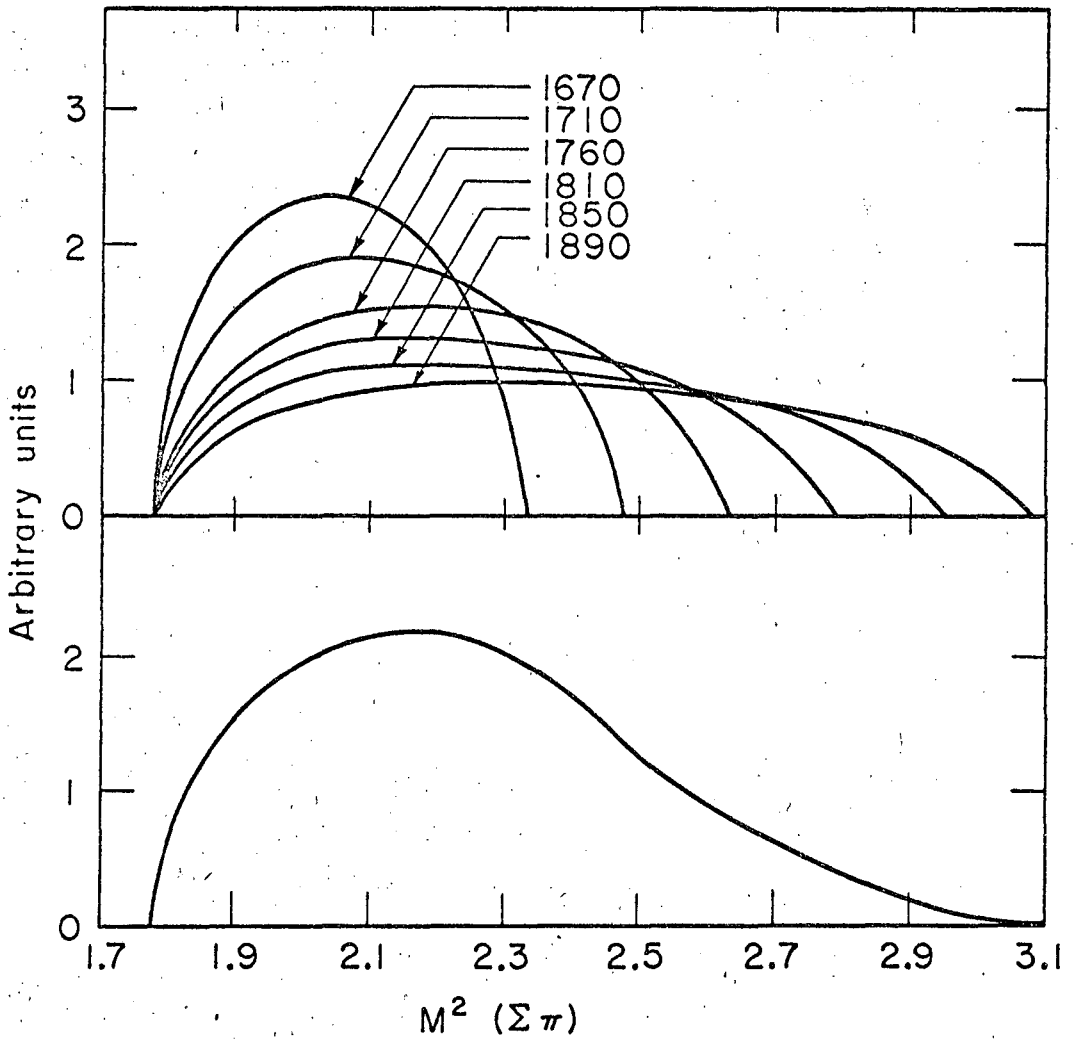
Fig. 10

into the cross section values to be presented in the next section.

The available K^- n energy range was divided into a number of intervals, the phase space for the central energy of that interval, examples of which are shown in Fig. 11a, weighted by the appropriate effective path length, and all curves added to yield the distribution shown in Fig. 11b which can be interpreted as the expected three-body phase space.

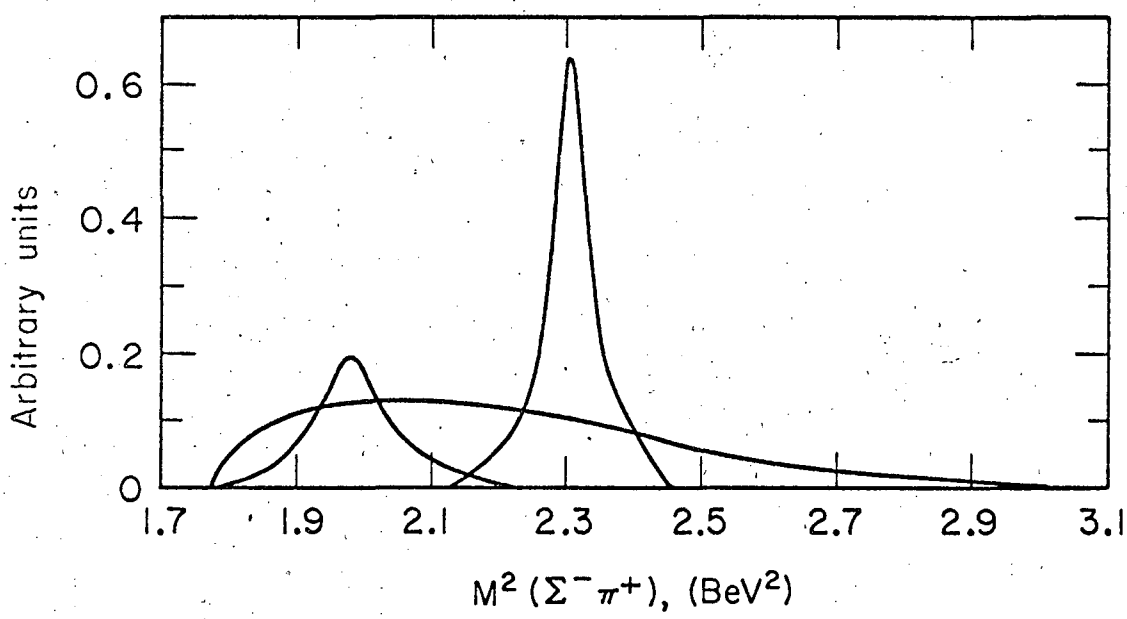
A. $\Sigma^- \pi^+$ Spectrum

The $\Sigma^- \pi^+$ mass squared distribution of Fig. 9 was fitted assuming the presence of the $Y_0^*(1520)$, the $Y_0^*(1405)$, and the derived three-body phase space. The only other structure which exists in the $\Sigma^- \pi^+$ spectrum is the $Y_1^*(1385)$ which is known to have a very small branching ratio into the sigma pi channel.[13] It would not be possible to resolve $Y_1^*(1385)$ events from $Y_0^*(1405)$ events in this experiment. The fitting program determined the best percentage of each of these contributions to fit the experimental histogram by minimizing chi-squared. The widths of the $Y_0^*(1520)$ and $Y_0^*(1405)$ were allowed to vary and the best values for those parameters were found to be Γ_{1520} = 20 MeV and Γ_{1405} = 50 MeV. The currently quoted width for the $Y_0^*(1520)$ is 16 ± 2 MeV and for the $Y_0^*(1405)$, 35 ± 10 MeV.[14] Fitting our distribution with these values did not make the fit significantly poorer. The best fit had a probability of 17%. The curve of Fig. 9, which represents the best fit to the $\Sigma^- \pi^+$ mass squared spectrum, is made up of the three distributions shown in Fig. 12. The ratio $Y_0^*(1520)$ to background appears to be 3 to 1; the ratio of $Y_0^*(1405)$ to background is approximately 0.75 to 1. It was of interest to see if the ratio of resonance to background changed markedly as a function of K^- n



MUB 11585

Fig. 11



MUB-11593

Fig. 12

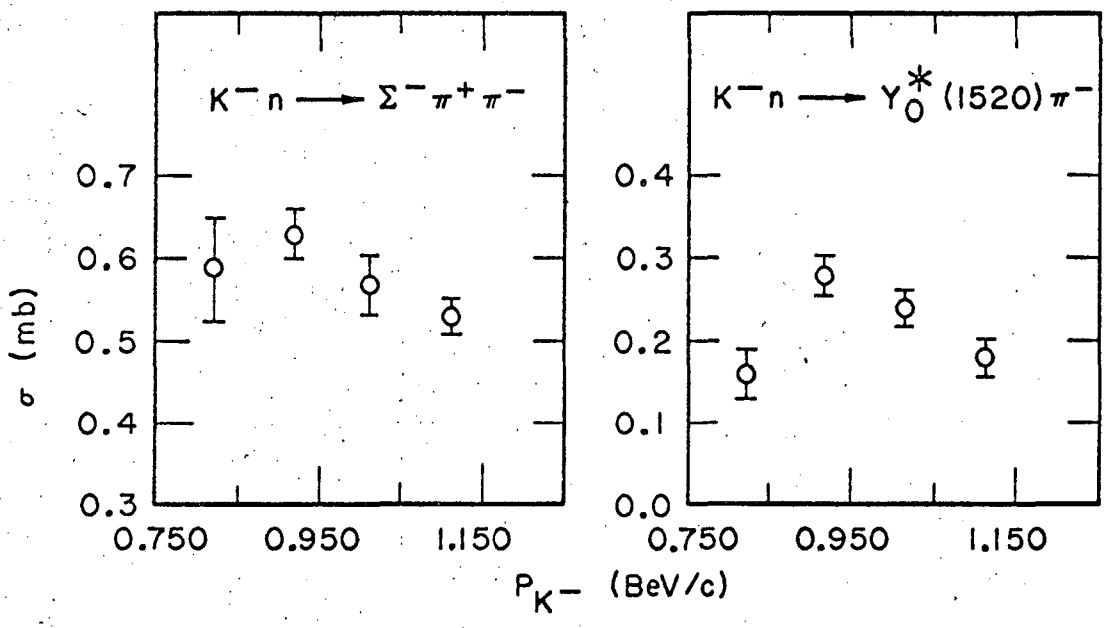
c.m. energy. The above fitting procedure was repeated for various energy intervals. It was found that in the range 1720 MeV $\leq E_{KN} \leq$ 1800 MeV the $Y_0^*(1520)$ to background ratio is slightly greater than outside this interval; this is suggestive of resonant production in this channel. This increase in the resonant to background ratio also takes place for the $Y_0^*(1405)$ in the interval 1660 MeV $\leq E_{KN} \leq$ 1720 MeV. Thus there is the possibility that we are observing the decay of two isospin one resonances, one into $Y_0^*(1520)\ \pi^-$ and the other into $Y_0^*(1405)\ \pi^-$.

1. $\underline{Y_0^*(1520)\ \pi^-}$ Events

The above reasoning led us to determine the cross section for not only $K^- n \rightarrow \Sigma^- \pi^+ \pi^-$ but also for the reaction $K^- n \rightarrow Y_0^*(1520)\ \pi^-$. The criteria for production of a $Y_0^*(1520)$ was that the invariant mass of the $\Sigma^- \pi^+$ system be in the interval from 1495 MeV to 1545 MeV; the qualitative features of the cross sections do not depend on the exact choice of the resonance's width. The cross sections for the two reactions of interest are shown in Fig. 13a as a function of K^- beam momentum and in Fig. 13b as a function of K^- n c.m. energy. Also shown in Fig. 13b is the non-$Y_0^*(1520)$ cross section. The peaking near 1760 MeV in the $Y_0^*(1520)$ cross section is evident and we attributed this enhancement to the production of an isospin one resonance. The non-$Y_0^*(1520)\ \pi^-$ cross section is rather flat except at the high energy end where it is rising. This effect may be due to one or more of the higher isospin resonances recently reported.[15]

We assumed that the resonant cross section to be of the Breit-Wigner form

(a)



MUB-11592

Fig. 13a

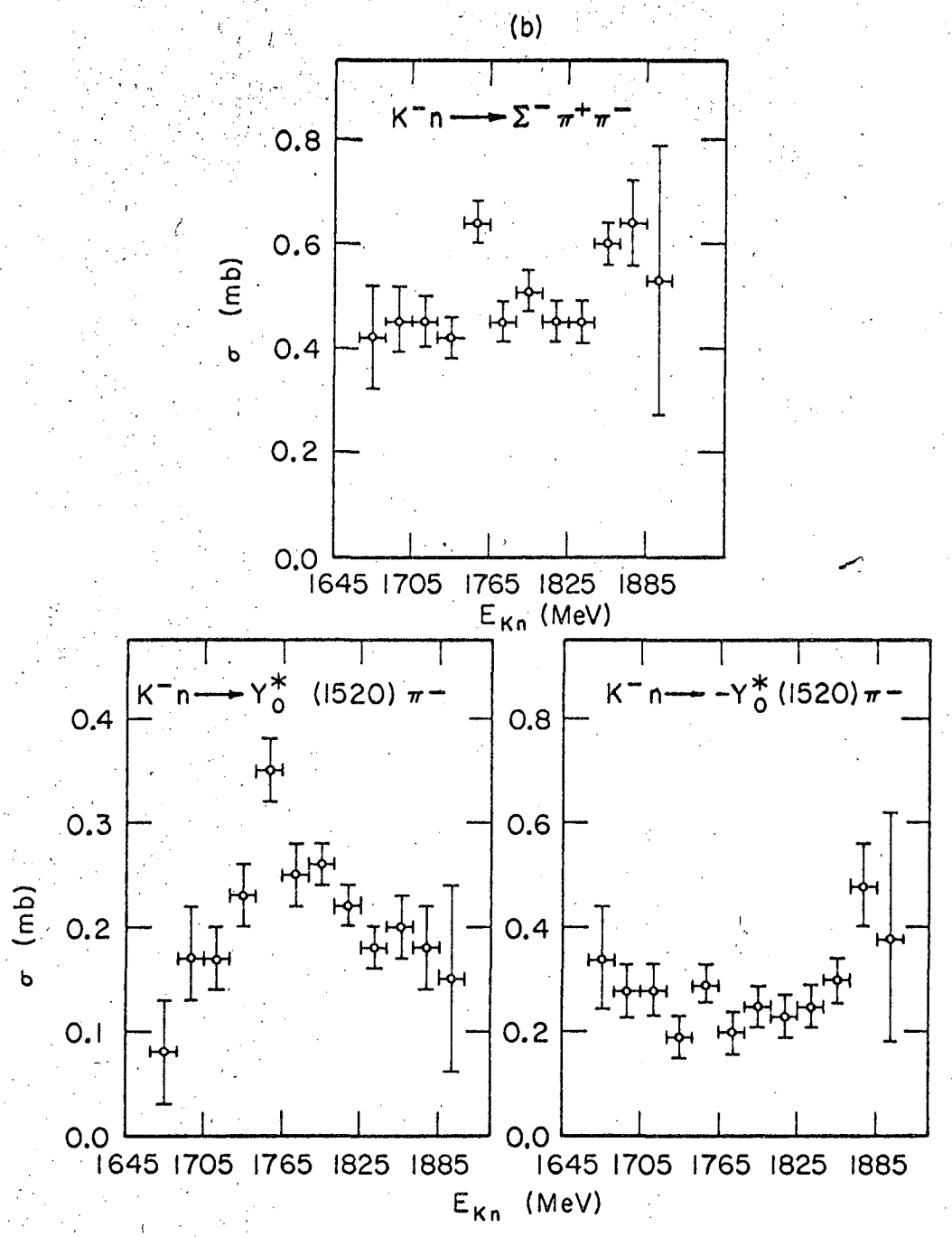

(b)
$K^- n \rightarrow \Sigma^- \pi^+ \pi^-$
$K^- n \rightarrow Y_0^*(1520)\pi^-$
$K^- n \rightarrow -Y_0^*(1520)\pi^-$
σ (mb)
E_{Kn} (MeV)
1645 1705 1765 1825 1885
0.0 0.1 0.2 0.3 0.4 0.6 0.8
MUB 11594

Fig. 13b

$$\sigma = \frac{(2J + 1)}{(2j_1 + 1)(2j_2 + 1)} \cdot \frac{\omega_0^2 \Gamma_e \Gamma_r}{(\omega_0^2 - \omega^2)^2 + \omega_0^2 \Gamma^2}$$

where: J is the spin of the parent resonance;

j_1 and j_2 are the decay products' spin (3/2 for the $Y_0^*(1520)$ and 0 for the pion);

ω_0 is the mass of the resonance;

Γ_e and Γ_r are the partial widths of the elastic and reaction channels, respectively;

Γ is the total width.[16]

As is shown in the next section, the $Y_1^*(1760)$ does not decay by an S wave orbital angular momentum state; thus both the partial and total widths are not constant but have an angular momentum dependence. We assumed the following form for the partial widths:

$$\frac{\Gamma(\omega)}{\Gamma(\omega_0)} = \left(\frac{\omega_0}{\omega}\right) \cdot \left(\frac{q}{q_0}\right)^{2L+1} \cdot \left(\frac{X + q_0^2}{X + q^2}\right)^L$$

where: $\Gamma(\omega_0)$ is the width at the central mass value ω_0;

ω is the mass;

q is the $Y_0^*(1520)$ momentum in the $Y_1^*(1760)$ rest frame;

L is the decay orbital angular momentum.[16]

The empirical SU_3 prediction for X is 350 MeV/c.[17] The partial widths do not depend strongly on the particular value of X taken.

As we shall show in the next section, the most probable value of L for the decay $Y_1^*(1760) \rightarrow Y_0^*(1520)\ \pi^-$ is one; conservation of spin and parity then predicts that a decay into any other final state will proceed with L = 2. There are several problems connected with fitting the resonance curve to our data:

(1) It is necessary to know the branching ratio of the $Y_1^*(1760)$ into

every channel. These ratios are not accurately known at this time. The best available values are an elasticity of 0.5 and a branching ratio into $Y_0^*(1520)$ of 0.15; it was assumed that the remaining 25% of the decays are divided evenly into the other possible final states. It was found that the values of the $Y_1^*(1760)$ mass and width do not depend strongly on the exact choice of the branching ratios.

(2) We have seen that there is a considerable amount of background under the $Y_0^*(1520)$ peak. It was found that the percentage of background is approximately the same above and below the interval $1720 \leq E_{KN} \leq 1800$ MeV; therefore it was assumed that the background rises rapidly from threshold at 1660 MeV and remains constant throughout the remaining energy range. The exact amount of this non-resonant background was allowed to vary in the fitting procedure; the best fit was obtained with a background value of 0.07 mb.

(3) Some of the $Y_0^*(1520)\ \pi^-$ events may not result from the decay of the $Y_1^*(1760)$. It was possible to fit the production cross section with a Breit-Wigner after removing the background mentioned in (2). Thus, it appears that almost all of the $Y_0^*(1520)$ do result from the decay of the $Y_1^*(1760)$.

Of course, the cross section curves implicitly contain all the unknown information mentioned above, but poor statistics would prevent a determination of a large number of parameters.

The fit was accomplished by allowing the values of the resonant mass and width and background to vary until chi-squared was minimized. The best values obtained for the resonant parameters were

$$M = 1760 \pm 5 \text{ MeV}$$

$$\Gamma = 70 \pm 20 \text{ MeV}.$$

As mentioned above, these parameters do not depend strongly on the choice of the branching ratios. It turned out that the resonance mass is also insensitive to the choice of the amount of background; however the width does change rapidly with changing amounts of background. Because the mass is so well determined, we have assumed that the width does not depend on the mass and have quoted the errors assuming no correlations between the resonant parameters rather than attempting to calculate an error matrix.

The decay of the $Y_1^*(1760)$ into the final state $Y_0^*(1520)\,\pi^-$ is a fortunate circumstance from the point of view of the determination of the parent resonance's quantum numbers. This final state contains a particle of spin 3/2 and a particle of spin zero. This system does not display the ambiguities associated with a final state composed of a spin 1/2 particle and spin zero particle; angular distributions alone will be seen to be sufficient to uniquely characterize a particular state of spin and parity of the $Y_1^*(1760)$.[18] This is very important in our reaction because the Σ^- is known to have a very small decay asymmetry parameter which precludes the possibility of measuring any polarizations. Too, the decay orbital angular momentum is expected to be lower for a 3/2 - 0 system than for a 1/2 - 0 system; this leads to simpler angular distributions.

We shall be concerned with two types of angular distributions, namely the production angular distribution of the $Y_0^*(1520)$ in the K^- n c.m. and the decay distribution of the sigma from the $Y_0^*(1520)$ in that resonance's rest frame. For a given choice of the $Y_1^*(1760)$ spin and parity, both of these distributions can be determined. If the direction of the incident K^- meson is used as the axis of quantization,

then no matter what spin the $Y_1^*(1760)$, it is allowed to have two projections along this axis, $m_j = \pm 1/2$. These are just the original spin projections of the target neutron. Since the decay process $Y_1^*(1760) \rightarrow Y_0^*(1520)\ \pi^-$ is strong and parity conserving, both of these states must give the same $Y_0^*(1520)\ \pi^-$ final state; this is because the $m_j = \pm 1/2$ states are related by a parity inversion. For a given $Y_1^*(1760)$ spin, conservation of angular momentum limits the decay orbital angular momentum to four possibilities; further, if a choice of parity is made, then only two of these states, L and L+2, are allowed. For example, if the $Y_1^*(1760)$ has spin 5/2 then L can be 1, 2, 3, or 4; if the parity is assumed to be negative, L must then be either 1 or 3. At the low Q values in this experiment, about 100 MeV, it is natural to assume that the lower of the two angular momentum states predominates. Simple centrifugal barrier considerations favor the P wave decay by a factor of 10^4 over the F wave state. (The possibility that both states do indeed enter into the decay has been considered recently.[19])

Assuming that only the lower of the two possible L values is present and that there are no non-resonant backgrounds, the initial state of the $Y_1^*(1760)$ can be composed in terms of the final state of the $Y_0^*(1520)\ \pi^-$ in the following manner:

$$|J^P,\ 1/2> = a_3\ |3/2,\ 3/2>\ Y_L^{-1} + a_1\ |3/2\ 1/2>\ Y_L^0 + a_{-1}\ |3/2,$$
$$-1/2>\ Y_L^1 + a_{-3}\ |3/2,\ -3/2>\ Y_L^2$$

where $|3/2,\ m_J>$ is the $Y_0^*(1520)$ spinor with $m_j = \pm 1/2, \pm 3/2$; Y_L^M is the spherical harmonic describing the relative orbital angular momentum, and a_j is the appropriate Clebsch-Gordon coefficient. Then the $Y_0^*(1520)$ production angular distribution with respect to the beam direction is simply

$$\frac{d\sigma}{d\Omega} = |a_3 Y_L^{-1}|^2 + |a_1 Y_L^0|^2 + |a_{-1} Y_L^1|^2 + |a_{-3} Y_L^2|^2 .$$

The decay angular distribution of the sigma in the $Y_0^*(1520)$ c.m. can now be calculated with the aid of the expression for the production distribution. The $Y_0^*(1520)$ has four possible spin projections along any quantization axes, $m_j = \pm 3/2, \pm 1/2$. Since the decay is strong and parity conserving, the m_j and $-m_j$ states must give the same decay distribution in the $Y_0^*(1520)$ rest frame. As is discussed more fully in the Appendix, decay from the $m_j = 3/2$ state must yield a distribution of the form $1 - P_2(\cos \Phi)$ where $P_2(\cos \Phi)$ is the second order Legendre polynomial in $\cos \Phi$ and $\cos \Phi = \frac{\vec{P}_\Sigma \cdot n}{P_\Sigma}$; n is a unit vector along the quantization axis and P_Σ is the sigma momentum in the $Y_0^*(1520)$ c.m.; from the $m_j = 1/2$ state the distribution is of the form $1 + P_2(\cos \Phi)$. If the $Y_0^*(1520)$ results from the decay of the $Y_1^*(1760)$, then the relative populations of the $m_j = \pm 3/2$ and $\pm 1/2$ states are known. Using the correct weighting factors and integrating over all $Y_0^*(1520)$ production angles, the angular distribution of the sigma with respect to any quantization axes can be determined for any spin and parity choice for the $Y_1^*(1760)$. The natural axes to use for the quantization are the beam direction and production normal defined as $n = \frac{\vec{P}_K \times Y_0^*(1520)}{|\vec{P}_K \times Y_0^*(1520)|}$. As would be expected, the sigma distribution is of the form $1 + AP_2(\cos \Phi)$ where A is a constant that depends on the $Y_1^*(1760)$ spin and parity and on the particular quantization axis chosen. A complete table of A values is found in the Appendix (together with expansion coefficients for the production angular distributions). It can be shown that the normal gives the most distinct distributions for different spin and parity choices.[20]

We now turn to a comparison of the experimental distributions with the various theoretical predictions. The production angular distributions for the $Y_0^*(1520)$ for various energy intervals throughout the available K^- n c.m. energy region are shown in Fig. 14. As before, the criterion used to determine the production of a $Y_0^*(1520)$ was that the invariant mass of the $\Sigma^- \pi^+$ system be in the range from 1495 MeV to 1545 MeV; the qualitative features of the angular distributions are insensitive to this choice for the resonance's width. The expected distributions for $5/2^+$ and $5/2^-$ are indicated on the histogram of Fig. 14 which represents events in the K^- n energy range from 1740 MeV to 1780 MeV. A Legendre polynomial expansion was fitted to the experimental distributions; the expansion coefficients are plotted in Fig. 15 and tabulated in Table III. In general, expansion to second order is sufficient to fit the data; the small systematically positive A_3 term does not increase the goodness of fit. Coefficients above third order are essentially zero except for the first fifth order coefficient which is due entirely to the small number of events in the experimental distribution in that energy interval. In particular, the A_4 is seen to be zero throughout the entire energy range. The behavior of the A_1 term is particularly interesting as it is seen to change sign as we pass through the resonant energy; this is suggestive of an interference of a resonant amplitude with a background as the resonant phase shift passes through 90 (or 0) degrees. We shall return to this point later.

Next we turn to the decay distributions of the sigma; the experimental data are shown in Fig. 16 with both the beam direction and production normal used as quantization axes for events with 1740 MeV $\leq K^- n \leq$ 1780 MeV and 1495 MeV $\leq M(\Sigma^- \pi^+) \leq$ 1545 MeV. Also shown are the $5/2^+$ and

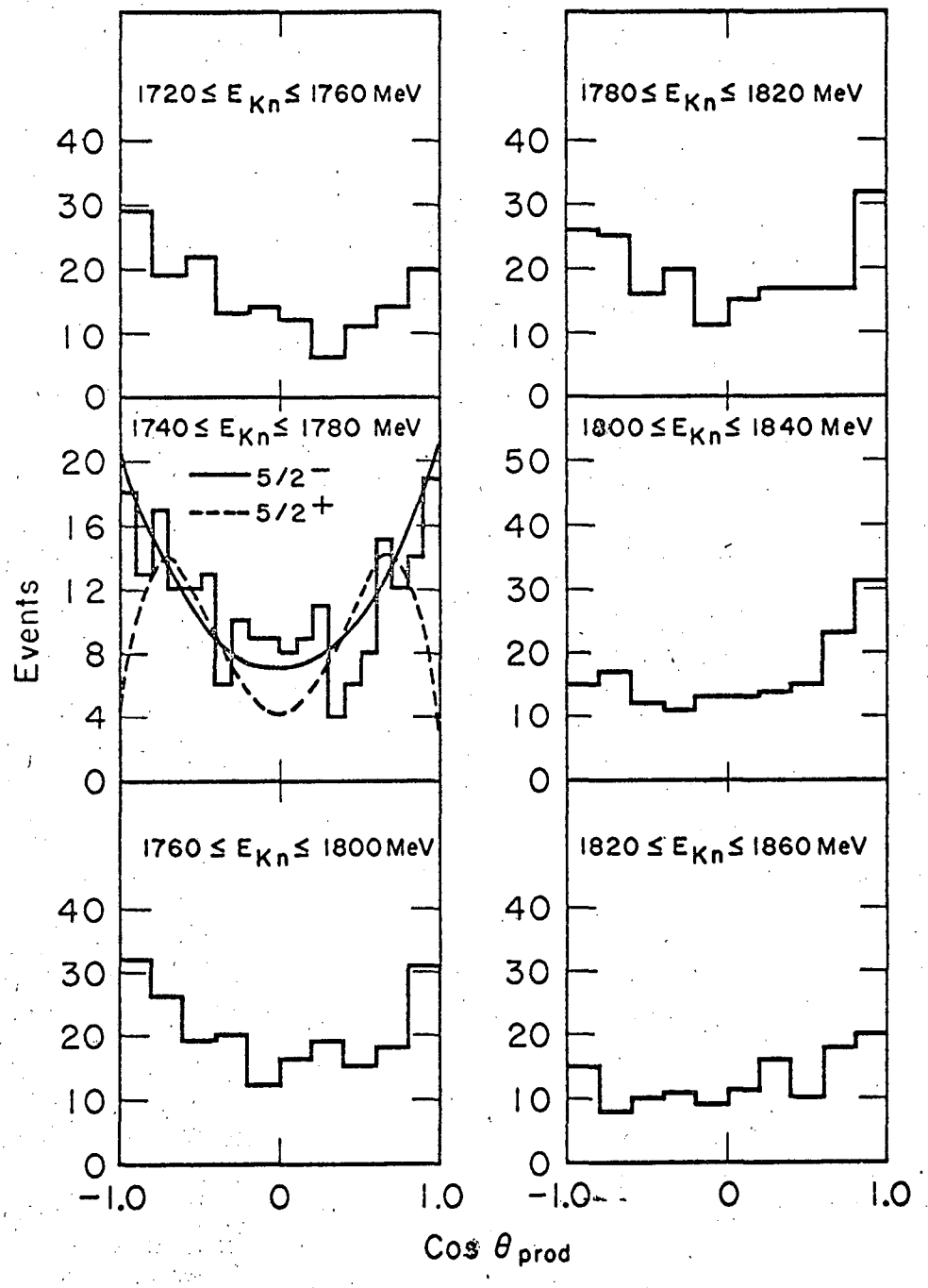
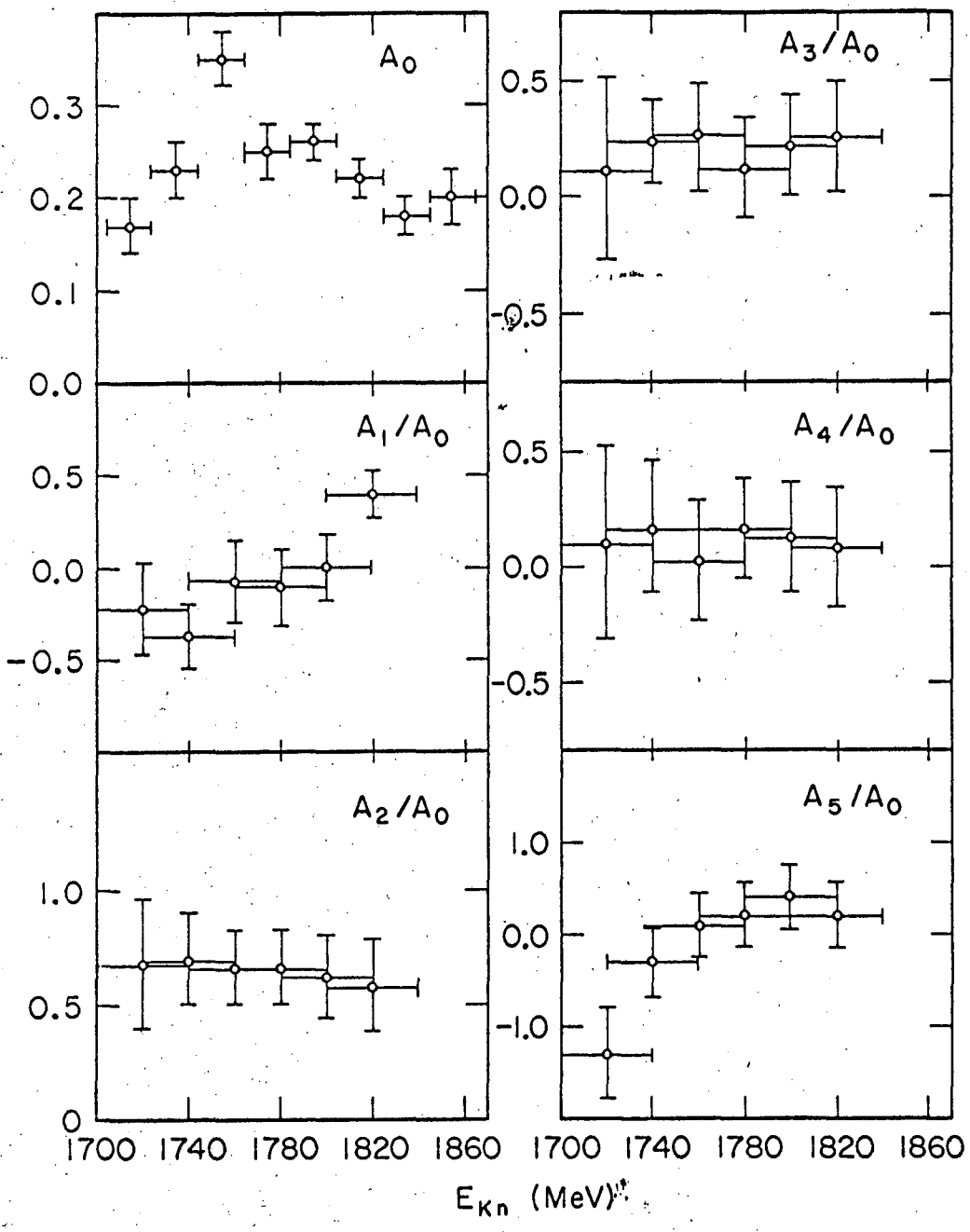

1720 ≤ E Kn ≤ 1760 MeV
1740 ≤ E Kn ≤ 1780 MeV
1760 ≤ E Kn ≤ 1800 MeV
1780 ≤ E Kn ≤ 1820 MeV
1800 ≤ E Kn ≤ 1840 MeV
1820 ≤ E Kn ≤ 1860 MeV
5/2−
5/2+
Events
Cos θ prod
MUB 11588

Fig. 14

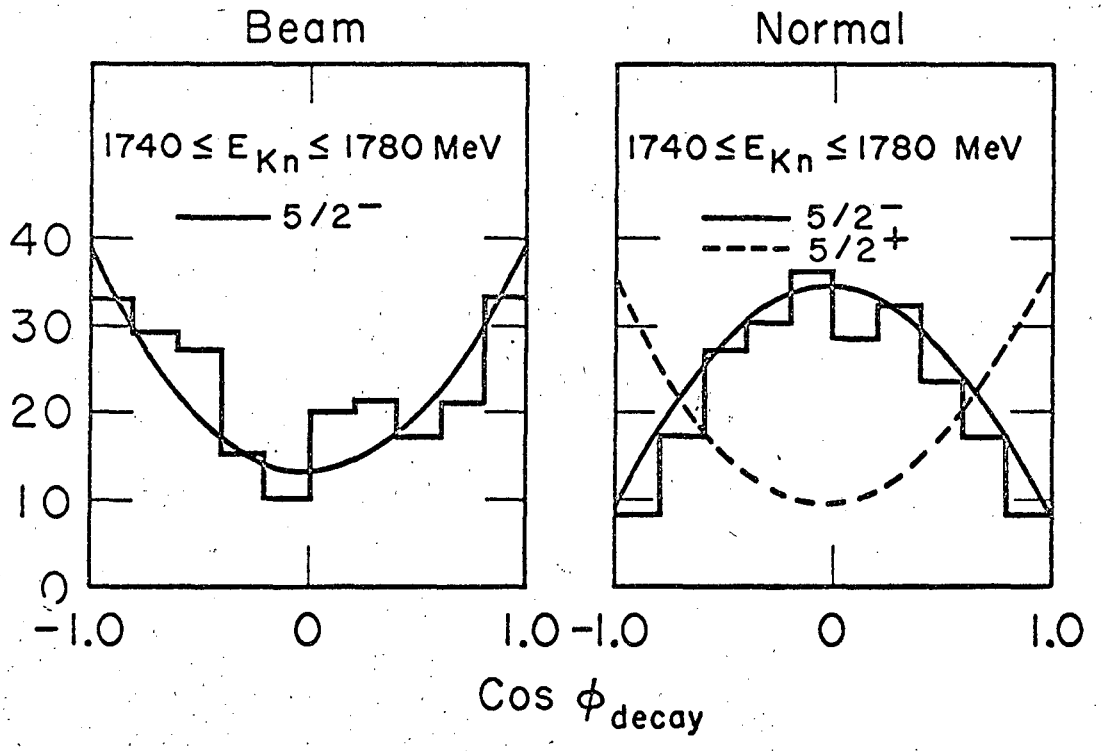
Table III. Legendre polynomial expansion coefficients for a fit to the experimental $Y_0^*(1520)$ production angular distribution for the K^- n c.m. energy intervals indicated.

K^- n c.m. energy	A_0	A_1	A_2	A_3	A_4	A_5
1700 to 1740 MeV	1.0	-0.22 ± 0.24	0.66 ± 0.32	0.11 ± 0.40	0.10 ± 0.42	-1.26 ± 0.51
1720 to 1760 MeV	1.0	-0.37 ± 0.16	0.70 ± 0.20	0.15 ± 0.26	0.17 ± 0.29	-0.31 ± 0.34
1740 to 1780 MeV	1.0	-0.08 ± 0.13	0.69 ± 0.16	0.26 ± 0.21	0.02 ± 0.24	0.09 ± 0.31
1760 to 1800 MeV	1.0	-0.10 ± 0.14	0.65 ± 0.18	0.12 ± 0.22	0.15 ± 0.24	0.28 ± 0.32
1780 to 1820 MeV	1.0	-0.01 ± 0.14	0.63 ± 0.18	0.21 ± 0.23	0.12 ± 0.25	0.41 ± 0.33
1800 to 1840 MeV	1.0	0.40 ± 0.15	0.59 ± 0.20	0.26 ± 0.24	0.09 ± 0.28	0.19 ± 0.36
1820 to 1860 MeV	1.0	0.26 ± 0.16	0.50 ± 0.22	0.06 ± 0.26	0.47 ± 0.30	-0.16 ± 0.38



MUB 11598

Fig. 15



MUB 11586

Fig. 16

$5/2^-$ theoretical curves. Legendre polynomial expansion coefficients are given in Table IV.

Table V contains the theoretical predictions for the decay of the $Y_1^*(1760)$ for spin up to 7/2, together with the probability that the experimental distribution fits the particular spin and parity assignment. As can be seen, the production and decay distributions rule out spin 1/2 and 3/2 and spin 5/2 with positive parity. The $7/2^-$ state is allowed by the production distribution but rejected by the decay prediction. What remains are two possibilities, namely $5/2^-$ and $7/2^+$, the former having a probability of 65% and the latter having a probability of 9%. While the $5/2^-$ is clearly preferred, there is, at first thought, a significant probability that $7/2^+$ is the correct assignment.

We shall show that even though the $7/2^+$ theoretical distribution yields a probability of 9% for fitting the data, the $5/2^-$ is an overwhelmingly better choice. An examination of Fig. 17a, which shows the $7/2^+$ and $5/2^-$ distributions, reveals that in the center of the angular distribution, from $-0.4 \leq \cos\Theta \leq 0.4$, the curves for the two spin-parity choices are almost identical. Since this region is expected to have a smaller number of events than is the case at the ends of the distribution, it is not surprising that our data are incapable of detecting the small difference of the two distributions in this range. However, at the extremes of the histogram, $|\cos\Theta| > 0.4$, the situation is very different; therefore we fitted the $7/2^+$ and $5/2^-$ theoretical distributions to the two regions $|\cos\Theta| > 0.4$ and $|\cos\Theta| \leq 0.4$ separately. The results are given in Table VI. The $5/2^-$ choice gives an adequate fit in all parts of the angular distribution; the $7/2^+$ distribution, on the other hand, fits the center of the histogram

Table IV. Legendre polynomial expansion coefficients for a fit to the experimental $Y_0^*(1520)$ decay distribution for events with 1740 MeV $\leq E_{KN}$ M.V. $\leq$ 1780 MeV.

Coef. \ Axis	Production Normal	Beam Direction
A_0	1.0	1.0
A_1	-0.03 ± 0.09	-0.10 ± 0.13
A_2	-0.91 ± 0.13	0.71 ± 0.16
A_3	0.06 ± 0.17	0.08 ± 0.19
A_4	0.04 ± 0.21	0.10 ± 0.24
A_5	-0.07 ± 0.29	-0.01 ± 0.31

Table V. $Y_0^*(1520)$ production and decay theoretical distributions for various spin and parity choices for the $Y_1^*(1760)$ and the probability of fit for these assignments.

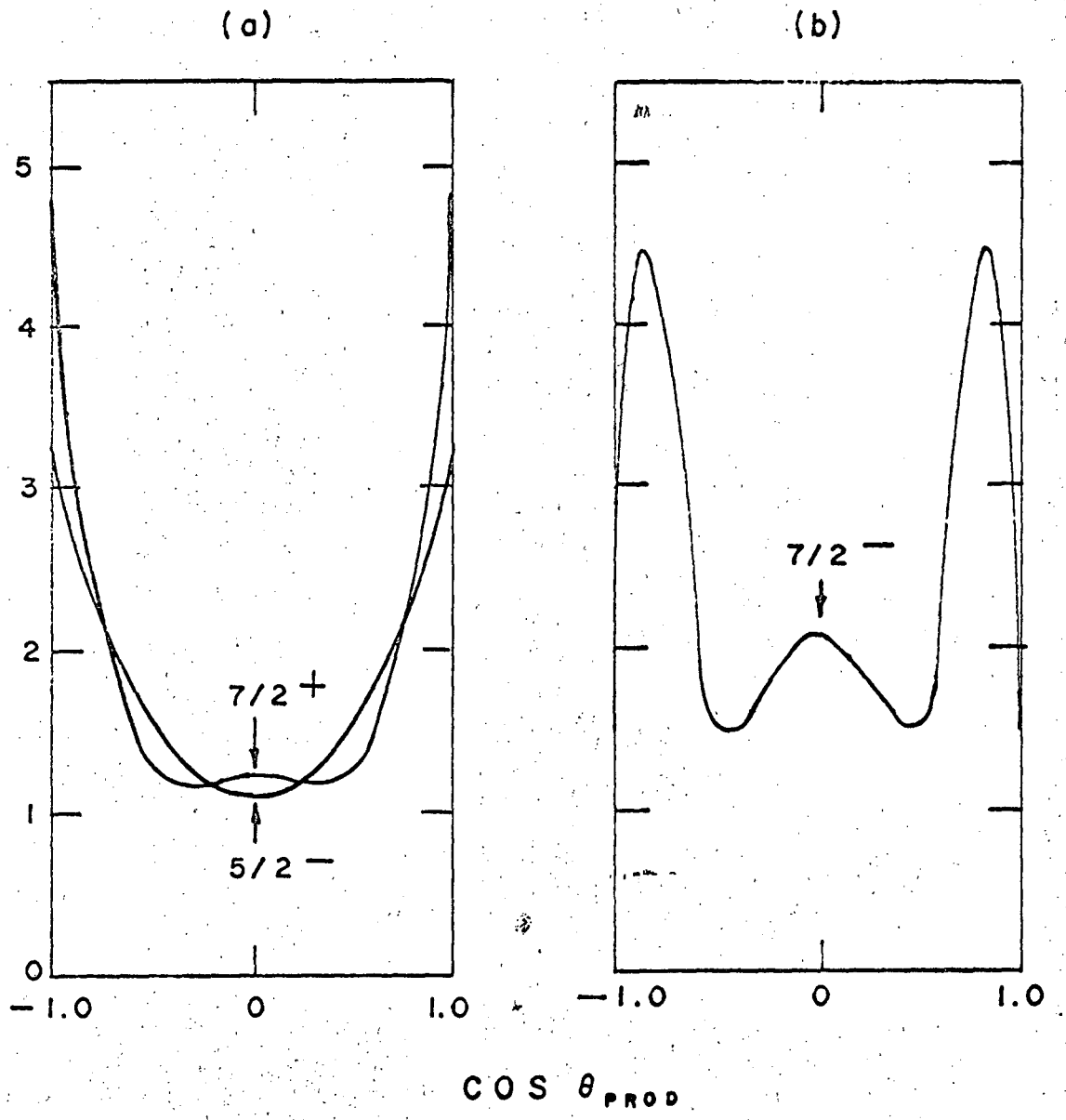
J^PL	$Y_0^*(1520)$ Theoretical Production Angular Distribution	Probability of fit %
$1/2^-P$	1.0	0.8
$1/2^+D$	1.0	0.8
$3/2^-P$	$1.0-0.80\ P_2(\cos\Theta)$	$<<.01$
$3/2^+S$	1.0	0.8
$5/2^-P$	$1.0+0.80\ P_2(\cos\Theta)$	65
$5/2^+D$	$1.0+0.41\ P_2(\cos\Theta)-0.98\ P_4(\cos\Theta)$	0.5
$7/2^-F$	$1.0+6.2\ P_2(\cos\Theta)-0.23\ P_4(\cos\Theta)-1.16\ P_6(\cos\Theta)$	43
$7/2^+D$	$1.0+1.02\ P_2(\cos\Theta)+0.55\ P_4(\cos\Theta)$	9

J^PL	$Y_0^*(1520)$ Theoretical Decay Distribution w.r.t. Production Normal	Probability of fit %
$1/2^-P$	$1.0-0.5\ P_2(\cos\Phi)$	21
$1/2^+D$	$1.0-0.5\ P_2(\cos\Phi)$	21
$3/2^-P$	$1.0+0.7\ P_2(\cos\Phi)$	$<<.01$
$3/2^+S$	$1.0-0.5\ P_2(\cos\Phi)$	21
$5/2^-P$	$1.0-0.7\ P_2(\cos\Phi)$	83
$5/2^+D$	$1.0+0.79\ P_2(\cos\Phi)$	$<<.01$
$7/2^-F$	$1.0+0.83\ P_2(\cos\Phi)$	$<<.01$
$7/2^+D$	$1.0-0.79\ P_2(\cos\Phi)$	95

(Table V, cont.)

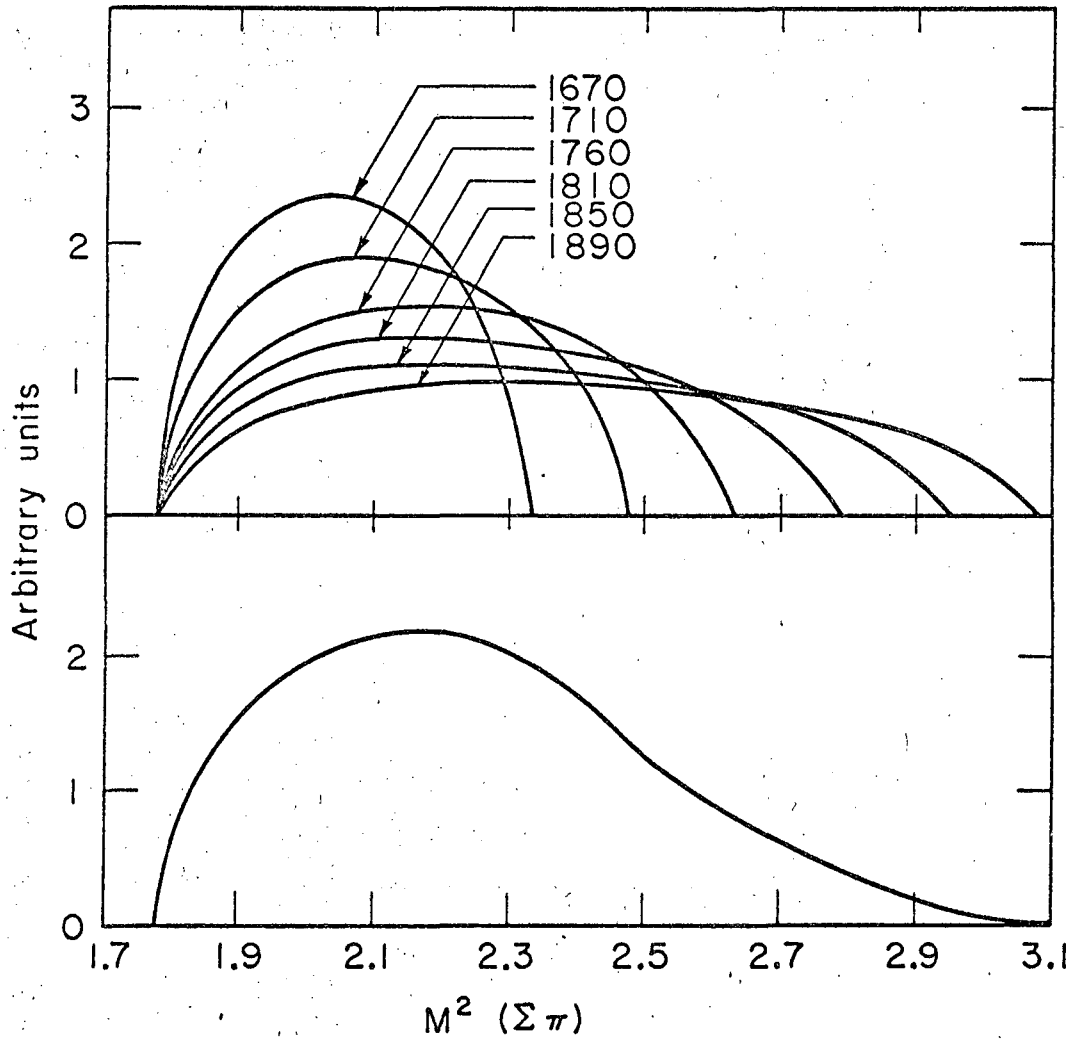
Table V
(cont.)

J^P_L	$Y_0^*(1520)$ Theoretical Decay Distribution w.r.t. Incident K^- Direction	Probability of fit %
$1/2^-P$	1.0	0.5
$1/2^+D$	1.0	0.5
$3/2^-P$	$1.0+0.2\ P_2(\cos\Theta)$	5
$3/2^+S$	$1.0+P_2(\cos\Theta)$	4
$5/2^-P$	$1.0+0.8\ P_2(\cos\Theta)$	24
$5/2^+D$	$1.0-0.14\ P_2(\cos\Theta)$	2
$7/2^-F$	$1.0-0.24\ P_2(\cos\Theta)$	<0.1
$7/2^+D$	$1.0+0.71\ P_2(\cos\Theta)$	34



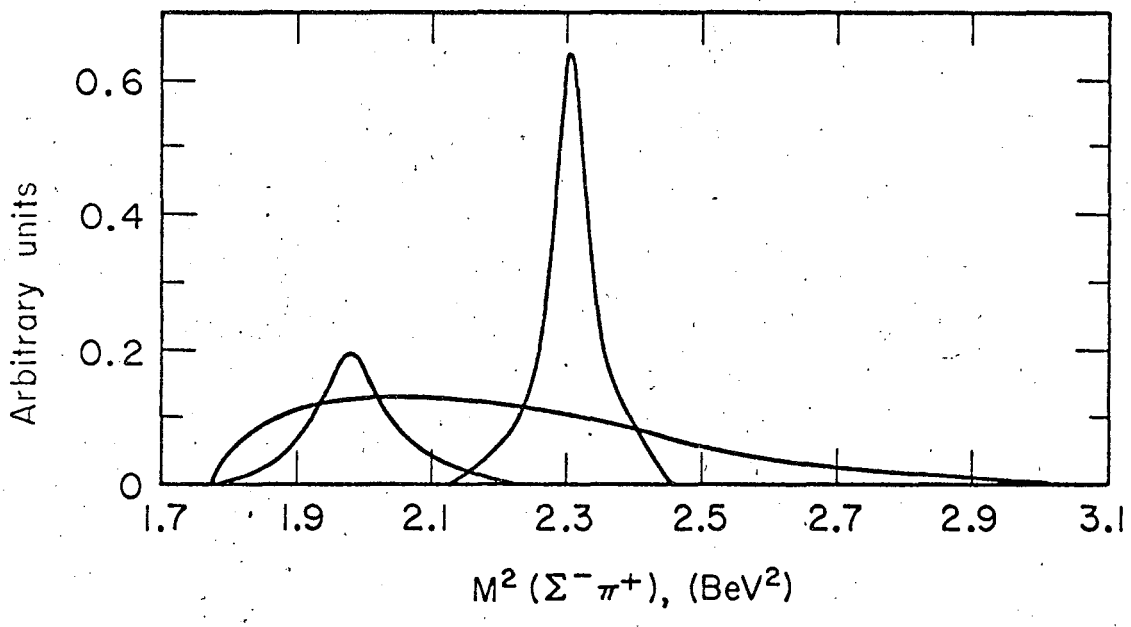
MUB-12010

Fig. 17



MUB-11585

Fig. 11



MUB-11593

Fig. 12

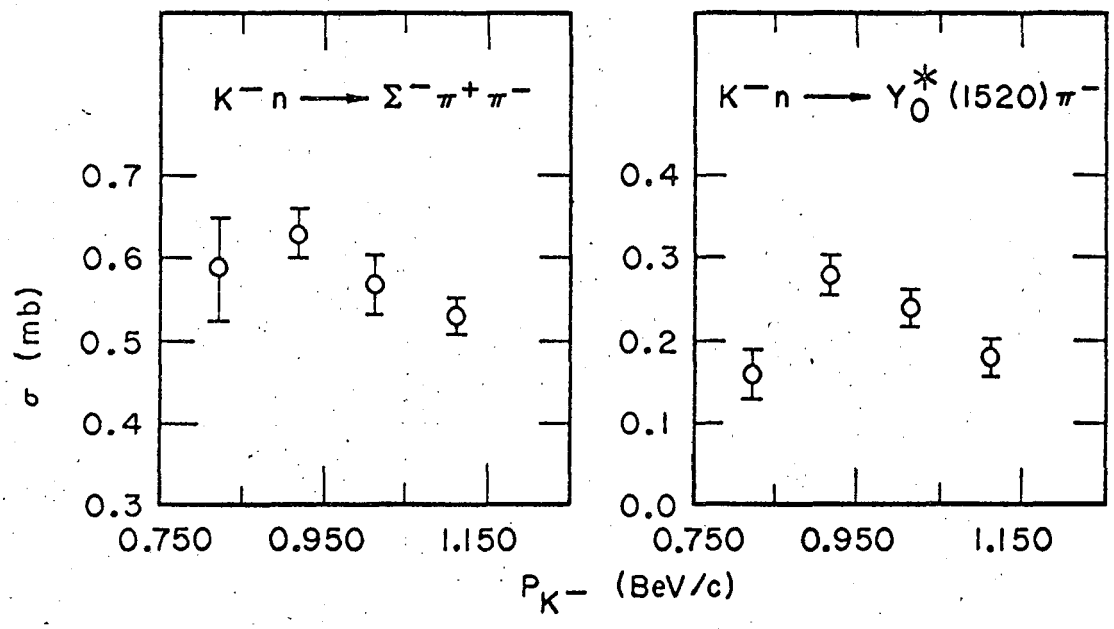
c.m. energy. The above fitting procedure was repeated for various energy intervals. It was found that in the range 1720 MeV $\leq E_{KN} \leq$ 1800 MeV the $Y_0^*(1520)$ to background ratio is slightly greater than outside this interval; this is suggestive of resonant production in this channel. This increase in the resonant to background ratio also takes place for the $Y_0^*(1405)$ in the interval 1660 MeV $\leq E_{KN} \leq$ 1720 MeV. Thus there is the possibility that we are observing the decay of two isospin one resonances, one into $Y_0^*(1520)\ \pi^-$ and the other into $Y_0^*(1405)\ \pi^-$.

1. $\underline{Y_0^*(1520)\ \pi^-}$ Events

The above reasoning led us to determine the cross section for not only $K^- n \rightarrow \Sigma^- \pi^+ \pi^-$ but also for the reaction $K^- n \rightarrow Y_0^*(1520)\ \pi^-$. The criteria for production of a $Y_0^*(1520)$ was that the invariant mass of the $\Sigma^- \pi^+$ system be in the interval from 1495 MeV to 1545 MeV; the qualitative features of the cross sections do not depend on the exact choice of the resonance's width. The cross sections for the two reactions of interest are shown in Fig. 13a as a function of K^- beam momentum and in Fig. 13b as a function of K^- n c.m. energy. Also shown in Fig. 13b is the non-$Y_0^*(1520)$ cross section. The peaking near 1760 MeV in the $Y_0^*(1520)$ cross section is evident and we attributed this enhancement to the production of an isospin one resonance. The non-$Y_0^*(1520)\ \pi^-$ cross section is rather flat except at the high energy end where it is rising. This effect may be due to one or more of the higher isospin resonances recently reported.[15]

We assumed that the resonant cross section to be of the Breit-Wigner form

(a)



MUB-11592

Fig. 13a

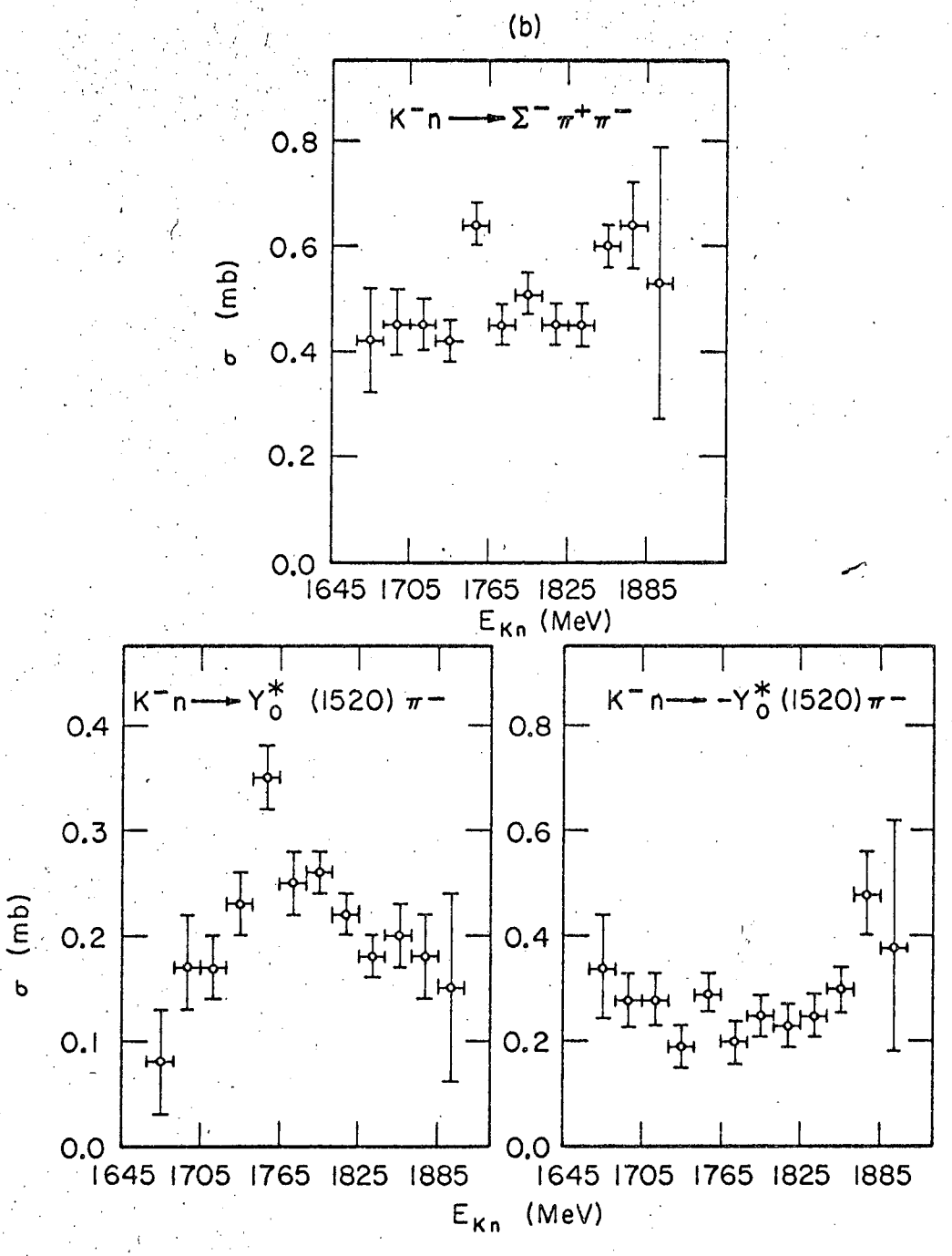

(b)
$K^- n \rightarrow \Sigma^- \pi^+ \pi^-$
$K^- n \rightarrow Y_0^*(1520)\pi^-$
$K^- n \rightarrow -Y_0^*(1520)\pi^-$
σ (mb)
E_{Kn} (MeV)
1645 1705 1765 1825 1885
0.0 0.2 0.4 0.6 0.8
0.0 0.1 0.2 0.3 0.4
MUB 11594

Fig. 13b

$$\sigma = \frac{(2J + 1)}{(2j_1 + 1)(2j_2 + 1)} \cdot \frac{\omega_0^2 \Gamma_e \Gamma_r}{(\omega_0^2 - \omega^2)^2 + \omega_0^2 \Gamma^2}$$

where: J is the spin of the parent resonance;

j_1 and j_2 are the decay products' spin (3/2 for the $Y_0^*(1520)$ and 0 for the pion);

ω_0 is the mass of the resonance;

Γ_e and Γ_r are the partial widths of the elastic and reaction channels, respectively;

Γ is the total width.[16]

As is shown in the next section, the $Y_1^*(1760)$ does not decay by an S wave orbital angular momentum state; thus both the partial and total widths are not constant but have an angular momentum dependence. We assumed the following form for the partial widths:

$$\frac{\Gamma(\omega)}{\Gamma(\omega_0)} = \left(\frac{\omega_0}{\omega}\right) \cdot \left(\frac{q}{q_0}\right)^{2L+1} \cdot \left(\frac{X + q_0^2}{X + q^2}\right)^L$$

where: $\Gamma(\omega_0)$ is the width at the central mass value ω_0;

ω is the mass;

q is the $Y_0^*(1520)$ momentum in the $Y_1^*(1760)$ rest frame;

L is the decay orbital angular momentum.[16]

The empirical SU_3 prediction for X is 350 MeV/c.[17] The partial widths do not depend strongly on the particular value of X taken.

As we shall show in the next section, the most probable value of L for the decay $Y_1^*(1760) \rightarrow Y_0^*(1520)\ \pi^-$ is one; conservation of spin and parity then predicts that a decay into any other final state will proceed with L = 2. There are several problems connected with fitting the resonance curve to our data:

(1) It is necessary to know the branching ratio of the $Y_1^*(1760)$ into

every channel. These ratios are not accurately known at this time. The best available values are an elasticity of 0.5 and a branching ratio into $Y_0^*(1520)$ of 0.15; it was assumed that the remaining 25% of the decays are divided evenly into the other possible final states. It was found that the values of the $Y_1^*(1760)$ mass and width do not depend strongly on the exact choice of the branching ratios.

(2) We have seen that there is a considerable amount of background under the $Y_0^*(1520)$ peak. It was found that the percentage of background is approximately the same above and below the interval $1720 \leq E_{KN} \leq 1800$ MeV; therefore it was assumed that the background rises rapidly from threshold at 1660 MeV and remains constant throughout the remaining energy range. The exact amount of this non-resonant background was allowed to vary in the fitting procedure; the best fit was obtained with a background value of 0.07 mb.

(3) Some of the $Y_0^*(1520)\ \pi^-$ events may not result from the decay of the $Y_1^*(1760)$. It was possible to fit the production cross section with a Breit-Wigner after removing the background mentioned in (2). Thus, it appears that almost all of the $Y_0^*(1520)$ do result from the decay of the $Y_1^*(1760)$.

Of course, the cross section curves implicitly contain all the unknown information mentioned above, but poor statistics would prevent a determination of a large number of parameters.

The fit was accomplished by allowing the values of the resonant mass and width and background to vary until chi-squared was minimized. The best values obtained for the resonant parameters were

$$M = 1760 \pm 5 \text{ MeV}$$

$$\Gamma = 70 \pm 20 \text{ MeV}.$$

As mentioned above, these parameters do not depend strongly on the choice of the branching ratios. It turned out that the resonance mass is also insensitive to the choice of the amount of background; however the width does change rapidly with changing amounts of background. Because the mass is so well determined, we have assumed that the width does not depend on the mass and have quoted the errors assuming no correlations between the resonant parameters rather than attempting to calculate an error matrix.

The decay of the $Y_1^*(1760)$ into the final state $Y_0^*(1520)\ \pi^-$ is a fortunate circumstance from the point of view of the determination of the parent resonance's quantum numbers. This final state contains a particle of spin 3/2 and a particle of spin zero. This system does not display the ambiguities associated with a final state composed of a spin 1/2 particle and spin zero particle; angular distributions alone will be seen to be sufficient to uniquely characterize a particular state of spin and parity of the $Y_1^*(1760)$.[18] This is very important in our reaction because the Σ^- is known to have a very small decay asymmetry parameter which precludes the possibility of measuring any polarizations. Too, the decay orbital angular momentum is expected to be lower for a 3/2 - 0 system than for a 1/2 - 0 system; this leads to simpler angular distributions.

We shall be concerned with two types of angular distributions, namely the production angular distribution of the $Y_0^*(1520)$ in the K^- n c.m. and the decay distribution of the sigma from the $Y_0^*(1520)$ in that resonance's rest frame. For a given choice of the $Y_1^*(1760)$ spin and parity, both of these distributions can be determined. If the direction of the incident K^- meson is used as the axis of quantization,

then no matter what spin the $Y_1^*(1760)$, it is allowed to have two projections along this axis, $m_j = \pm 1/2$. These are just the original spin projections of the target neutron. Since the decay process $Y_1^*(1760) \rightarrow Y_0^*(1520)\,\pi^-$ is strong and parity conserving, both of these states must give the same $Y_0^*(1520)\,\pi^-$ final state; this is because the $m_j = \pm 1/2$ states are related by a parity inversion. For a given $Y_1^*(1760)$ spin, conservation of angular momentum limits the decay orbital angular momentum to four possibilities; further, if a choice of parity is made, then only two of these states, L and L+2, are allowed. For example, if the $Y_1^*(1760)$ has spin 5/2 then L can be 1, 2, 3, or 4; if the parity is assumed to be negative, L must then be either 1 or 3. At the low Q values in this experiment, about 100 MeV, it is natural to assume that the lower of the two angular momentum states predominates. Simple centrifugal barrier considerations favor the P wave decay by a factor of 10^4 over the F wave state. (The possibility that both states do indeed enter into the decay has been considered recently.[19])

Assuming that only the lower of the two possible L values is present and that there are no non-resonant backgrounds, the initial state of the $Y_1^*(1760)$ can be composed in terms of the final state of the $Y_0^*(1520)\,\pi^-$ in the following manner:

$$|J^P,\ 1/2> = a_3\ |3/2,\ 3/2>\ Y_L^{-1} + a_1\ |3/2\ 1/2>\ Y_L^0 + a_{-1}\ |3/2,$$
$$-1/2>\ Y_L^1 + a_{-3}\ |3/2,\ -3/2>\ Y_L^2$$

where $|3/2,\ m_j>$ is the $Y_0^*(1520)$ spinor with $m_j = \pm 1/2, \pm 3/2$; Y_L^M is the spherical harmonic describing the relative orbital angular momentum, and a_j is the appropriate Clebsch-Gordon coefficient. Then the $Y_0^*(1520)$ production angular distribution with respect to the beam direction is simply

$$\frac{d\sigma}{d\Omega} = |a_3 Y_L^{-1}|^2 + |a_1 Y_L^0|^2 + |a_{-1} Y_L^1|^2 + |a_{-3} Y_L^2|^2 .$$

The decay angular distribution of the sigma in the $Y_0^*(1520)$ c.m. can now be calculated with the aid of the expression for the production distribution. The $Y_0^*(1520)$ has four possible spin projections along any quantization axes, $m_j = \pm 3/2, \pm 1/2$. Since the decay is strong and parity conserving, the m_j and $-m_j$ states must give the same decay distribution in the $Y_0^*(1520)$ rest frame. As is discussed more fully in the Appendix, decay from the $m_j = 3/2$ state must yield a distribution of the form $1 - P_2(\cos \Phi)$ where $P_2(\cos \Phi)$ is the second order Legendre polynomial in $\cos \Phi$ and $\cos \Phi = \frac{\vec{P}_\Sigma \cdot n}{P_\Sigma}$; n is a unit vector along the quantization axis and P_Σ is the sigma momentum in the $Y_0^*(1520)$ c.m.; from the $m_j = 1/2$ state the distribution is of the form $1 + P_2(\cos \Phi)$. If the $Y_0^*(1520)$ results from the decay of the $Y_1^*(1760)$, then the relative populations of the $m_j = \pm 3/2$ and $\pm 1/2$ states are known. Using the correct weighting factors and integrating over all $Y_0^*(1520)$ production angles, the angular distribution of the sigma with respect to any quantization axes can be determined for any spin and parity choice for the $Y_1^*(1760)$. The natural axes to use for the quantization are the beam direction and production normal defined as $n = \frac{\vec{P}_K \times Y_0^*(1520)}{|\vec{P}_K \times Y_0^*(1520)|}$. As would be expected, the sigma distribution is of the form $1 + AP_2(\cos \Phi)$ where A is a constant that depends on the $Y_1^*(1760)$ spin and parity and on the particular quantization axis chosen. A complete table of A values is found in the Appendix (together with expansion coefficients for the production angular distributions). It can be shown that the normal gives the most distinct distributions for different spin and parity choices.[20]

We now turn to a comparison of the experimental distributions with the various theoretical predictions. The production angular distributions for the $Y_0^*(1520)$ for various energy intervals throughout the available K^- n c.m. energy region are shown in Fig. 14. As before, the criterion used to determine the production of a $Y_0^*(1520)$ was that the invariant mass of the $\Sigma^- \pi^+$ system be in the range from 1495 MeV to 1545 MeV; the qualitative features of the angular distributions are insensitive to this choice for the resonance's width. The expected distributions for $5/2^+$ and $5/2^-$ are indicated on the histogram of Fig. 14 which represents events in the K^- n energy range from 1740 MeV to 1780 MeV. A Legendre polynomial expansion was fitted to the experimental distributions; the expansion coefficients are plotted in Fig. 15 and tabulated in Table III. In general, expansion to second order is sufficient to fit the data; the small systematically positive A_3 term does not increase the goodness of fit. Coefficients above third order are essentially zero except for the first fifth order coefficient which is due entirely to the small number of events in the experimental distribution in that energy interval. In particular, the A_4 is seen to be zero throughout the entire energy range. The behavior of the A_1 term is particularly interesting as it is seen to change sign as we pass through the resonant energy; this is suggestive of an interference of a resonant amplitude with a background as the resonant phase shift passes through 90 (or 0) degrees. We shall return to this point later.

Next we turn to the decay distributions of the sigma; the experimental data are shown in Fig. 16 with both the beam direction and production normal used as quantization axes for events with 1740 MeV $\leq K^- n \leq$ 1780 MeV and 1495 MeV $\leq M(\Sigma^- \pi^+) \leq$ 1545 MeV. Also shown are the $5/2^+$ and

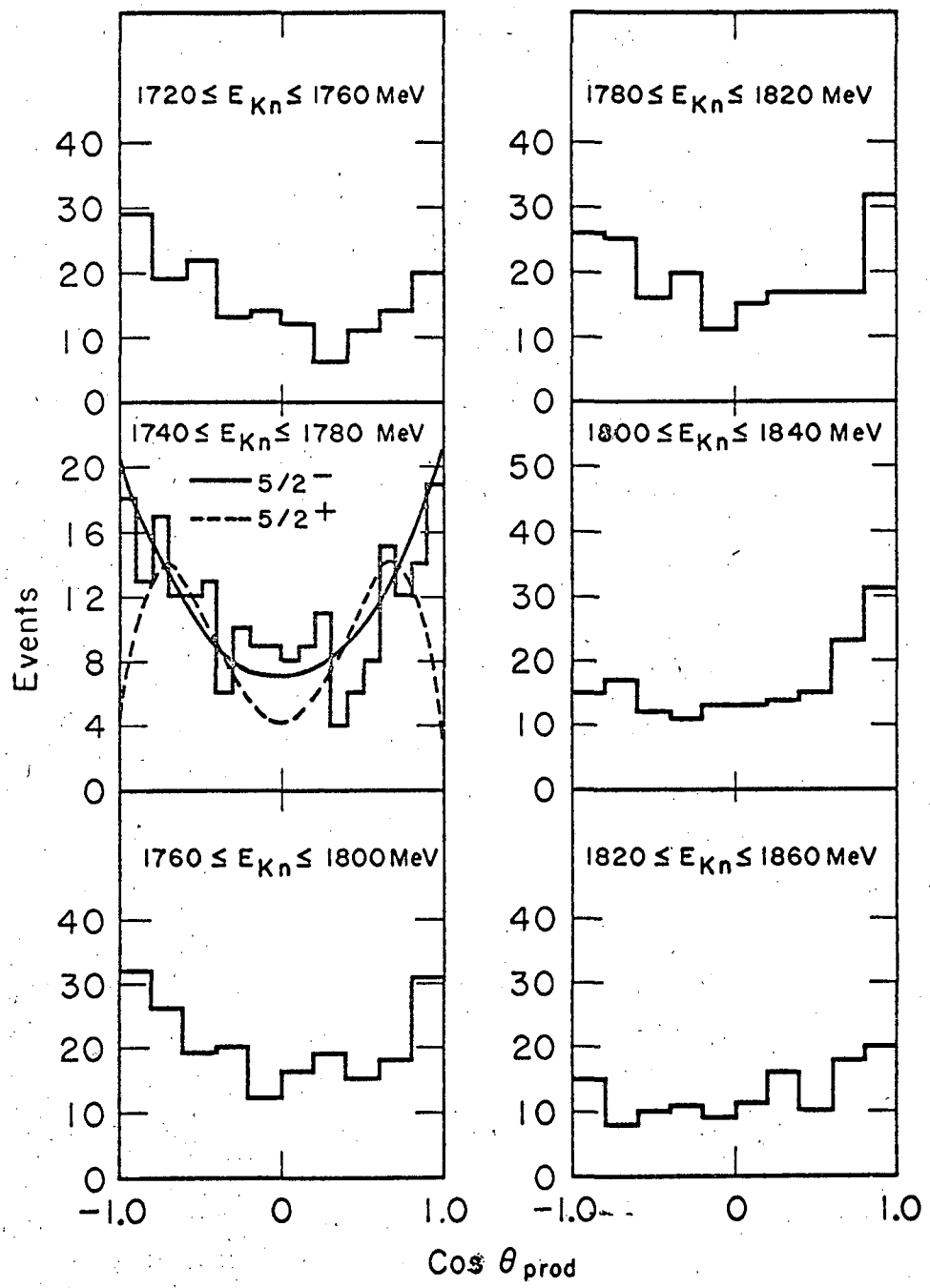
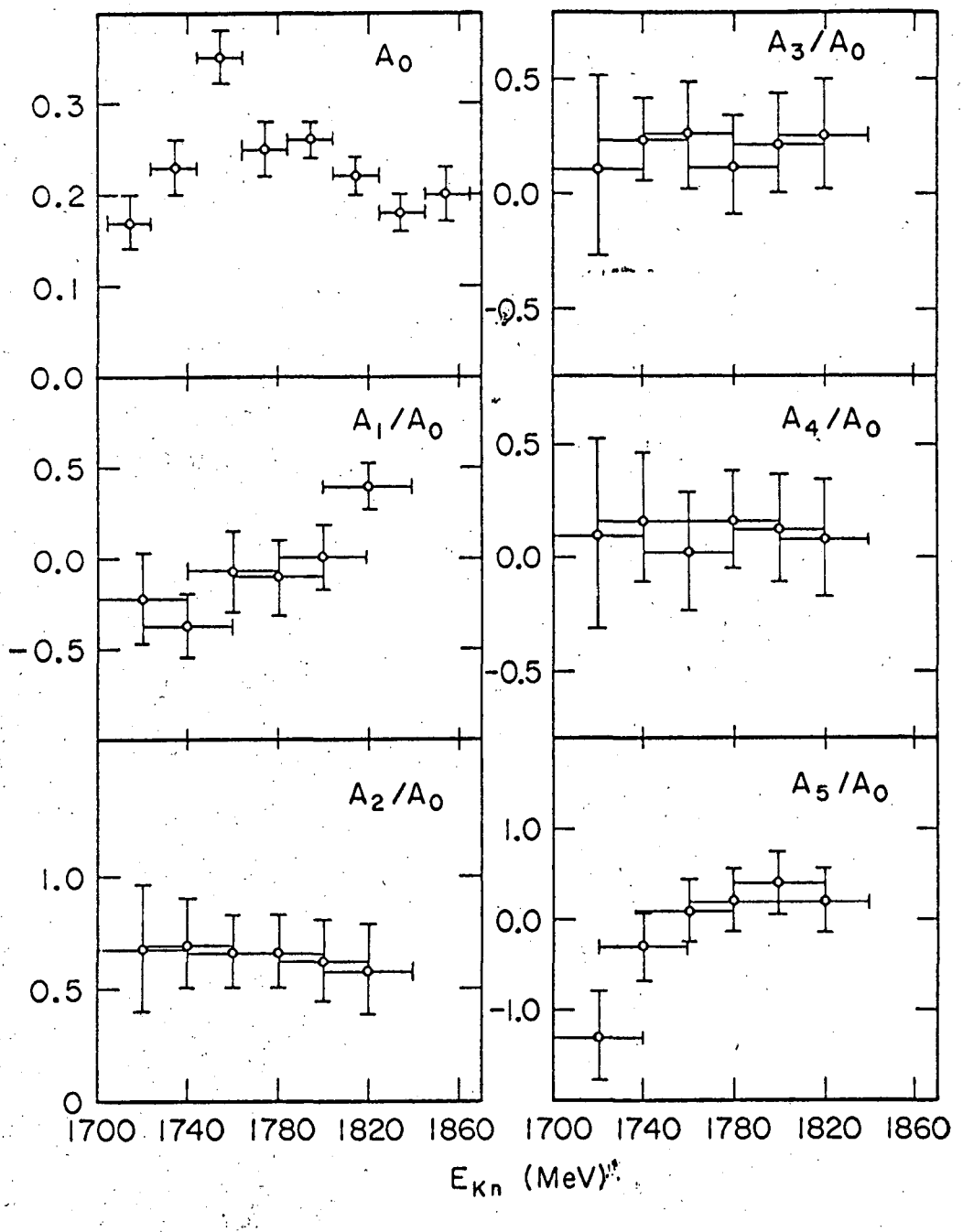

1720 ≤ E Kn ≤ 1760 MeV
1740 ≤ E Kn ≤ 1780 MeV
1760 ≤ E Kn ≤ 1800 MeV
1780 ≤ E Kn ≤ 1820 MeV
1800 ≤ E Kn ≤ 1840 MeV
1820 ≤ E Kn ≤ 1860 MeV
5/2−
5/2+
Events
Cos θ prod
MUB 11588

Fig. 14

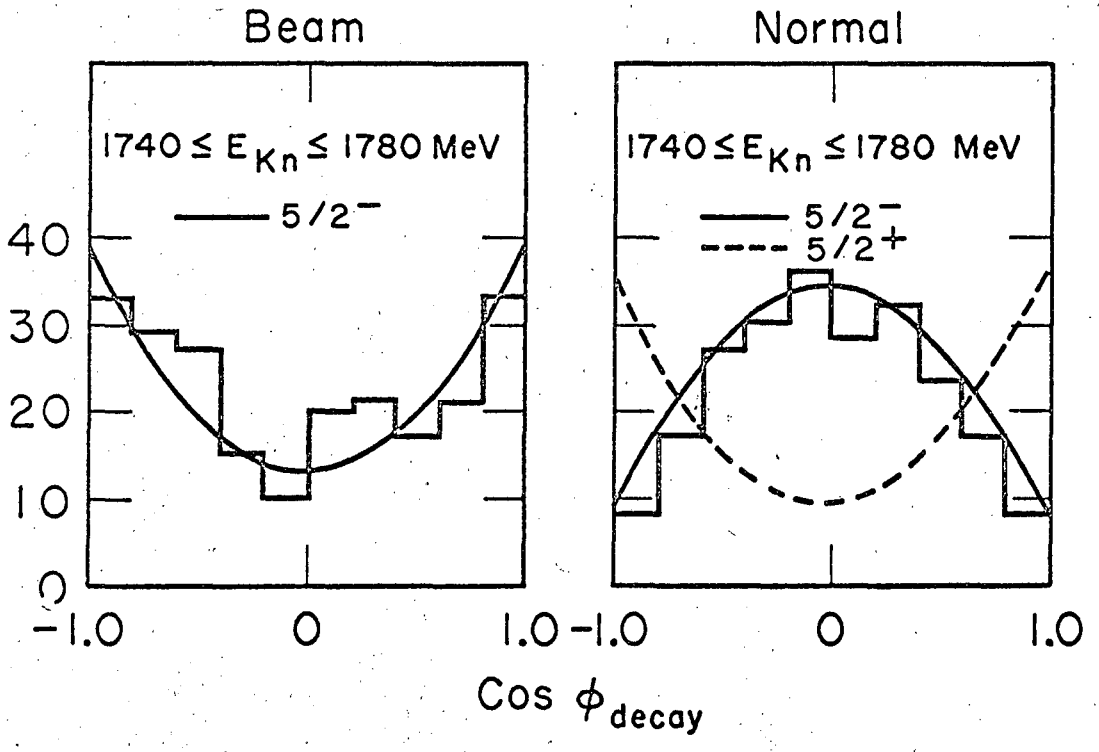
Table III. Legendre polynomial expansion coefficients for a fit to the experimental $Y_0^*(1520)$ production angular distribution for the K^- n c.m. energy intervals indicated.

K^- n c.m. energy	A_0	A_1	A_2	A_3	A_4	A_5
1700 to 1740 MeV	1.0	-0.22 ± 0.24	0.66 ± 0.32	0.11 ± 0.40	0.10 ± 0.42	-1.26 ± 0.51
1720 to 1760 MeV	1.0	-0.37 ± 0.16	0.70 ± 0.20	0.15 ± 0.26	0.17 ± 0.29	-0.31 ± 0.34
1740 to 1780 MeV	1.0	-0.08 ± 0.13	0.69 ± 0.16	0.26 ± 0.21	0.02 ± 0.24	0.09 ± 0.31
1760 to 1800 MeV	1.0	-0.10 ± 0.14	0.65 ± 0.18	0.12 ± 0.22	0.15 ± 0.24	0.28 ± 0.32
1780 to 1820 MeV	1.0	-0.01 ± 0.14	0.63 ± 0.18	0.21 ± 0.23	0.12 ± 0.25	0.41 ± 0.33
1800 to 1840 MeV	1.0	0.40 ± 0.15	0.59 ± 0.20	0.26 ± 0.24	0.09 ± 0.28	0.19 ± 0.36
1820 to 1860 MeV	1.0	0.26 ± 0.16	0.50 ± 0.22	0.06 ± 0.26	0.47 ± 0.30	-0.16 ± 0.38



MUB 11598

Fig. 15



MUB 11586

Fig. 16

$5/2^-$ theoretical curves. Legendre polynomial expansion coefficients are given in Table IV.

Table V contains the theoretical predictions for the decay of the $Y_1^*(1760)$ for spin up to 7/2, together with the probability that the experimental distribution fits the particular spin and parity assignment. As can be seen, the production and decay distributions rule out spin 1/2 and 3/2 and spin 5/2 with positive parity. The $7/2^-$ state is allowed by the production distribution but rejected by the decay prediction. What remains are two possibilities, namely $5/2^-$ and $7/2^+$, the former having a probability of 65% and the latter having a probability of 9%. While the $5/2^-$ is clearly preferred, there is, at first thought, a significant probability that $7/2^+$ is the correct assignment.

We shall show that even though the $7/2^+$ theoretical distribution yields a probability of 9% for fitting the data, the $5/2^-$ is an overwhelmingly better choice. An examination of Fig. 17a, which shows the $7/2^+$ and $5/2^-$ distributions, reveals that in the center of the angular distribution, from $-0.4 \leq \cos\Theta \leq 0.4$, the curves for the two spin-parity choices are almost identical. Since this region is expected to have a smaller number of events than is the case at the ends of the distribution, it is not surprising that our data are incapable of detecting the small difference of the two distributions in this range. However, at the extremes of the histogram, $|\cos\Theta| > 0.4$, the situation is very different; therefore we fitted the $7/2^+$ and $5/2^-$ theoretical distributions to the two regions $|\cos\Theta| > 0.4$ and $|\cos\Theta| \leq 0.4$ separately. The results are given in Table VI. The $5/2^-$ choice gives an adequate fit in all parts of the angular distribution; the $7/2^+$ distribution, on the other hand, fits the center of the histogram

Table IV. Legendre polynomial expansion coefficients for a fit to the experimental $Y_0^*(1520)$ decay distribution for events with 1740 MeV $\leq E_{KN}$ M.V. $\leq$ 1780 MeV.

Coef. \ Axis	Production Normal	Beam Direction
A_0	1.0	1.0
A_1	-0.03 ± 0.09	-0.10 ± 0.13
A_2	-0.91 ± 0.13	0.71 ± 0.16
A_3	0.06 ± 0.17	0.08 ± 0.19
A_4	0.04 ± 0.21	0.10 ± 0.24
A_5	-0.07 ± 0.29	-0.01 ± 0.31

Table V. $Y_0^*(1520)$ production and decay theoretical distributions for various spin and parity choices for the $Y_1^*(1760)$ and the probability of fit for these assignments.

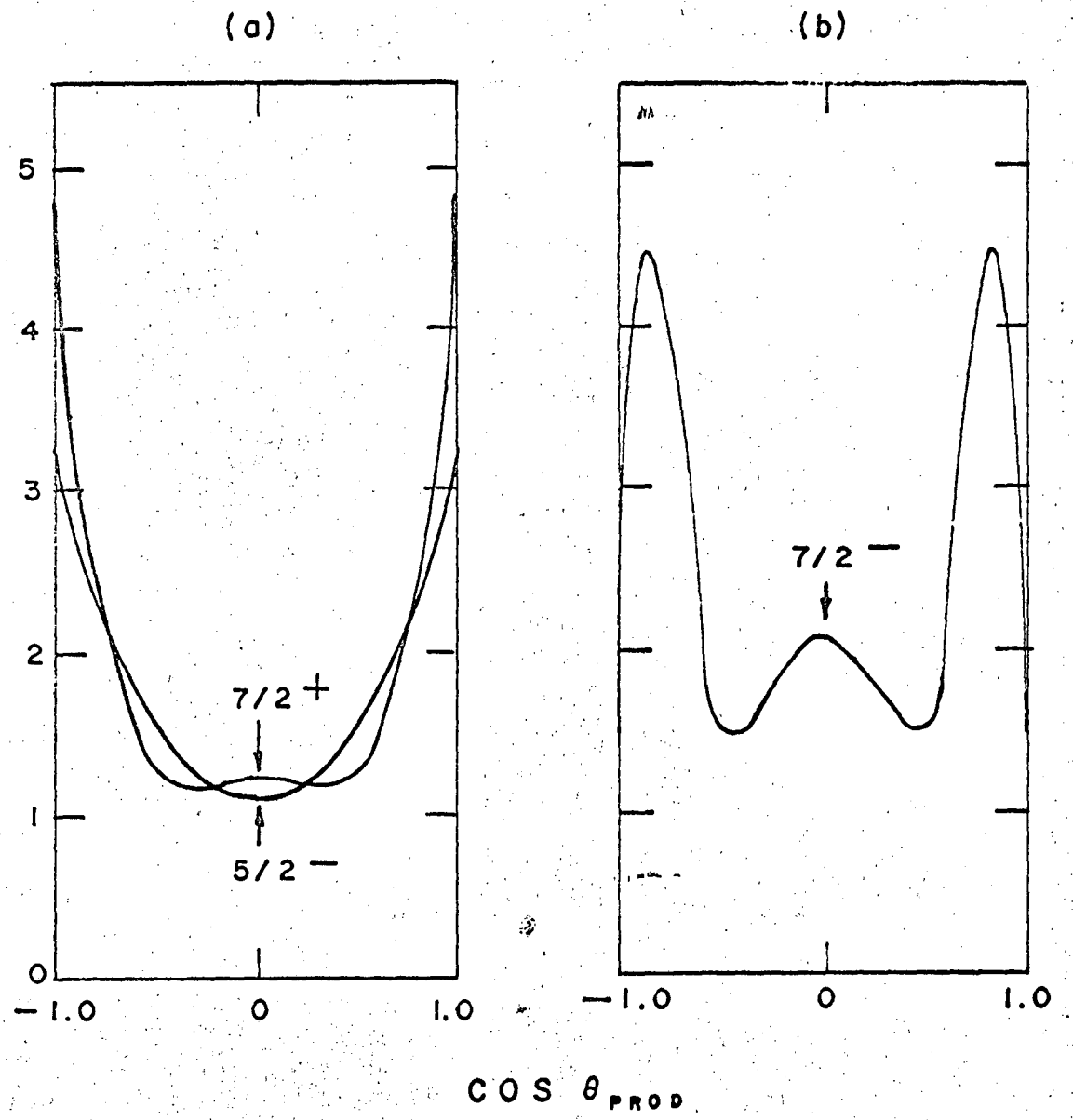
J^PL	$Y_0^*(1520)$ Theoretical Production Angular Distribution	Probability of fit %
$1/2^-P$	1.0	0.8
$1/2^+D$	1.0	0.8
$3/2^-P$	$1.0-0.80\ P_2(\cos\Theta)$	$<<.01$
$3/2^+S$	1.0	0.8
$5/2^-P$	$1.0+0.80\ P_2(\cos\Theta)$	65
$5/2^+D$	$1.0+0.41\ P_2(\cos\Theta)-0.98\ P_4(\cos\Theta)$	0.5
$7/2^-F$	$1.0+6.2\ P_2(\cos\Theta)-0.23\ P_4(\cos\Theta)-1.16\ P_6(\cos\Theta)$	43
$7/2^+D$	$1.0+1.02\ P_2(\cos\Theta)+0.55\ P_4(\cos\Theta)$	9

J^PL	$Y_0^*(1520)$ Theoretical Decay Distribution w.r.t. Production Normal	Probability of fit %
$1/2^-P$	$1.0-0.5\ P_2(\cos\Phi)$	21
$1/2^+D$	$1.0-0.5\ P_2(\cos\Phi)$	21
$3/2^-P$	$1.0+0.7\ P_2(\cos\Phi)$	$<<.01$
$3/2^+S$	$1.0-0.5\ P_2(\cos\Phi)$	21
$5/2^-P$	$1.0-0.7\ P_2(\cos\Phi)$	83
$5/2^+D$	$1.0+0.79\ P_2(\cos\Phi)$	$<<.01$
$7/2^-F$	$1.0+0.83\ P_2(\cos\Phi)$	$<<.01$
$7/2^+D$	$1.0-0.79\ P_2(\cos\Phi)$	95

(Table V, cont.)

Table V
(cont.)

J^P_L	$Y_0^*(1520)$ Theoretical Decay Distribution w.r.t. Incident K^- Direction	Probability of fit %
$1/2^-P$	1.0	0.5
$1/2^+D$	1.0	0.5
$3/2^-P$	$1.0+0.2\ P_2(\cos\Theta)$	5
$3/2^+S$	$1.0+P_2(\cos\Theta)$	4
$5/2^-P$	$1.0+0.8\ P_2(\cos\Theta)$	24
$5/2^+D$	$1.0-0.14\ P_2(\cos\Theta)$	2
$7/2^-F$	$1.0-0.24\ P_2(\cos\Theta)$	<0.1
$7/2^+D$	$1.0+0.71\ P_2(\cos\Theta)$	34



MUB-12010

Fig. 17

very well but has only a probability of 1% of fitting the ends of the experimental distribution. Actually, this could have been suspected from an examination of the expansion coefficients of Fig. 15; there is no indication of the term which would characterize the presence of D waves, namely A_4. Due to the lack of the A_4 and the inability of its theoretical distribution to adequately fit the production angular distribution throughout the entire range of cos Θ, we rejected the $7/2^+$ hypothesis in favor of an assignment of $5/2^-$ for the spin and parity of the $Y_1^*(1760)$.

We showed that the $7/2^-$ assignment was ruled out by the lack of fit to the observed decay distribution; however, on the basis of the production angular distribution alone, it seems that this choice has an excellent chance of fitting the data, namely 43%. A glance at the theoretical curve shown in Fig. 17b reveals that throughout most of the histogram the $7/2^-$ and $5/2^-$ fit the data equally well; but in the boxes with $|\cos \Theta| \geq 0.9$ the $7/2^-$ distribution disagrees violently with the experimental situation. Therefore, we would reject this hypothesis also even though it has a large overall probability of fitting the data.

Actually, the original experiment which suggested that the $Y_1^*(1760)$ might exist also indicated that amplitudes with spin greater than 5/2 were not required.[2] No subsequent work on other decay modes of the $Y_1^*(1760)$ has required spin 7/2 or greater for this isobar.[3]

With this choice of J^P we can explain the behavior of the Legendre polynomial expansion coefficients given in Fig. 15 and Table IV. The most reasonable assumption as to the nature of the non-resonant background is that it is in a state of $J = 3/2$ and $L = 0$, because of the low Q^-

Table VI. Probabilities of fit for the indicated cos Θ ranges and spin and parity choices to the $Y_0^*(1520)$ production angular distributions.

Range of $Y_0^*(1520)$ Production Angle	Probability of Fit	
	$5/2^-$	$7/2^+$
$\|\cos\Theta\| > 0.4$	55%	1%
$\|\cos\Theta\| \leq 0.4$	60%	92%

value available. If this is actually the case, then it is possible to write the expected angular distribution as

$$\frac{d\sigma}{d\Omega} = \frac{1}{4\pi}\left(|T_{30}|^2 + |T_{51}|^2\right) + \frac{R_e\, T_{30}^*\, T_{51}}{2\pi}\cdot\frac{3}{\sqrt{5}}\, P_1(\cos\Theta) + \frac{|T_{51}|^2}{5\pi}\, P_2(\cos\Theta)$$

where T_{JL} is the amplitude for a state with spin J/2 and orbital angular momentum L. This expression is seen to describe the nature of the change in the sign of A_1 and the reduction of the expected value of A_2. The only other possible non-negligible expansion coefficient is A_3; we shall show in the next section that backgrounds due to non $Y_0^*(1520)$ production can easily give rise to small A_3 terms.

In summary, all evidence indicates a spin and parity assignment of $5/2^-$ for the $Y_1^*(1760)$; the best values for the resonant parameters are

$$M = 1760 \pm 5 \text{ MeV}$$

$$\Gamma = 70 \pm 20 \text{ MeV}.$$

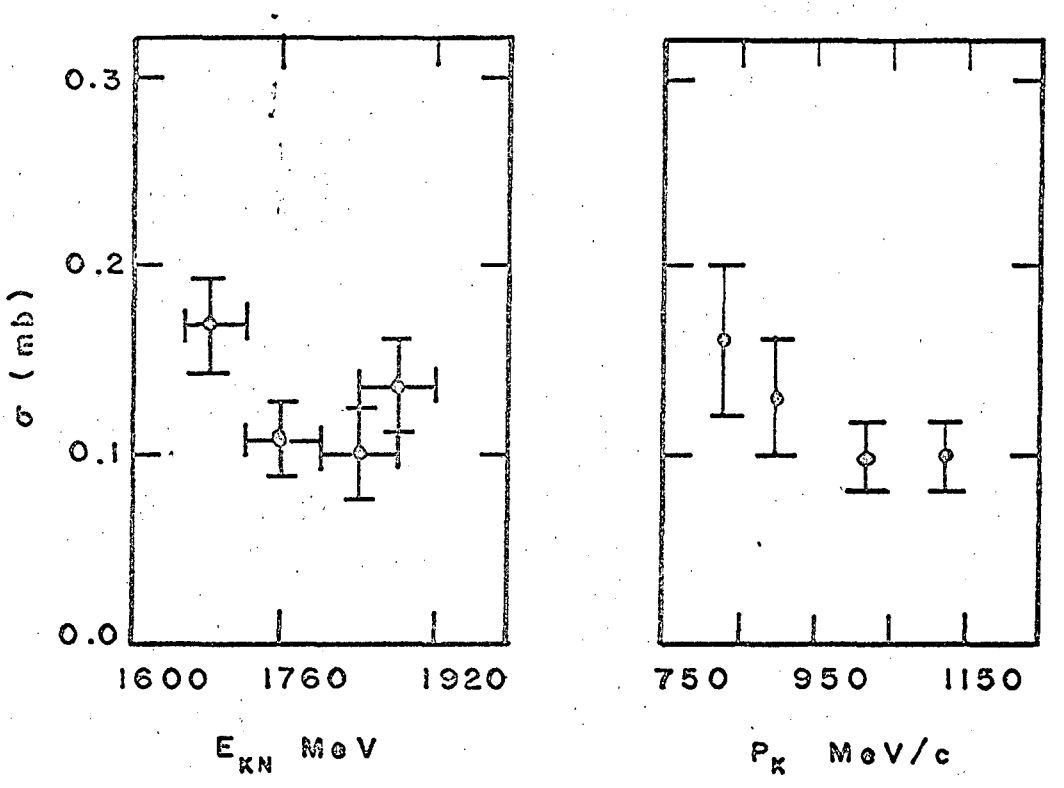
2. $Y_0^*(1405)$ Events

As we saw from Figs. 9 and 12 there is, in addition to the $Y_0^*(1520)$, another resonance produced in the $\Sigma^- \pi^+$ channel--the $Y_0^*(1405)$. It was originally thought that the $Y_1^*(1760)$ had spin 5/2 but there was no information concerning the parity. The fact that the $Y_1^*(1760)$ decays into $Y_0^*(1520)\,\pi^-$ rather than into $Y_0^*(1405)\,\pi^-$, which is certainly fully allowed, in itself indicates that the parity is most probably negative. The argument is as follows: If the $Y_1^*(1760)$ had positive parity, then it would decay into both the $J^P = 3/2^-$ $Y_0^*(1520)$ and $J^P = 1/2^-$ $Y_0^*(1405)$ by a D wave orbital angular momentum state. Since the Q value for the decay into the latter resonance is larger than

for decay into the $Y_0^*(1520)\,\pi^-$, the $Y_0^*(1405)\,\pi^-$ mode would be expected to dominate. However, if the $Y_1^*(1760)$ is $5/2^-$ then the $Y_0^*(1405)\,\pi^-$ decay is by F wave which is much less favored than the P wave process we discovered in the last section.

Actually, it is thought that the $Y_0^*(1405)\,\pi^-$ may be the result of the decay of an isospin one resonance--the $Y_1^*(1660)$.[21] While there is very little data in this experiment below 1700 MeV (and none at all below 1660 MeV) we attempted to see the high energy tail of the $Y_1^*(1660)$. To this end we plotted the production cross section as a function of K^- beam momentum and K^- n c.m. energy; these data are shown in Fig. 18. The criterion used to determine the production of a $Y_0^*(1405)$ was that the invariant mass of the $\Sigma^-\,\pi^+$ system be in the range 1380 MeV to 1430 MeV. The qualitative features of the cross sections of Fig. 18 are rather sensitive functions of the exact width of the resonance. This is due to the nature of the phase space in the 1660 MeV to 1700 MeV region, which is not at all unlike the shape of the Breit-Wigner curve which describes the $Y_0^*(1405)$. Because of the meager number of events in this range, it is not possible to make a reasonable estimate of the ratio of resonance to background. The cross section values are given with no attempt of a background subtraction. The increasing cross section seen in Fig. 18 may be due to the presence of the $Y_1^*(1660)$ but could just as well be due to our inability to estimate background.

Figure 19 shows the production angular distributions for the events for which $1380 \leq M(\Sigma^-\,\pi^+) \leq 1430$ MeV; it is at once evident that there are very large backgrounds producing significant odd $\cos\Theta$ terms. The coefficients of a Legendre polynomial expansion are shown in Fig. 20. Terms in A_4 or greater are essentially zero and are not shown. If we



MUB-12007

Fig. 18

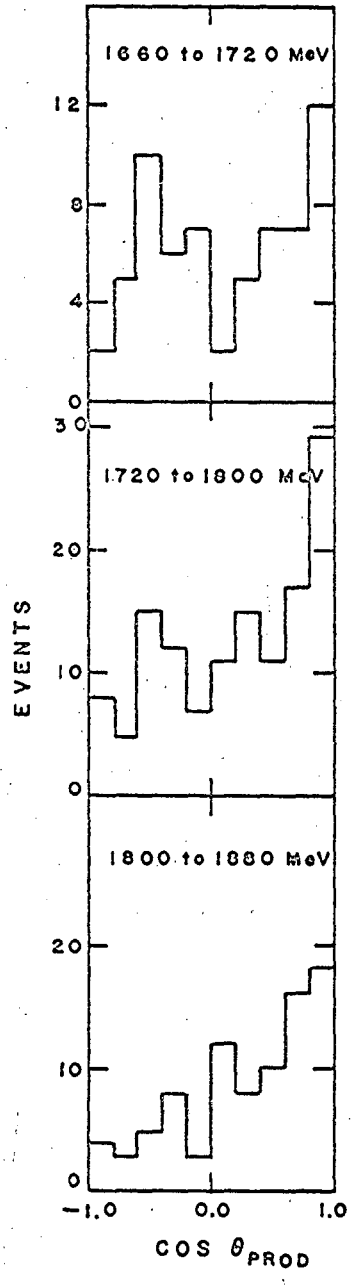
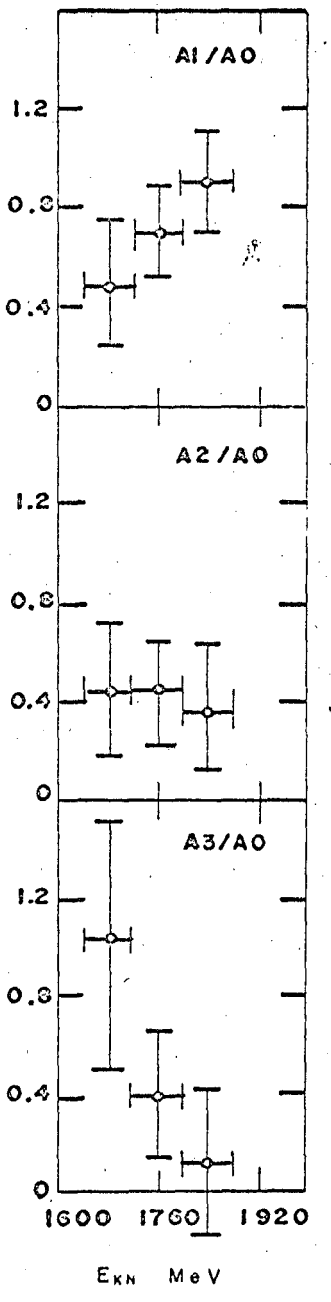

1660 to 1720 MeV
1720 to 1800 MeV
1800 to 1880 MeV
EVENTS
COS θPROD
-1.0
0.0
1.0
MUB-12008

Fig. 19



MUB-12009

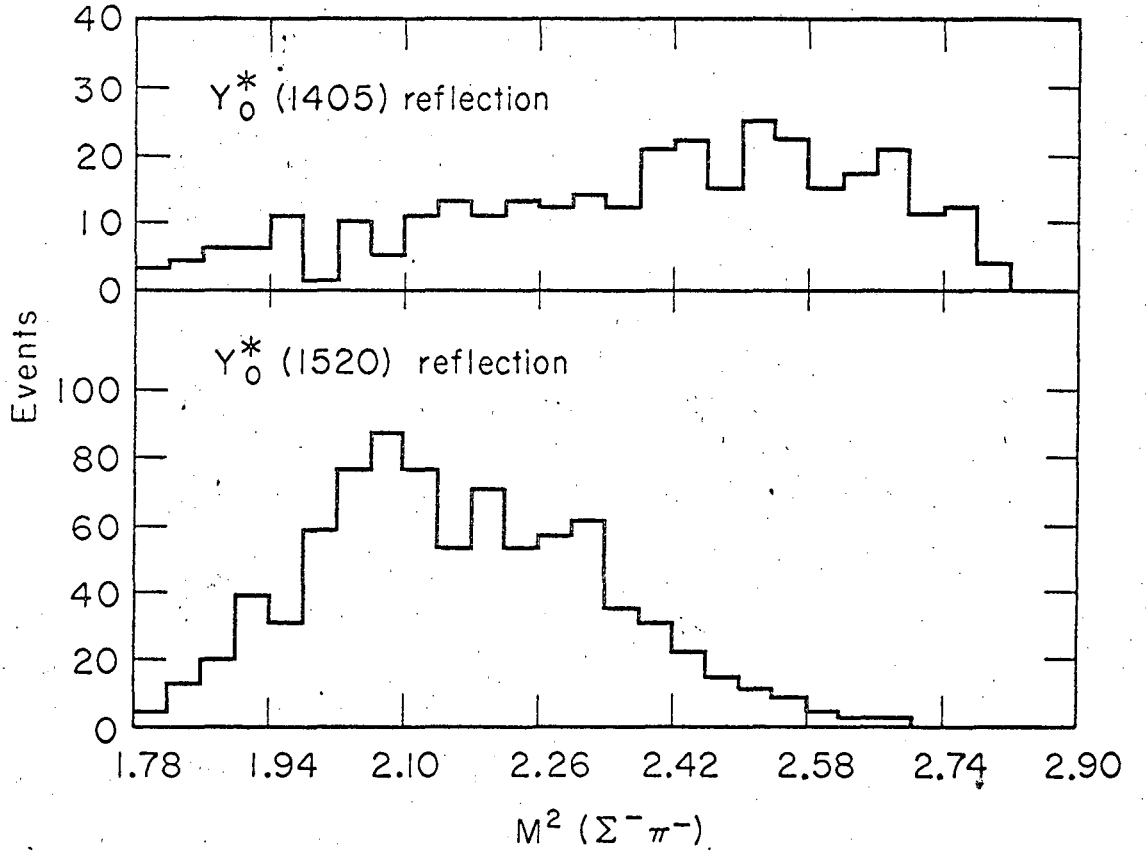
Fig. 20

are indeed observing the tail of the $Y_1^*(1660)$ then it is possible that the rapidly changing odd P_L (cos Θ) terms are due to a rapidly changing resonant phase interfering with background. The only statement that can be made about the nature of this possible resonant amplitude is that our data do not require a spin of greater than 3/2 for it. The $Y_0^*(1660)$ is thought to have spin 3/2.[22]

The parity of the $Y_0^*(1660)$ has not been definitely determined at this time; it is believed that the most probable assignment is negative.[21] If we had a knowledge of the backgrounds, then it might be possible to examine the interference terms and find the $Y_1^*(1660)$ parity. However, since we showed that there is a spin 5/2 $Y_1^*(1760)$ produced in this general K^- momentum region, it is necessary to assume non-resonant amplitudes up to D wave. Because there is also no possibility of observing any polarization of the sigma, our data sheds no light on the unresolved question of the $Y_1^*(1660)$ parity.

B. $\Sigma^- \pi^-$ Spectrum

The $\Sigma^- \pi^-$ final state is very interesting because it must have an isospin of two. The existence of a Y_2^* decaying into this channel near a mass value of 1420 MeV has been reported.[6] Because of the very strong production of the $Y_0^*(1520)$ in the cross channel, it is difficult to detect any structure in the $\Sigma^- \pi^-$ system from the Dalitz plot of Fig. 8. The projection on the M^2 ($\Sigma^- \pi^-$) axes shown in Fig. 9 shows no evidence of structure. However, it must be remembered that this plot contains events which are the reflection of the $Y_0^*(1520)$ or $Y_0^*(1405)$; these reflections are shown in Fig. 21. It is possible to effectively remove their effect in the $\Sigma^- \pi^-$ spectrum in the following way: From Fig. 12 we determined the ratio of $Y_0^*(1520)$ and $Y_0^*(1405)$ to background



MUB-11591

Fig. 21

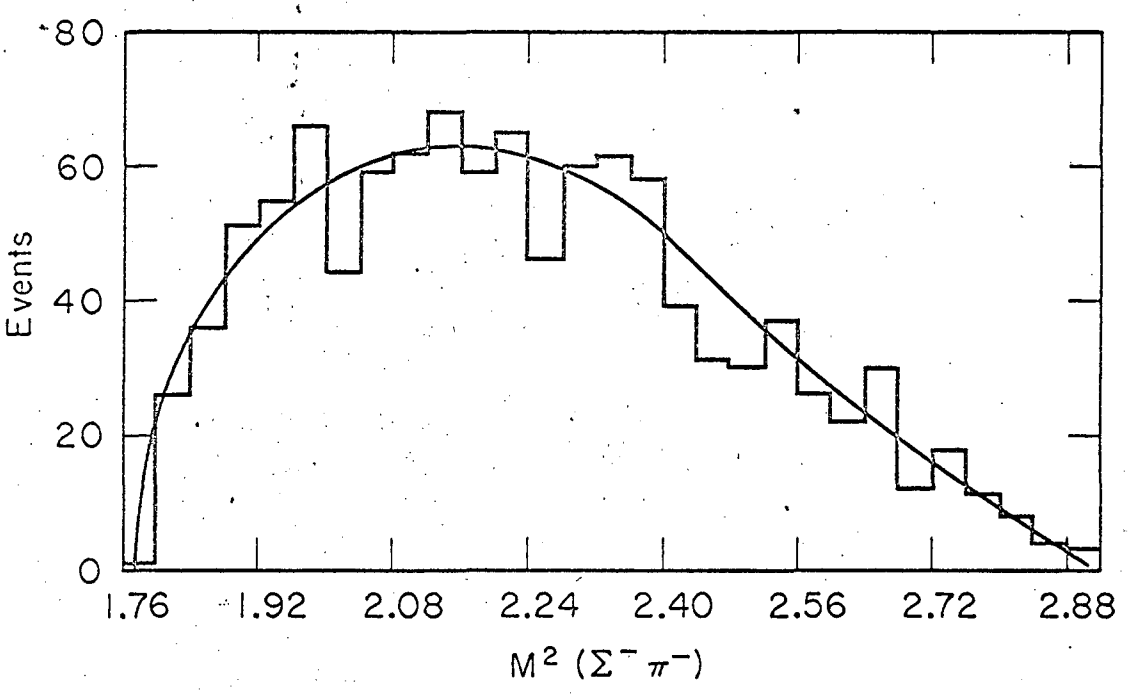
and, therefore, can remove the appropriate percentage of their reflections from the M^2 ($\Sigma^- \pi^-$) plot. The resulting distribution is shown in Fig. 22 with the expected three-body phase space derived in a previous section. As can be seen, there is no indication of an enhancement in the $\Sigma^- \pi^-$ final state.

If there were a significant interaction between the Σ^- and π^- around some energy value, then in the region of the Dalitz plot where their resonant band overlapped the $Y_0^*(1520)$ band interference effects could cause the $Y_0^*(1520)$ decay angular distributions to be distorted. In the abscence of such interference effects the strong parity conserving decay of the resonance must result in angular distributions which are symmetric in the cosine of the decay angle of the sigma with respect to any quantization axis. Essentially, we saw this in the Appendix in the derivation of the decay distributions with respect to the beam direction and production normal. The same reasoning leads us to expect that the $Y_0^*(1520)$ decay will yield a sigma distribution of the form $1 + BP_2 (\cos \Theta)$ where B is just an energy dependent parameter for a particular choice of quantization axis.

A particularly good direction to use is the $Y_0^*(1520)$ line of flight since

$$\cos \Theta = \frac{\vec{P}_\Sigma \cdot \vec{Y}_0^*(1520)}{|\vec{P}_\Sigma \cdot \vec{Y}_0^*(1520)|}$$

varies from +1 to -1 along lines of constant M^2 ($\Sigma^- \pi^+$). Unless the Y_2^* were very wide, we would expect to see a distortion in the distribution in cos Θ plot which changed its position in the histogram as the $K^- n$ c.m. energy interval is varied. The Y_2^* reported at 1420 MeV was very narrow and should give a distinct effect in a small range of cos Θ

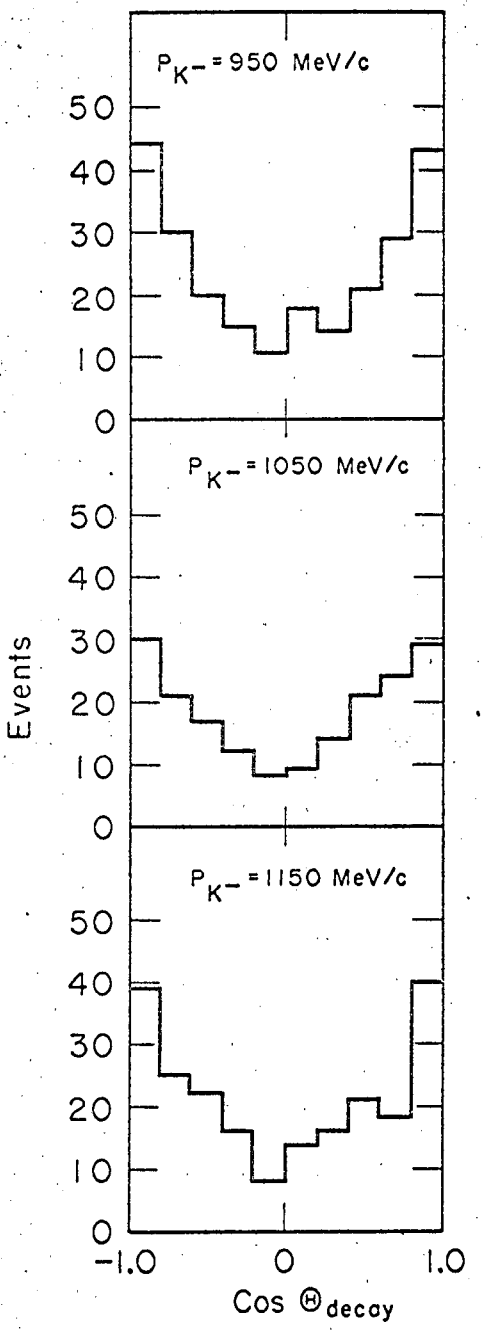


MUB 11587

Fig. 22

values. In Fig. 23 these angular distributions are shown as a function of K^- beam momentum; they are perfectly symmetric. The available K^- n energy range was searched with various cuts on the energy interval and the cos Θ distributions were found to be symmetric in all cases.

Although there is no evidence for a Y_2^* in our data, the domination of the $Y_0^*(1520)$ in the mass spectra would make the detection of a broad resonance in $\Sigma^- \pi^-$ difficult. Further, the most favorable K^- n c.m. energy for the production of a Y_2^* near 1420 MeV is around 1760 MeV; at that energy the reflection of the $Y_0^*(1520)$ is very large and the presence of the $Y_1^*(1760)$ determines the form of the angular distributions. In an attempt to minimize the effects of the $Y_1^*(1760)$, we repeated the above analysis at various energies above and below 1760 MeV. The results do not change; there is no indication of any Y_2^*, especially a narrow one, anywhere in the available energy range.



MUB 11600

Fig. 23

ACKNOWLEDGMENTS

I am indebted to the many people who have helped me during my years as a graduate student; in particular I would like to express my appreciation to Dr. Robert W. Birge for his guidance and constant encouragement and to Dr. Robert T. Pu for many illuminating discussions on the subject of spin and parity analysis. All members of the Powell-Birge Physics group have aided me in gaining a better understanding of the techniques of high energy physics and in the preparation of this thesis. Without the fine support of the scanners and measurers under the direction of Mr. Wes Weber this work would not have been possible. I would especially like to thank Miss Jean Colton for an outstanding job in scanning the film.

There are numerous people outside the Powell-Birge group who have contributed to the data of this thesis, the Bevatron staff, the 25-inch bubble chamber crew, and the members of the Data Handling group under Mr. Howard S. White being the most important. Mr. Loren Shalz of this latter group deserves special mention for the aid he rendered me in the use of the FAIR system.

Finally I would like to thank Mrs. Kathy Pierce for a fine job in the preparation of the manuscript and Dr. Robert P. Ely, Jr. for his criticism of the text.

This work was done under the auspices of the U. S. Atomic Energy Commission.

APPENDIX

Production and Decay of Particles of Spin 3/2

The particular spin 3/2 particle that we shall be considering is the $Y_0^*(1520)$ which is also known to have negative parity. The process to be considered is

$$K^- n \rightarrow Y_1^*(1760) \rightarrow Y_0^*(1520)\, \pi^-;\ Y_0^*(1520) \rightarrow \Sigma^- \pi^+.$$

However the techniques to be presented can be easily extended to positive parity particles, such as the $Y_1^*(1385)$, which decay into other spin 1/2-spin 0 final states.

We shall assume that there are no backgrounds present and first consider the production angular distribution of the $Y_0^*(1520)$. The quantization axis will be the incident beam direction and we shall use the K^- n center of mass frame. Whatever the spin of the $Y_1^*(1760)$ is, only two spin projection states are possible, namely the two initial spin projections of the target neutron, $m_j = \pm 1/2$. This is because the K^- n system cannot have a component of angular momentum along the beam direction. Moreover, these two states must yield the same $Y_0^*(1520)$ angular distributions since the decay $Y_1^*(1760) \rightarrow Y_0^*(1520)\, \pi^-$ is strong and parity conserving and the $m_j = \pm 1/2$ projections are related by a parity inversion. Then for any spin and parity choice for the parent resonance only two $Y_0^*(1520)$ relative orbital angular momentum states are available, L and L+2. The initial state of the $Y_1^*(1760)$ can be composed in terms of the spin 3/2 spin 0 and relative angular momentum state L. It is natural at the low Q values of this experiment to assume that the lower L state is dominant and write

$$| J^P\ 1/2 > = A_3 \mid 3/2\ 3/2 > + A_1 \mid 3/2\ 1/2 > + A_{-1} \mid 3/2\ -1/2 > + A_{-3} \mid 3/2, -3/2 >$$

where $| 3/2, m >$ is the $Y_0^*(1520)$ spinor and

$$A_3 = a_3 Y_L^{-1} \qquad A_1 = a_1 Y_L^0$$
$$A_{-1} = a_{-1} Y_L^1 \qquad A_{-3} = a_{-3} Y_L^2 ;$$

the Y_L^m is the spherical harmonic describing the relative orbital angular momentum and a_j is the appropriate Clebsch-Gordon coefficient. Then the $Y_0^*(1520)$ production angular distribution is

$$\frac{d\sigma}{d\Omega} = | a_3 Y_L^{-1} |^2 + | a_1 Y_L^0 |^2 + | a_{-1} Y_L^1 |^2 + | a_{-3} Y_L^2 |^2$$

since the spinors $| 3/2, m_j >$ are orthonormal. In particular, if $J^P = 5/2^-$, then $L = 1$ and

$$\frac{d\sigma}{d\Omega} = 1 + 2 \cos^2 \Theta ;$$

for $J^P = 5/2^+$ $L = 2$ and

$$\frac{d\sigma}{d\Omega} = 1 + 10 \cos^2 \Theta - 10 \cos^4 \Theta$$

A complete listing of distributions up to spin 7/2 is given in Table A-I; also included are the Clebsch-Gordon coefficients for interference terms of different spin and parity up to 5/2.

Next, consider the decay $Y_0^*(1520) \rightarrow \Sigma^- \pi^+$ which is symbolically $3/2^- \rightarrow 1/2^+ + 0^-$. The decay is strong and parity conserving so the relative angular momentum must be $L = 2$. Let us continue to quantize with respect to the beam direction but now work in the $Y_0^*(1520)$ rest frame. Then the initial spin states of the $Y_0^*(1520)$ can be composed in terms of the $\Sigma^- \pi^+$ final state as follows:

$$| 3/2\ 3/2 > = -\sqrt{1/5} \; | 1/2\ 1/2 > Y_2^1 + \sqrt{4/5} \; | 1/2\ -1/2 > Y_2^2$$

$$| 3/2\ 1/2 > = -\sqrt{2/5} \; | 1/2\ 1/2 > Y_2^0 + \sqrt{3/5} \; | 1/2\ -1/2 > Y_2^1$$

where $| 1/2, m_j >$, $m_j = \pm 1/2$, is the sigma spinor and Y_L^m and a_j have usual meaning. The states $| 3/2\ -1/2 >$ and $| 3/2\ -3/2 >$ are also

possible, but since they are related to $|\ 3/2\ 1/2\ >$ and $|\ 3/2\ 3/2\ >$, respectively, by a parity inversion, they must give the same sigma distribution.

Then the decay from the state $|\ 3/2\ 3/2\ >$ is of the form

$$\left(\frac{d\sigma}{d\Omega}\right)_{3/2\ 3/2} = 1 - P_2\ (\cos\Phi)$$

and from the $|\ 3/2\ 1/2\ >$ state is of the form

$$\left(\frac{d\sigma}{d\Omega}\right)_{3/2\ 1/2} = 1 + P_2\ (\cos\Phi)\ .$$

Next it is necessary to know the relative probabilities for the various $Y_0^*(1520)$ spin projections. If the $Y_0^*(1520)$ is the result of the decay of the $Y_1^*(1760)$ these weights are known; for a given production angle Θ^1 the probability, P, is

$$P\ (|\ 3/2\ 3/2\ >) = |\ a_3\ Y_L^{-1}\ |^2 + |\ a_{-3}\ Y_L^{2}\ |^2$$

for the $|\ 3/2\ 3/2\ >$ state and

$$P\ (|\ 3/2\ 1/2\ >) = |\ a_1\ Y_L^{0}\ |^2 + |\ a_{-1}\ Y_L^{1}\ |^2$$

for the $|\ 3/2\ 1/2\ >$ state. P is simply found by inspection of the form of the $Y_0^*(1520)$ production angular distribution. Then

$$\left(\frac{d\sigma}{d\Omega\ \Theta^1}\right) = (1 - P_2\ (\cos\Phi))\ (P\ (|\ 3/2\ 3/2\ >)) + (1 + P_2\ (\cos\Phi))\ (P\ (|\ 3/2\ 1/2\ >))$$

We integrate over the production angle Θ^1 and get

$$\left(\frac{d\sigma}{d\Omega}\right)_{\text{beam}} = (1 - P_2\ (\cos\Phi))\ (|\ a_3\ |^2 + |\ a_{-3}\ |^2) + (1 + P_2\ (\cos\Phi))\ (|\ a_1\ |^2 + |\ a_{-1}\ |^2)$$

Since, by unitarity, $|\ a_1\ |^2 + |\ a_{-1}\ |^2 + |\ a_3\ |^2 + |\ a_{-3}\ |^2 = 1$ we find that:

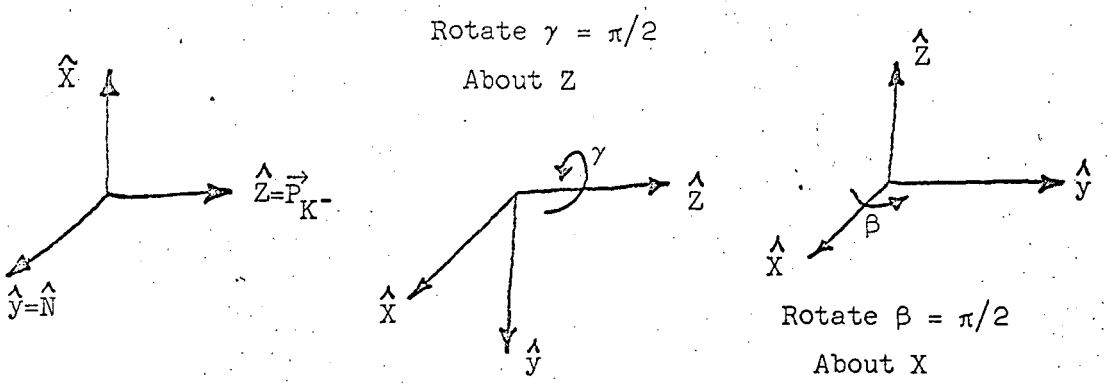
$$\left(\frac{d\sigma}{d\Omega}\right)_{\text{beam}} = 1 + (1 - 2\ (|\ a_3\ |^2 + |\ a_{-3}\ |^2))\ P_2\ (\cos\Phi)$$

There is a better axis along which to quantize than the beam

direction; it is the production normal defined as

$$\hat{n} = \frac{\vec{P}_{K^-} \times \vec{Y}^*_0(1520)}{|\vec{P}_{K^-} \times \vec{Y}^*_0(1520)|}$$

It is better in the sense that it gives a more distinct set of distributions for various spin and parity choices than the beam direction.[16] The simplest way to write the spin states with respect to the normal is to transform the states quantized along the beam direction with the two rotations shown below; these rotations interchange the normal and beam directions.



The rotation matrix is

$$D(\alpha\ \beta\ \gamma) = \frac{1}{\sqrt{8}} \begin{bmatrix} 1 & -\sqrt{3} & \sqrt{3} & -1 \\ \sqrt{3} & -1 & -1 & \sqrt{3} \\ \sqrt{3} & 1 & -1 & -\sqrt{3} \\ 1 & \sqrt{3} & \sqrt{3} & 1 \end{bmatrix} \epsilon^{-im\pi/2}$$

(See Edmonds, Angular Momentum in Quantum Mechanics, Princeton, 1963.)

Then

$$|\ J\ 1/2\ >_{norm} = A'_3\ |\ 3/2\ 3/2\ > + A'_1\ |\ 3/2\ 1/2\ > + A'_{-1}\ |\ 3/2\ -1/2\ > + A'_{-3}\ |\ 3/2\ -3/2\ >$$

where

$$\begin{bmatrix} A'_3 \\ A'_1 \\ A'_{-1} \\ A'_{-3} \end{bmatrix} = D \begin{bmatrix} a_3 Y_L^{-1} \\ a_1 Y_L^{0} \\ a_{-1} Y_L^{1} \\ a_{-3} Y_L^{2} \end{bmatrix}$$

Again this supplies us with the relative probabilities for the $\pm$ 3/2 and $\pm$ 1/2 spin projections of the $Y_0^*(1520)$; they are just $(|A'_3|^2 + |A_{-3}|^2)$ and $(|A'_1|^2 + |A_{-1}|^2)$. Integration over all $Y_0^*(1520)$ production angles Θ^1 gives

$$\left(\frac{d\sigma}{d\Omega}\right)_{\text{normal}} = 1 + (a_3^2 + a_{-3}^2 - 1/2 - \sqrt{3}\,(a_3\, a_{-1} + a_1\, a_{-3}\sqrt{\frac{L(L+1)}{(L+1)(L+2)}}))$$

The strange square root comes from

$$\int A_1\, A^*_{-3}\, d\Omega_{\text{prod}} = -\, a_1\, a_{-3}\sqrt{\frac{L(L+1)}{(L+1)(L+2)}}$$

In summary,

$$\left(\frac{d\sigma}{d\Omega}\right)_{\text{decay}} = 1 + A\, P_2\,(\cos\Phi)$$

where:

along the beam $\quad A = 1 - 2(|a_3|^2 + |a_{-3}|^2)$

along the normal $\quad A = |a_3|^2 + |a_{-3}|^2 - 1/2 - \sqrt{3}\left[a_3\, a_{-1} + a_1\, a_{-3}\sqrt{\frac{L(L+1)}{(L+1)(L+2)}}\right]$

The general form of the Clebsch-Gordon coefficients are

$$J = L + 3/2$$

$$a_3 = (L(L+1)(L+2) \,/\, (2L+1)(2L+2)(2L+3))^{1/2}$$

$$a_1 = (3(L+1)^2\,(L+2) \,/\, (2L+1)(2L+2)(2L+3))^{1/2}$$

$$a_{-1} = (3L(L+1)(L+2) \,/\, (2L+1)(2L+2)(2L+3))^{1/2}$$

$$a_{-3} = ((L-1)(L)(L+1) \,/\, (2L+1)(2L+2)(2L+3))^{1/2}$$

$$J = L + 1/2$$

$$a_3 = -(3L(L+1)^2 / 2L(2L+1)(2L+3))^{1/2}$$

$$a_1 = -L((L+1) / 2L(2L+1)(2L+3))^{1/2}$$

$$a_{-1} = (L+3)(L / 2L(2L+1)(2L+3))^{1/2}$$

$$a_{-3} = (3(L-1)L(L+2) / 2L(2L+1)(2L+3))^{1/2}$$

Using these values we find that

along the beam	$J = L + 3/2$	$A = (2J+3)/4J$
	$J = L + 1/2$	$A = -(2J-4)(2J+3) / 4J(2J+2)$
and along the normal	$J = L + 3/2$	$A = -(4J-3)/4J$
	$J = L + 1/2$	$A = (4J+1)/(J+4)$

where J is the $Y_1^*(1760)$ spin. A table of A values up to spin 7/2 is given in Table A-II.

The above treatment has been clearly non relativistic; we can derive the angular distributions from the relativistic helicity formalism also. Consider the amplitude for the strong decay $R \to B + M$ where R has spin J' and B has spin J and M is spinless. For decay from the state $|J'M'\rangle$ into the final state in which B has momentum $\vec{p}$, in the R c.m., $A(\vec{p}\lambda_B) = \langle \vec{p}\lambda_B | M | J'M' \rangle$ where λ_B is the helicity of B. In terms of helicity states

$$|\vec{p}\lambda\rangle = \sum_{Jm} |Jm\lambda\rangle \sqrt{\frac{2J+1}{4\pi}} D^J_{m\lambda}(\omega)$$

so

$$A(\vec{p}\lambda_B) = \sqrt{\frac{2J'+1}{4\pi}} \langle J'M'\lambda_B | M | J'M' \rangle D^{J'*}_{M'\lambda_B}(\omega)$$

Since M is a scalar under P for this strong process

$$M(-\lambda_B) = \eta_R \eta_B \eta_M (-)^{J'-S_R-S_B} M(\lambda_B)$$

where η is the relative parity. If the density matrix for R is ρ, then the production angular distribution of B in the R c.m. is

$$W(\theta,\phi) = N \sum_{\substack{mm' \\ \lambda_B}} |M(\lambda_B)|^2 D^{J'*}_{m\lambda_B}(\omega) D^{J'}_{m'\lambda_B}(\omega) \rho_{mm'}$$

For our reaction with an unpolarized target ρ is diagonal with $m = \pm 1/2$ both equally probable so that

$$W(\theta,\phi) = N \sum_{\lambda_B} |M(\lambda_B)|^2 \left[\left(d^J_{1/2\lambda_B}(\theta)\right)^2 + \left(d^J_{-1/2\lambda}(\theta)\right)^2 \right]$$

where we have used $D^J_{mm'}(\omega) = \epsilon^{-im\alpha} d^J_{mm'}(\theta) \epsilon^{-im'\gamma}$

If $S_B = 3/2$ we have both M(3/2) and m(1/2) and must make some assumption about them to proceed further. In the same spirit as above we shall

assume that only the lowest possible L value is present. The ratio of M(3/2) to M(1/2) is then determined by Clebsh Gordon coefficients.

$$\frac{M(3/2)}{M(1/2)} = \frac{(J\,3/2 \mid L\;3/2\;0\;3/2)}{(J\,1/2 \mid L\;3/2\;0\;1/2)} = \begin{cases} \sqrt{\frac{2J+3}{3(2J-1)}} & l = J - 3/2 \\ \sqrt{\frac{3(2J+3)}{2J-1}} & l = J - 1/2 \end{cases}$$

Table I then follows directly.

As before we now have the B density matrix.

$$\langle \lambda_{13} | \rho_B | \lambda_B \rangle = N' \frac{M(\lambda_B) M^*(\lambda_{13})}{W(\theta,\phi)} \sum_{mm'} \rho_{mm'} D^{J*}_{m\lambda_{13}} D^{J}_{m'\lambda_B}(\omega)$$

Note that ρ_B is a helicity density matrix. As before we average over production angles

$$\langle \rho_{B\lambda\lambda'} \rangle = \frac{\int d\Omega_p \rho_{B\lambda\lambda'}(\omega) W(\omega)}{\int d\Omega_p W(\omega)}$$

and find

$$\langle \rho_{\pm 1/2, \pm 1/2} \rangle = \begin{cases} \frac{3(2J-1)}{16J} & l = J - 3/2 \\ \frac{(2J-1)}{16(J+1)} & l = J - 1/2 \end{cases} \qquad \langle \rho_{\pm 3/2, \pm 3/2} \rangle = \begin{cases} \frac{2J+3}{16J} & l = J - 3/2 \\ \frac{3(2J+3)}{16(J+1)} & l = J - 1/2 \end{cases}$$

again $\left(\frac{d\sigma}{d\Omega}\right)_{\text{DECAY}} \sim (1 + A P_2(\cos\phi))$ with

$$A = \begin{cases} \frac{(2J-3)}{4J} & l = J - 3/2 \\ -\frac{(2J+5)}{4(J+1)} & l = J - 1/2 \end{cases}$$

from which we may determine I_{decay} with respect to the B line of flight.

It should be pointed out that if the assumption of the dominance of the lowest L value is not true then the entire analysis above breaks down. In that case it is necessary to do a modified moments type analysis and observe the angular distributions of B decay decay and B polarizations as a function of B production angle. This would require a very much larger number of events than currently availible.

Table A-I. Partial-wave-amplitude contributions to the $Y_0^*(1520)$ production angular distribution $I = \Sigma A_N P_N(\cos\Theta)$. (J^P, L) implies decay from a state of spin and parity J^P via L wave.

Partial amplitude		Inter-ference terms	Coefficients						
Term	$J^P L$		A_0	A_1	A_2	A_3	A_4	A_5	A_6
1	$(1/2^-P)$		0.56						
2	$(1/2^+D)$		0.56						
3	$(3/2^+S)$		1.1						
4	$(3/2^+D)$		1.1						
5	$(3/2^-P)$		1.1		-0.9				
6	$(3/2^-F)$		1.1		+0.9				
7	$(5/2^-P)$		1.7		1.4				
8	$(5/2^-F)$		1.7		1.1		-0.7		
9	$(5/2^+D)$		1.7		0.7		-1.7		
10	$(5/2^+G)$		1.7		1.7		0.93		
11	$(7/2^-F)$		1.0		6.2		-0.23		-1.16
12	$(7/2^+D)$		1.0		1.02		0.55		
		(2,1)		1.1					
		(3,1)		-1.6					
		(3,2)			-1.6				
		(4,1)		1.6					
		(4,2)			1.6				
		(4,3)			-2.3				
		(5,1)			-0.7				
		(5,2)		-0.7					
		(5,3)		1.0					

(Table A-I., cont.)

Table A-I.
(cont.)

Partial amplitude		Interference terms	Coefficients						
Term	$J^P L$		A_0	A_1	A_2	A_3	A_4	A_5	A_6
		(5,4)		0.8		-1.8			
		(6,1)			2.1				
		(6,2)		2.1					
		(6,3)				-3.0			
		(6,4)		0.6		2.4			
		(6,5)			-1.4				
		(7,1)			-2.6				
		(7,2)				-2.6			
		(7,3)		3.7					
		(7,4)		-0.74		-3.0			
		(7,5)			1.7				
		(7,6)			-0.24		-4.7		
		(8,1)			2.1				
		(8,2)				2.1			
		(8,3)				-3.0			
		(8,4)		3.6		-0.6			
		(8,5)			1.5		-2.9		
		(8,6)			1.2		+2.9		
		(8,7)			-1.4		-3.6		
		(9,1)				-1.3			
		(9,2)				-1.3			
		(9,3)				1.8			

(Table A-I., cont.)

Table A-I
(cont.)

Partial amplitude		Inter-ference terms	Coefficients						
Term	$J^P L$		A_0	A_1	A_2	A_3	A_4	A_5	A_6
		(9,4)			1.3		-3.1		
		(9,5)		3.4		-2.6			
		(9,6)		-0.5		-1.9			
		(9,7)		0.6		2.4			
		(9,8)		0.55		1.8		-4.8	
		(10,1)				3.1			
		(10,2)			3.1				
		(10,3)					-4.4		
		(10,4)			1.3		3.2		
		(10,5)				-2.0			
		(10,6)		4.0		2.0			
		(10,7)				-0.5		-6.7	
		(10,8)		0.4		2.0		3.5	
		(10,9)			-1.0		-2.5		

Table A-II. "A" values for the indicated spin and parity choices

$J^{P}L$	A_{beam}	A_{normal}
$1/2^{-}P$	0.00	-0.50
$1/2^{+}D$	0.00	-0.50
$3/2^{-}P$	0.20	0.70
$3/2^{+}S$	1.00	-0.50
$5/2^{-}P$	0.80	-0.70
$5/2^{+}D$	-0.14	0.79
$7/2^{-}F$	-0.24	0.83
$7/2^{+}D$	0.71	-0.79

REFERENCES

1. O. Chamberlain, K. M. Crowe, D. Keefe, L. T. Kerth, A. Liminick, T. Maung, and T. F. Zipf, Phys. Rev. Letters 125, 1696 (1962).

2. A. Barbaro-Galtieri, A. Hussain, and R. D. Tripp, Physics Letters 6, 296 (1963).

3. R. W. Birge, R. P. Ely, G. E. Kalmus, A. Kernan, J. Louie, J. S. Sahouria, W. M. Smart, The Spin and Parity of the $Y_0^*(1815)$ and the $Y_1^*(1765)$, Proceedings of the Athens Conference on High Energy Physics, Athens, Ohio (1965).

4. R. B. Bell, R. W. Birge, Y.-L. Pan, and R. T. Pu, Phys. Rev. Letters 16, 203 (1966) and R. Armenteros, M. Ferro Luzzi, D. W. Leith, R. Levi Setti, A. Minter, R. D. Tripp, H. Futhuth, V. Hepp, E. Kluge, H. Schneider, R. Barloutard, P. Granet, J. Meyer, and J. P. Porte, Physics Letters 19, 338 (1965).

5. P. Eberhard, F. T. Shively, R. Ross, S. Seigel, J. R. Ficenee, R. I. Hulsizer, R. W. Mortara, M. Pripstein, and W. P. Swanson, Phys. Rev. Letters 14, 466 (1965).

6. Y.-L. Pan and R. P. Ely, Phys. Rev. Letters 13, 277 (1965).

7. R. B. Bell, R. W. Bland, M. G. Bowler, J. L. Brown, R. P. Ely, S.-Y. Fung, G. Goldhaber, A. Hirata, J. A. Kadyk, J. Louie, C. T. Murphy, J. S. Sahouria, V. H. Sieger, W. M. Smart and G. H. Trilling, A Variable Momentum Separated $K^{\pm}$ Beam at the Bevatron, Lawrence Radiation Laboratory report UCRL-11527, July 1964 (unpublished).

8. R. L. Cool, G. Giacomelli, T. F. Kycia, B. A. Leontie, K. K. Li, A. Lundby, and J. Teiger, Phys. Rev. Letters 16, 1228 (1966).

9. Reference manuals, FOG CLOUDY FAIR Bubble Chamber Data Processing System, Lawrence Radiation Laboratory report UCID-1340, 1965 (unpublished).

10. B. Ronne, Analysis of Bubble Chamber Data, Proceedings of the 1964 School for Physicists at CERN.

11. M. B. Watson, M. Ferro Luzzi, and R. D. Tripp, Phys. Rev. 5, 2248 (1963).

12. A. H. Rosenfeld, A. Barbaro-Galtieri, W. H. Barkas, and P. L. Bastian, Data on Particles and Resonant States, Lawrence Radiation Laboratory report UCRL-8030, 1959 (unpublished).

13. R. Armenteros, M. Ferro Luzzi, D. W. Leith, R. Levi Setti, A. Minter, R. D. Tripp, H. Futhuth, V. Hepp, E. Kluge, H. Schneider, R. Barloutard, P. Granet, J. Meyer, and J. P. Porte, Physics Letters 19, 338 (1965).

14. A. H. Rosenfeld, A. Barbaro-Galtieri, W. H. Barkas, and P. L. Bastian, Data on Particles and Resonant States, Lawrence Radiation Laboratory report UCRL-8030, 1959 (unpublished).

15. R. L. Cool, G. Giacomelli, T. F. Kycia, B. A. Leontie, K. K. Li, A. Lundby, and J. Teiger, Phys. Rev. Letters 16, 1228 (1966).

16. R. D. Tripp, Proceedings of the International School of Physics Enrico Fermi, Varenna, Course 33, Academic Press, 1966.

17. S. L. Glashow and A. H. Rosenfeld, Phys. Rev. Letters 10, 192 (1963).

18. S. Minami, Nuovo Cimento 31, 258 (1964).

19. G. I. Wolters and D. J. Holthuizen, Physics Letters 19, 701 (1966).

20. R. D. Tripp, Proceedings of the International School of Physics Enrico Fermi, Varenna, Course 33, Academic Press, 1966.

21. P. Eberhard, F. T. Shively, R. R. Ross, D. M. Siegel, J. R. Ficenec, R. I. Hullsizer, D. W. Mortara, M. Pripstein, and W. P. Swanson, Phys. Rev. Letters 14, 466 (1965).

22. M. Taher-Azdeh, D. J. Prowse, P. E. Schlein, W. E. Slater, P. H. Stork, and H. Ticho, Phys. Rev. Letters 11, 470 (1963).

FIGURE CAPTIONS

Fig. 1. Beam line used to provide the K^- mesons in this experiment.

Fig. 2. Histograms of the measured K^- beam momenta.

Fig. 3. Distribution of the recoil proton momentum and prediction of the deuteron wave function.

Fig. 4. Example of a three- and four-prong event in the bubble chamber.

Fig. 5. Chi squared distributions for: a. 3C or 4C fits with visible recoil protons; b. 1C fits at the sigma decay vertex for all events.

Fig. 6. Distribution of sigma lifetimes.

Fig. 7. a. Azimuthal angular distribution of the sigma for various production angle regions.

b. Azimuthal angular distribution in the lab and decay angular distribution in the sigma center of mass of the decay pion from the sigma.

Fig. 8. Dalitz plot of good events and allowed regions for various K^- n c.m. energies in this experiment.

Fig. 9. a. $\Sigma^- \pi^+$ spectrum;

b. $\pi^+ \pi^-$ spectrum;

c. $\Sigma^- \pi^-$ spectrum.

Fig. 10. a. Expected K^- n c.m. energy distributions for the four momenta of this experiment;

b. Total expected K^- n c.m. energy distribution.

Fig. 11. Phase spaces for various K^- n c.m. energies (unweighted) and the total expected phase space.

Fig. 12. $Y_0^*(1520)$, $Y_0^*(1405)$ resonance curves and three body phase space which compose the best fit to the $\Sigma^- \pi^+$ spectrum.

Fig. 13. Cross sections for $K^- n \to \Sigma^- \pi^+ \pi^-$ and $K^- n \to Y_0^*(1520) \pi^-$ as a function of: a. K^- momentum, and b. K^- n c.m. energy; also shown in the non-$Y_0^*(1520) \pi^-$ cross section.

Fig. 14. $Y_0^*(1520)$ production angular distributions as a function of K^- n c.m. energy.

Fig. 15. Legendre polynomial expansion coefficients, up to fifth order, as a function of K^- n c.m. energy.

Fig. 16. Decay angular distributions of the sigma for 1495 MeV $\leq M(\Sigma^- \pi^+) \leq$ 1545 MeV and 1740 MeV $\leq E_{KN} \leq$ 1780 MeV.

Fig. 17. Theoretical production angular distributions of the $Y_0^*(1520)$ for a $Y_1^*(1760)$ of spin and parity: a. $5/2^-$ and $7/2^+$, and b. $7/2^-$.

Fig. 18. Cross section for production of the $Y_0^*(1405) \pi^-$ as a function of K^- momentum and K^- n c.m. energy.

Fig. 19. $Y_0^*(1405)$ production angular distributions.

Fig. 20. Legendre polynomial expansion coefficients for the $Y_0^*(1405)$ production angular distributions.

Fig. 21. Reflection of the $Y_0^*(1520)$ and $Y_0^*(1405)$.

Fig. 22. $\Sigma^- \pi^-$ spectrum with the $Y_0^*(1520)$ and $Y_0^*(1405)$ reflections removed.

Fig. 23. $Y_0^*(1520)$ decay angular distributions with respect to its line of flight as a function of K^- momentum.

This report was prepared as an account of Government sponsored work. Neither the United States, nor the Commission, nor any person acting on behalf of the Commission:

A. Makes any warranty or representation, expressed or implied, with respect to the accuracy, completeness, or usefulness of the information contained in this report, or that the use of any information, apparatus, method, or process disclosed in this report may not infringe privately owned rights; or

B. Assumes any liabilities with respect to the use of, or for damages resulting from the use of any information, apparatus, method, or process disclosed in this report.

As used in the above, "person acting on behalf of the Commission" includes any employee or contractor of the Commission, or employee of such contractor, to the extent that such employee or contractor of the Commission, or employee of such contractor prepares, disseminates, or provides access to, any information pursuant to his employment or contract with the Commission, or his employment with such contractor.